MASTERARBEIT | MASTER'S THESIS

Titel | Title

Investigation of the influence of polyoxometalates on the cellular uptake of diverse peptides

verfasst von | submitted by

Nina Scherrer BSc

angestrebter akademischer Grad | in partial fulfilment of the requirements for the degree of

Master of Science (MSc)

Wien | Vienna, 2026

Studienkennzahl lt. Studienblatt | Degree programme code as it appears on the student record sheet:	UA 066 863
Studienrichtung lt. Studienblatt | Degree programme as it appears on the student record sheet:	Masterstudium Biologische Chemie
Betreut von | Supervisor:	Mag. Dr. Markus Mitterhauser
Mitbetreut von | Co-Supervisor:	Nadiia Gumerova PhD

Acknowledgement

I would like to express my gratitude to all people who were involved in the creation of this master's thesis. I want to emphasize how much knowledge was transferred to me during these months, not only in theoretical matters, but also especially in practical terms. I learned a lot and I am grateful for this experience.

I want to express my gratitude to Univ.-Prof. Dr. Markus Mitterhauser, who not only made this thesis possible, but also supported it with great enthusiasm and scientific curiosity from the very beginning. Also, I want to thank Katarína Benčurová, MSc., who introduced and guided me in lab work with patience and provided essential support in the interpretation of results as well as in troubleshooting practical challenges. Many thanks to Mag. Dr. Theresa Balber for her consistent and thoughtful input during the evaluation of results, as well as for her practical suggestions that helped refine both the experiments and their interpretation.

I also want to express my gratefulness to Nadiia Gumerova, PhD, as she co-supervised this thesis and supplied the polyoxometalates used in this work and generously shared her expertise on this topic, which helped a lot in data interpretation and in understanding the chemistry behind these fascinating compounds. I am thankful to Dr. Marie Brandt and Dr. Karsten Bamminger who supported me during my attempt to synthesize FITC-octaarginine and gave me helpful insights into organic synthesis and LC-MS methods, even if only briefly, it was very much appreciated.

Finally, my sincere thanks go to all those involved in the PET tracer synthesis at the Division of Nuclear Medicine at the General Hospital of Vienna, for providing me with a small amount of PET tracers that had been synthesized for patient use. Your willingness to share these materials was essential to the success of my work.

Table of Content

Acknowledgement I
List of abbreviations IV
List of figures VIII
List of tables XI
Zusammenfassung 1
Abstract 2
1. Introduction 3
1.1. Aim 3
1.2. POM 3
1.2.1. Properties 3
1.2.2. Medical applications 4
1.2.3. Synthesis 5
1.2.4. Superchaotropic membrane carriers 7
1.3. Cell Membranes 8
1.3.1. Structure, fluidity and membrane lipids 8
1.3.2. Membrane proteins 10
1.3.3. Membrane transport 10
1.3.4. Uptake of peptides 13
1.4. Targets and PET tracers of interest 14
1.4.1. CXCR4 and [^{68}Ga]Ga-Pentixafor 14
1.4.2. PSMA and [^{68}Ga]Ga-PSMA-11 18
2. Experiments 20
2.1. Cell culture maintenance 20
2.1.1. Principle 20
2.1.2. Chemicals, materials and devices 24
2.1.3. Procedure 25
2.2. Cytotoxicity experiments 27
2.2.1. Method 27
2.2.2. Chemicals, materials and devices 28
2.2.3. Procedure 29
2.2.4. Results 30
2.2.5. Discussion 31
2.3. Synthesis of FITC-octaarginine 32
2.3.1. Method 32
2.3.2. Devices and chemicals 34
2.3.3. Procedure 35

2.3.4. Results 36
2.3.5. Discussion 39
2.4. Fluorescence experiments....40
2.4.1. Method 40
2.4.2. Chemicals, materials and devices....42
2.4.3. Procedure....42
2.4.4. Results 44
2.4.5. Discussion 51
2.5. LigandTracer® experiments 53
2.5.1. Method 53
2.5.2. Chemicals, materials and devices....54
2.5.3. Procedure....55
2.5.4. Results 55
2.5.5. Discussion 57
2.6. Conventional well plate uptake experiments with PET tracers 58
2.6.1. Method 58
2.6.2. Chemicals and devices....58
2.6.3. Procedure....59
2.6.4. Calculations and statistical analysis....60
2.6.5. Results 62
2.6.6. Discussion 78
3. General discussion and conclusions....82
4. Summary 84
5. References 85
6. Appendix....91
6.1. Detailed results cell toxicity experiments 91
6.2. Results cell uptake experiments....97
6.3. Calculation and statistical evaluation of cell uptake experiments 105

List of abbreviations

%AD/5.0e5 cells	percentage of applied dose per 500,000 cells
2-PMPA	2-phosphonomethylpentanedioic acid
4-AMBA	4-aminomethylbenzoic acid
ACN	acetonitrile
AHX	6-aminohexanoic acid
AMP	adenosine monophosphate
AP-2	adaptor protein 2
ATCC	American Type Culture Collection
ATP	adenosine triphosphate
C	actual cell count of an experiment
cAMP	cyclic adenosine monophosphate
CD4+	cluster of differentiation 4 positive
CHO	Chinese hamster ovary
CPM	counts per minute
CXCL12	C-X-C motif chemokine ligand 12
CXCR4	C-X-C chemokine receptor type 4
DAG	diacylglycerol
DAPI	4',6-diamidino-2-phenylindol
DIPEA	*N,N*-diisopropylethylamine
DMSO	dimethyl sulfoxide
DNA	deoxyribonucleic acid
DOTA	1,4,7,10-tetraazacyclododecane-1,4,7,10-tetraacetic acid
DPBS	Dulbecco’s phosphate-buffered saline
ER	endoplasmic reticulum
ERK1/2	extracellular signal-regulated kinase

FACS	fluorescence activated cell sorting
FBS	fetal bovine serum
FITC	fluorescein isothiocyanate
GDP	guanosine diphosphate
GFP	green fluorescent protein
GRKs	G-protein coupled receptor kinases
GTP	guanosine triphosphate
GTPase	guanosine triphosphatase
HBED-CC diacetic acid	*N,N′*-bis[2-hydroxy-5-carboxyethylbenzyl]ethylenediamine-N,N'-diacetic acid
HBSS	Hank’s balanced salt solution
HIV	human immunodeficiency virus
IP_3	inositol-1,4,5-triphosphate
JAK	Janus kinase
LC-MS	liquid chromatography coupled with MS
M	molecular mass
m/z	mass-to-charge ratio
MAPK/ERK kinase	mitogen-activated protein kinase/extracellular signal-regulated kinase
MEK1/2	mitogen-activated protein kinase kinase
mGluRs	metabotropic glutamate receptors
MO_x	metal oxygen
MTT	thiazolyl blue tetrazolium bromide
N_c	decay-corrected activity
N_m	measured activity
N_n	normalized activity
NPP1	nucleotide pyrophosphatase/phosphodiesterase 1

N_s	activity of the standard representing 100% applied dose
ns	not significant
NTPDase	nucleoside triphosphate diphosphohydrolase 1
PBS	phosphate-buffered saline
PDK1	PIP_3 dependent protein kinase 1
PET	positron emission tomography
PH domain	Pleckstrin-homology domain
PI3K	phosphoinositide-3 kinase
PIP_2	phosphatidylinositol-4,5-bisphosphate
PIP_3	phosphatidylinositol-3,4,5-triphosphate
PKA	protein kinase A
PKB	protein kinase B
PKC	protein kinase C
PLC-β	phospholipase C-β
POM	polyoxometalates
POMs	polyoxometalates
PSMA	prostate-specific membrane antigen
qPCR	qualitative polymerase chain reaction
RCF	relative centrifugal force
RFC	reduced folate carrier
RH	relative humidity
RhoGEFs	guanine nucleotide exchange factors
ROCK	Rho-associated kinases
RPMI	Roswell Park Memorial Institute
SDF-1	stromal cell-derived factor 1α
SIM	selected ion monitoring

STAT	signal transducer and activator of transcription
t	time
$t_{1/2}$	half-life
TAT	trans-activator of transcription
TBA	tributylamine
TCA	tricarboxylic acid
TFA	trifluoroacetic acid
TIC	total ion chromatogram

List of figures

Figure 1 Different POM structures [4] 4
Figure 2 Structure of $SiMoW_{11}$ – Keggin type [16] 6
Figure 3 Structure of $GaMo_6$ – Anderson type [16] 6
Figure 4 Structure of $GaMo_{12}$ – Keggin type [16] 7
Figure 5 Structure of phosphatidylcholine, the most abundant phospholipid in mammalian cell membranes 8
Figure 6 Different head groups of phospholipids 9
Figure 7 Permeability of different classes of molecules through a synthetic membrane 11
Figure 8 Forms of transport across a lipid bilayer 11
Figure 9 Kinetics of transporter-mediated diffusion versus simple diffusion 12
Figure 10 Types of active transporters and types of coupled transporters 12
Figure 11 Schematic illustration of the process of endocytosis [22] 13
Figure 12 Schematic demonstration of entry ways for small molecules, peptides and proteins [23] 14
Figure 13 Structure of [^{68}Ga]Ga-Pentixafor 15
Figure 14 Overview of the signalling cascade initiated by CXCL12 binding to CXCR4 [41] 16
Figure 15 Endocytosis of agonist-bound GPCR via β-arrestin binding 18
Figure 16 Structure of [^{68}Ga]Ga-PSMA-11 19
Figure 17 Illustration of the cellular function of PSMA [54] 20
Figure 18 Air flow in horizontal (left) and vertical laminar flow hoods (right) [63] 21
Figure 19 CHO-K1 cells at low (left) and high confluency (right) [66] 22
Figure 20 HT29 cells at low (left) and high confluency (right) [67] 23
Figure 21 T47D cells at low (left) and high confluency (right) [69] 23
Figure 22 Formazan structure (left) dissolved formazan crystals in DMSO (right) 28
Figure 23 Applied concentrations of $GaMo_6$ and $GaMo_{12}$ to the cell lines CHO-K1, HT29 and T47D 29
Figure 24 Representative inhibition curves of $GaMo_6$ and $GaMo_{12}$ in CHO-K1 30
Figure 25 Representative inhibition curves of $GaMo_6$ and $GaMo_{12}$ in HT29 30
Figure 26 Representative inhibition curves of $GaMo_6$ and $GaMo_{12}$ in T47D 31
Figure 27 Reaction of FITC with a protein [77] 32
Figure 28 Unwanted cyclisation after FITC conjugation [76] 33
Figure 29 Schematic illustration of the principal behind chromatography 33
Figure 30 Basic principle of MS [82] 34
Figure 31 Chromatogram of octaarginine (right) and FITC (left), SIM (selected ion monitoring) plot (top) and TIC (total ion chromatogram) (bottom) 36
Figure 32 Chromatogram of FITC and octaargine in the presence of DIPEA after 40, 90, 130 minutes and overnight at 4 °C, SIM plot (top), TIC (bottom) 37
Figure 33 Chromatogram of FITC and octaargine in the presence of DIPEA after overnight incubation at room temperature, SIM plot (top), TIC (bottom) 38
Figure 34 Chromatogram of FITC and octaargine in the presence of DIPEA at higher concentrations incubated for 2 and 4 h at room temperature, SIM plot (top), TIC (bottom) 38
Figure 35 Schematic illustration of fluorescence [85] 40
Figure 36 Schematic illustration and comparison between widefield (A) and confocal microscopy (B) [87] 41
Figure 37 Images of triple-labelled cell aggregate obtained using widefield (A) and confocal (B) fluorescent microscopy [88] 41
Figure 38 Uptake of FITC-protamine in the presence of different POMs 45

Figure 39 Uptake of FITC-protamine at different concentrations in the presence of 10 µM $SiMoW_{11}$.....45
Figure 40 Uptake of FITC-protamine at different concentrations without membrane carrier 46
Figure 41 FITC-protamine uptake at higher concentrations, with increased heparin concentration and incubated in DPBS in the presence of 10 µM $SiMoW_{11}$ 46
Figure 42 FITC-protamine uptake at higher concentrations, with increased heparin concentration and incubated in DPBS in the absence of a membrane carrier 47
Figure 43 Uptake of FITC-protamine after permeabilization, in the absence of heparin and following preincubation with $SiMoW_{11}$ 48
Figure 44 Uptake of FITC-protamine after permeabilization, in the absence of heparin and following preincubation with water.....48
Figure 45 Uptake of FITC-protamine after overnight incubation 49
Figure 46 Uptake of FITC-octaarginine in the presence of different POMs.....49
Figure 47 Uptake of FITC-octaarginine in the presence of different POMs after extended incubation 50
Figure 48 Uptake of FITC-octaarginine in the presence of different POMs at a higher peptide concentration.....51
Figure 49 Uptake of FITC-octaarginine in the presence of different POMs after overnight incubation 51
Figure 50 LigandTracer® methodology [93] 54
Figure 51 Different types of LigandTracer® [92].....54
Figure 52 Cell culture dish preparation for LigandTracer® experiment. In the publication, as opposed to this thesis, cells were seeded two days prior to an experiment [94] 55
Figure 53 Binding curves of [^{68}Ga]Ga-Pentixafor to HT29 cells.....56
Figure 54 Binding curves of [^{68}Ga]Ga-Pentixafor to HT29 cells.....57
Figure 55 Scheme of cell uptake experiment Filled and striped wells represent the cells in absence or presence of an inhibitor, respectively. From each well, three fractions were collected, blue representing the supernatant fraction, orange representing the membrane bound fraction and purple representing the internalized fraction. 60
Figure 56 internalized and membrane bound percentage of applied dosage (%AD) of [^{68}Ga]Ga-Pentixafor in HT29 cells at 37 °C 66
Figure 57 Relative membrane-bound and internalized fractions of [^{68}Ga]Ga–Pentixafor in HT29 at 37 °C.....66
Figure 58 Membrane bound and internalized percentage of applied dosage (%AD) of [^{68}Ga]Ga-Pentixafor in HT29 cells at 4 °C 67
Figure 59 Relative membrane-bound and internalized fractions of [^{68}Ga]Ga–Pentixafor in HT29 cells at 4 °C.....67
Figure 60 Membrane bound and internalized percentage of applied dosage (%AD) of [^{68}Ga]Ga-Pentixafor in CHO-K1 cells at 37 °C.....68
Figure 61 Relative membrane-bound and internalized fractions of [^{68}Ga]Ga–Pentixafor in CHO–K1 cells at 37 °C 68
Figure 62 Membrane bound and internalized percentage of applied dosage (%AD) of [^{68}Ga]Ga-Pentixafor in CHO-K1 cells at 4 °C 69
Figure 63 Relative membrane-bound and internalized fractions of [^{68}Ga]Ga–Pentixafor in CHO–K1 cells at 4 °C 69
Figure 64 Membrane bound and internalized percentage of applied dosage (%AD) of [^{68}Ga]Ga-PSMA-11 in CHO-K1 PSMA cells at 37 °C.....74
Figure 65 Relative membrane-bound and internalized fractions of [^{68}Ga]Ga–PSMA-11 in CHO–K1 PSMA cells at 37 °C.....74
Figure 66 Membrane bound and internalized percentage of applied dosage (%AD) of [^{68}Ga]Ga-PSMA-11 in CHO-K1 PSMA cells at 4 °C.....75

Figure 67 Relative membrane-bound and internalized fractions of [^{68}Ga]Ga–PSMA-11 in CHO–K1 PSMA cells at 4 °C.....75
Figure 68 Membrane bound and internalized percentage of applied dosage (%AD) of [^{68}Ga]Ga-PSMA-11 in CHO-K1 cells at 37 °C.....76
Figure 69 Relative membrane-bound and internalized fractions of [^{68}Ga]Ga–PSMA-11 in CHO–K1 cells at 37 °C 76
Figure 70 Membrane bound and internalized percentage of applied dosage (%AD) of [^{68}Ga]Ga-PSMA-11 in CHO-K1 cells at 4 °C.....77
Figure 71 Relative membrane-bound and internalized fractions of [^{68}Ga]Ga–PSMA-11 in CHO–K1 cells at 4 °C 77
Figure 72 Appendix - IC_{50} results $GaMo_6$ in CHO-K1 91
Figure 73 Appendix - IC_{50} results $GaMo_{12}$ in CHO-K1 92
Figure 74 Appendix – IC_{50} results $GaMo_6$ in HT29 93
Figure 75 Appendix - IC_{50} results $GaMo_{12}$ in CHO-K1 95
Figure 76 Appendix - IC_{50} results $GaMo_6$ in T47D 96
Figure 77 Appendix - IC_{50} results $GaMo_{12}$ in T47D.....97

List of tables

Table 1 Medium composition for each cell line 25
Table 2 Splitting fractions 26
Table 3 IC50 results of POMs in the cell lines CHO-K1, HT29 and T47D 31
Table 4 Concentration gradient of mobile phase applied on the column 35
Table 5 Relevant m/z values for the starting materials and the desired product and their most probable multiply charged ions 35
Table 6 Final concentrations of [^{68}Ga]Ga-Pentixafor and $SiMoW_{11}$ after each addition (related to Figure 53) 56
Table 7 Final concentrations of [^{68}Ga]Ga-Pentixafor and $SiMoW_{11}$ after each addition (related to Figure 54) 57
Table 8 Overview of tested conditions 60
Table 9 Statistical comparison between no carrier and POM mediated internalization (int) and membrane binding (mb) of [^{68}Ga]Ga-Pentixafor 63
Table 10 Statistical comparison between inhibited and not inhibited internalization (int) and membrane binding (mb) of [^{68}Ga]Ga-Pentixafor 64
Table 11 Statistical comparison between 10 µM and 30 µM of applied POM in terms of internalization (int) and membrane binding (mb) of [^{68}Ga]Ga-Pentixafor 65
Table 12 Statistical comparison between no carrier and POM mediated internalization (int) and membrane binding (mb) of [^{68}Ga]Ga-PSMA-11, concentrations of POM in µM.....71
Table 13 Statistical comparison between inhibited and not inhibited internalization (int) and membrane binding (mb) of [^{68}Ga]Ga-PSMA-11 72
Table 14 Statistical comparison between 10 µM and 30 µM of applied POM in terms of internalization (int) and membrane binding (mb) of [^{68}Ga]Ga-PSMA-11 73
Table 15 Appendix - IC_{50} results $GaMo_6$ in CHO-K1 91
Table 16 Appendix - IC_{50} results $GaMo_{12}$ in CHO-K1 92
Table 17 Appendix – IC_{50} results $GaMo_6$ in HT29 92
Table 18 Appendix - IC_{50} results $GaMo_{12}$ in CHO-K1 94
Table 19 Appendix - IC_{50} results $GaMo_6$ in T47D 95
Table 20 Appendix - IC_{50} results $GaMo_{12}$ in T47D 96
Table 21 Appendix – [^{68}Ga]Ga-PSMA-11 internalized 97
Table 22 Appendix – [^{68}Ga]Ga- PSMA-11 membrane bound 99
Table 23 Appendix – [^{68}Ga]Ga-Pentixafor internalized 101
Table 24 Appendix – [^{68}Ga]Ga-Pentixafor membrane bound 103

Zusammenfassung

Diese Masterarbeit beschäftigt sich weitestgehend mit der Erforschung der Membrancarrier-Eigenschaften von POMs (Polyoxometallate), im speziellen $GaMo_6$ und $GaMo_{12}$. Hierzu wurde zuerst die Zelltoxizität beider POMs in den in weiterer Folge verwendeten Zelllinien CHO-K1 und HT29 ermittelt, um sicherzustellen, dass es zu keinen Interferenzen durch bestehende Zelltoxizität kommt. Ebenfalls wurde auch geprüft, ob POMs einen proliferativen Effekt auf eine östrogenrezeptor-positive Krebszelllinie T47D besitzen. Es wurde kein proliferativer Effekt der beiden getesteten POMs auf T47D festgestellt. Alle folgenden Versuche wurden mit einer maximalen Konzentration von 30 µM POM durchgeführt, was unter der ermittelten Zytotoxizität liegt. Anschließend wurden Peptidaufnahmeversuche mit verschiedenen Methoden und Peptiden durchgeführt. Zuerst wurde die Aufnahme von FITC (Fluoresceinisothiocyanat)-Protamin und FITC-Octaarginin unter Anwesenheit von $GaMo_6$, $GaMo_{12}$ und $SiMoW_{11}$ als Positivkontrolle in CHO-K1 Zellen mittels Fluoreszenzmikroskopie untersucht. Hierbei konnte keine Aussage über die Aufnahme der getesteten Peptide getroffen werden, da sich das Hintergrundsignal trotz mehrerer Protokolladaptionen nicht reduzieren ließ. Es ist empfohlen, eine andere Methode zur Bestimmung der Aufnahme dieser Peptide heranzuziehen. Die Aufnahme von den Peptidhaltigen PET-Tracern Pentixafor und PSMA-11, die mit Gallium-68 markiert waren, wurde in der Anwesenheit von $GaMo_6$, $GaMo_{12}$ und $SiMoW_{11}$ als Positivkontrolle mittels eines Aufnahme-Assays bestimmt, welcher zwischen membrangebundenes und internalisiertes Peptid differenziert. Hierbei wurde im Fall von $SiMoW_{11}$ und $GaMo_{12}$ eine Erhöhung der Internalisierung von Pentixafor und eine Erniedrigung der Internalisierung von PSMA-11 beobachtet, während $GaMo_6$ für Pentixafor keine und für PSMA-11 nur partiell eine signifikante Änderung beobachtet wurde. Ebenso wurde versucht, mit der LigandTracer® Technologie kinetische Daten zu der POM-Unterstützen Aufnahme zu erheben, welches allerdings durch die unspezifische Bindung der Tracer an der Gefäßwand nicht glückte. Nebenbei wurde noch versucht, eine in-house Synthese von FITC-Octaarginin durchzuführen. Da die Optimierung dieser Synthese nicht im Fokus dieser Masterarbeit lag, wurde dieses Ziel aufgrund des hohen zeitlichen Aufwands nicht weiterverfolgt.

Abstract

This master's thesis primarily investigates the membrane carrier properties of POMs, specifically $GaMo_6$ and $GaMo_{12}$. The cytotoxicity of both POMs was first determined in the cell lines CHO-K1 and HT29, which were used in later experiments, to rule out interferences from cytotoxic effects. A potential proliferative effect on the estrogen receptor-positive cancer cell line T47D was also investigated. No proliferative effect of the two tested POMs on T47D was observed. All subsequent experiments were conducted with a maximum concentration of 30 µM POM, which is below the determined cytotoxicity. Peptide uptake experiments were conducted using various methods and peptides. First, the uptake of FITC-protamine and FITC-octaarginine in CHO-K1 cells was investigated using fluorescence microscopy in the presence of $GaMo_6$ and $GaMo_{12}$, while $SiMoW_{11}$ was used as positive control. No conclusions could be made regarding the uptake of the tested peptides because the background signal could not be reduced despite several protocol adaptations. It is recommended to use another method to determine peptide uptake. The internalization of peptide-containing PET tracers Pentixafor and PSMA-11, which were labelled with gallium-68, was determined in the presence of $GaMo_6$, $GaMo_{12}$, and $SiMoW_{11}$ using an uptake assay that differentiates between membrane-bound and internalized peptide. In the case of $SiMoW_{11}$ and $GaMo_{12}$, an increase in the internalization of Pentixafor and a decrease in the internalization of PSMA-11 was observed, while no significant change for Pentixafor and only partially decreased internalization of PSMA-11 was observed with $GaMo_6$. Attempts were also made to collect kinetic data on POM-assisted uptake using LigandTracer® technology, but this was unsuccessful due to the nonspecific binding of the tracer to the vessel wall. In addition, an in-house synthesis of FITC-octaarginine was also attempted. Since the optimization of this synthesis was not the focus of this master's thesis, this goal was not pursued further.

1. Introduction

1.1. Aim

POMs possess superchaotropic properties, which has been previously shown to exhibit membrane carrier activity.[1] This master's thesis aimed at elaborating on those properties for the Anderson-type disk shaped $GaMo_6$ and Keggin-type spherical $GaMo_{12}$ with different peptides, using Keggin-type $SiMoW_{11}$ as a previously established positive control. First, internalization of FITC-labelled protamine and octaarginine in the presence of the POMs was examined via fluorescence microscopy. To reduce the waiting time due to the shipping period, an in-house synthesis of FITC-octaarginine was attempted. Then, the internalization and membrane binding of peptide containing [^{68}Ga]Ga-labelled PET tracers Pentixafor and PSMA-11 was tested in conjunction with the POMs using an internalization assay. It was also attempted to gain kinetic data on the internalization of Pentixafor with $SiMoW_{11}$ present using LigandTracer® technology. To ensure that no cytotoxic interferences occurred, the toxicity of $GaMo_6$ and $GaMo_{12}$ were determined using an MTT assay. During this assay, potential proliferative effects of POMs on estrogen receptor positive cancer cells were also tested, since some molybdenum containing structures have shown such activity.[2]

1.2. POM

1.2.1. Properties

POMs are anionic metal-oxygen nanoclusters with highly variable structures and different electronic, compositional and reactive properties. Due to the combination of charge and ionic radius, transition metals from group 5 and 6 form POMs while being their highest oxidation state. An electronic back-donation, which occurs during the formation of a π-bond between metal and oxygen, is possible due to their empty and accessible d-orbitals. Recent years have also brought forward POMs containing noble metals. The acidic condensation of a variable number of $\{MO_x\}$ (x = 4 – 7, M = Mo(VI), W(VI), V(V), Nb(V), Ta(V)) polyhedra leads to the formation of POMs. The most common subunit is $\{MO_6\}$, possessing a coordination number of 6. However, oligomerization is not without limits: due to the polarization of the peripheral metal centers towards the outer oxygen shell, the formation of double bonds between the metal and the oxygen prevents further formation of bridges to additional polyhedra. Each metal center in the polyhedron is displaced toward the terminal oxygen atoms because of the participation of d-orbitals in the π metal-oxygen bonding. Consequently, the metal center can become polarized toward a single terminal oxygen or two terminal oxygens arranged in a relative cis configuration. This results in a final product with markedly different electronic properties. Even though some properties vary between different POMs, there are some characteristics they all

have in common. All possess a large negative charge and are big in size. They have a high structural symmetry, are thermally stable, show oxidant resistance and they can also undergo redox reactions without conformational changes or degradation, which is due to their ability to delocalize electrons between several metal atoms. POMs are usually classified based on their composition. Iso-POMs only contain metals and oxygen and display a very basic surface, whereas hetero-POMs can also contain heteroatoms, which enhances their stability in comparison to their iso-counterparts.[3] POMs can also be classified based on their structure (Figure 1).

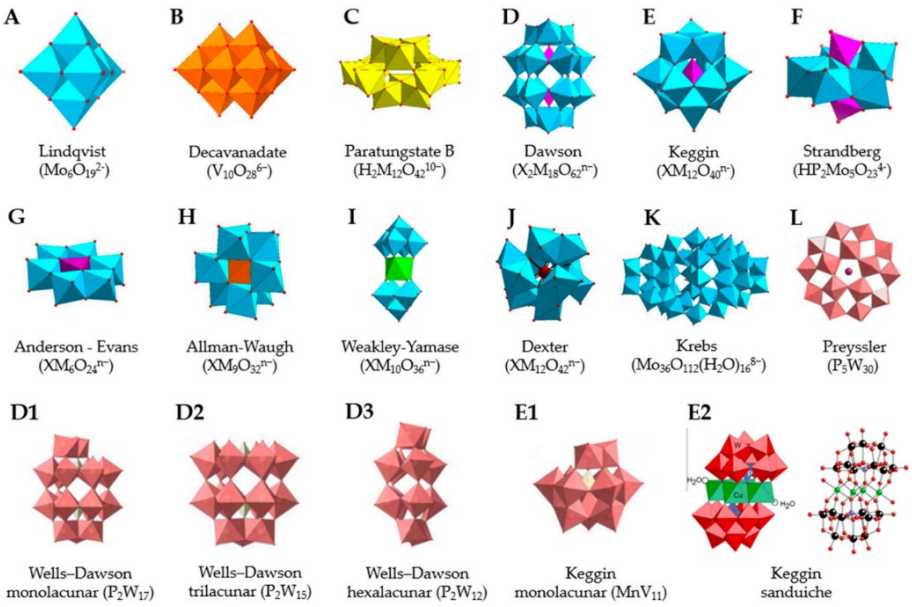

Figure 1 Different POM structures [4]

Due to their electron-donating oxygen atoms, POMs can be considered soft Lewis bases. Conversely, the unoccupied orbitals of the metal centers of POM structures can act as Lewis acids, as they can accept electrons.[5]

1.2.2. Medical applications

POMs have recently been shown to possess anticancer, antibacterial and antiviral properties, although their mechanisms of action are not yet fully understood. Not all POMs exhibit the same level of bioactivity: some are more effective antibacterial, antiviral or anticancer agents than others.

In the case of *Moraxella catarrhalis*, a gram-negative bacterium that causes lower respiratory tract infections, six POMs have been identified to exhibit antibacterial activity. One of these is of the Preyssler type, while the rest belongs to the Dawson family.[6] Also, some POM-based hybrid and nanocomposite structures have proven effective against *Helicobacter pylori* and *Streptococcus pneumoniae*.[7]

Regarding their anticancer potential, a proposed mechanism involves the inhibition of ecto-nucleotidases, enzymes which promote angiogenesis, tumor growth and immunosuppression due to the hydrolysis of extracellular AMP (adenosine monophosphate) resulting in free adenosine. A trivacant Keggin-derived sandwich structure was found to be a potent inhibitor of an ecto-nucleotidase, specifically NTPDase (nucleoside triphosphate diphosphohydrolase 1), whereas some other Keggin-, Preyssler- and crypt-structured POMs appear to selectively inhibit human NPP1 (nucleotide pyrophosphatase/phosphodiesterase 1).[8] They are also suspected of inducing cell apoptosis by DNA (deoxyribonucleic acid) modification, might also be able to hydrolyze carboxyesters and perform oxidative and hydrolytic protein cleavage due to their redox properties; both mechanisms have been hypothesized to contribute to their anticancer activity.[9] POM-like hybrids and nanocomposites have shown potential for cancer treatment *in vitro* exhibiting reduced overall toxicity towards normal cells compared to unmodified POMs.[10] Furthermore, diverse POMs have demonstrated anticancer activity *in vivo* using mouse models of diverse cancer types.[4]

A titanium containing polyoxotungstate showed antiviral activity against anti-influenza virus A in infected mice and a vanadium substituted polytungstate showed antiviral activity *in vitro* for parainfluenza, Dengue fever virus and HIV, which further elaborates on the versatility of applications for POMs in the medical field.[11]

POMs have further shown promising results in the treatment of neurodegenerative diseases such as Alzheimer's.[12] Due to the structural diversity of POMs, many more medical applications are theoretically possible.[3]

1.2.3. Synthesis

The synthesis of POMs is straightforward and consists of the following steps: first, salts of the metal that is to be incorporated into the POM need to be dissolved in a suitable solvent depending on what POM is to be synthesized. This is followed by an acidification, which causes condensation of those metals into metal-oxygen units. Subsequent heating drives the self-assembly of the POMs into larger structures such as Keggin or Anderson types. Once this larger architecture is formed, it is precipitated with a suitable counterion, such as potassium or TBA (tributylamine).[13], [14] The resulting structure is strongly influenced by the temperature applied during synthesis: higher temperatures favor the formation of larger and more ordered structures, such as Keggin and Wells-Dawson types, whereas intermediate temperatures might lead to intermediates and non-classical structures. Other reaction conditions, such as pH, also influence which structure is formed.[15]

$SiMoW_{11}$

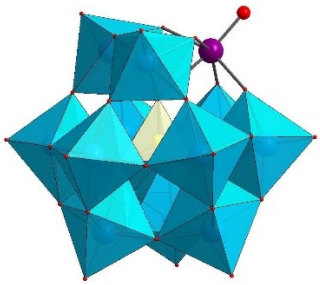

Figure 2 Structure of $SiMoW_{11}$ – Keggin type [16]

Color code: {WO_6} = blue; {SiO_4} = yellow; Mo = purple; O = red

$SiMoW_{11}$, which is an abbreviation for $K_4[SiMoW_{11}O_{40}]$, is a Keggin type POM containing molybdenum and tungsten. For synthesis, a solution of $NaMoO_4$ is acidified with HNO_3, followed by the addition of potassium moldybotungstosilicate. This results in the precipitation of a yellow solid, which is filtered and washed with a saturated KCl soliton, ethanol and ether. To purify, the precipitate is dissolved in water at room temperature and then stored at 0°C for 24 hours. Yellow needles can be obtained afterwards.[17]

$GaMo_6$

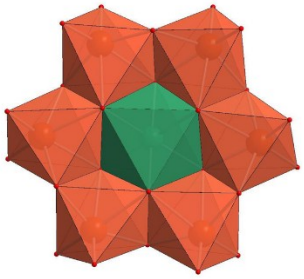

Figure 3 Structure of $GaMo_6$ – Anderson type [16]

Color code: {MoO_6} = orange; {GaO_6} = green; O = red

The Anderson type POM $GaMo_6$, which is short for $K_3[Ga(OH)_6Mo_6O_{18}]$, is synthesized by dissolving Na_2MoO_4 and $Ga(NO_3)_3$ in water, followed by acidification to a pH of 3 using HCl. After heating the mixture to 80°C for 30 minutes, the product is formed and can be precipitated using KCl, followed by filtration.[18]

$GaMo_{12}$

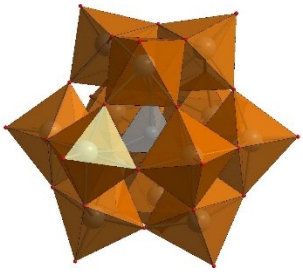

Figure 4 Structure of $GaMo_{12}$ – Keggin type [16]

Color code: {MoO_6} = orange; {GaO_4} = grey; O = red

$TBA_5[GaMo_{12}O_{40}]$, or $GaMo_{12}$ for short, is also a Keggin type POM, which is similarly to $GaMo_6$ synthesized by acidifying a solution containing $Ga(NO_3)_3$ and Na_2MoO_4 with HNO_3. First, a Na_2MoO_4 solution is acidified with HCl before $Ga(NO_3)_3$ is added. This is followed by the addition of CH_3CN, after which the solution is heated to 75°C for 20 hours. The precipitate that forms is then filtered and cooled to room temperature before TBABr is added to precipitate a yellow salt. This salt is then acquired by filtration.[19]

1.2.4. Superchaotropic membrane carriers

The most relevant characteristics of POMs in the context of this research are their superchaotropic properties.[1] Chaotropic substances disrupt hydrogen-bonding networks among water molecules, which in turn increases the solubility of certain molecules such as proteins and nucleic acids. However, chaotropic molecules can also influence how molecules interact with cellular membranes. While it is hypothesized that the disruption of the hydrogen bonding networks enables hydrophilic substances to interact with membranes, the exact mechanism underlying the membrane carrier activity exhibited by some POMs is not understood yet. Carrier molecules must exhibit affinity both for their cargo as well as the membrane itself to facilitate transport across the lipid bilayer. Some low-charged POMs have previously exhibited strong, but reversible, intermolecular interactions with cationic oligopeptides. It has also been confirmed that the carrier properties are not caused by the rupture of the membranes. Using experiments with membranes, it was shown that certain Keggin type POMs exhibited membrane carrier behaviors, whereas Anderson type POMs were inactive in this regard. One of the Keggin type POMs that demonstrated membrane carrier properties is $SiMoW_{11}$ [1], which was used in this master's thesis as a positive control.

1.3. Cell Membranes

1.3.1. Structure, fluidity and membrane lipids

The plasma membrane of a cell is of utmost importance, as it represents the border and interaction space between the organism and its environment. Receptors, channels and pores are the main interaction points between the cell and the surrounding molecules.

The lipid bilayer consists primarily of phospholipids, structures that contain a hydrophilic head consisting of a choline, phosphate and glycerol, with the glycerol connecting the head to the fatty acids that represent the hydrophobic tails (Figure 5).[20]

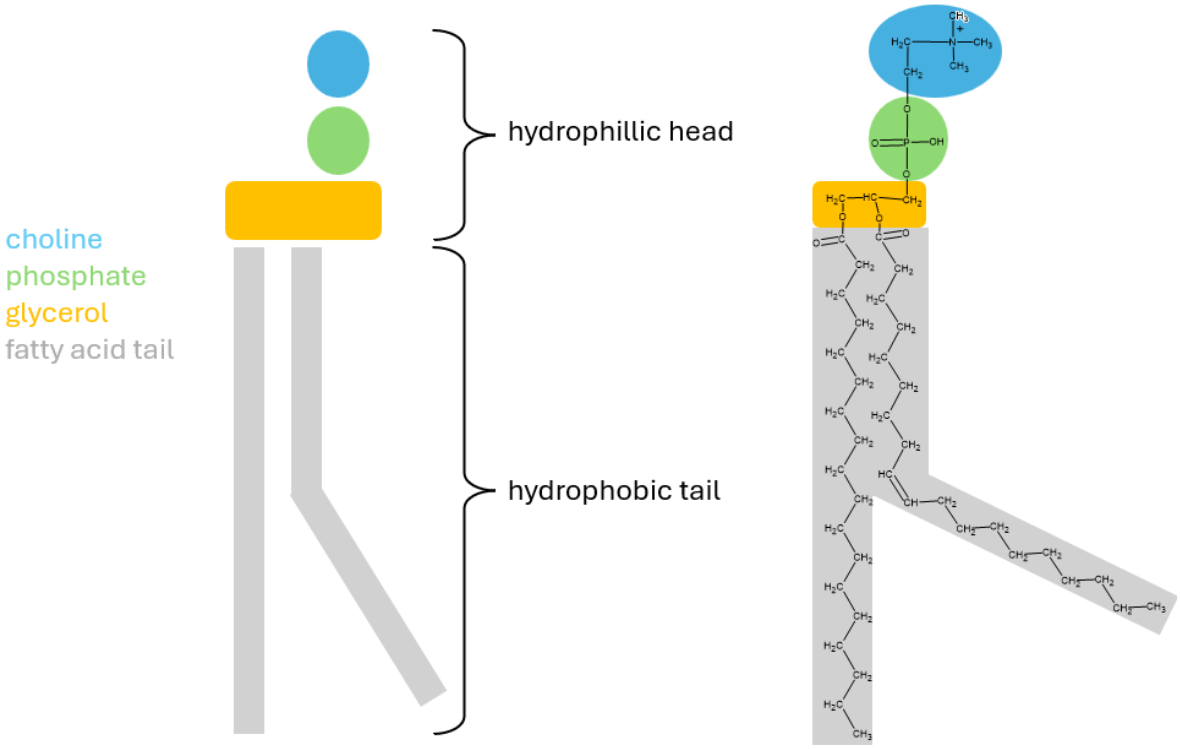

Figure 5 Structure of phosphatidylcholine, the most abundant phospholipid in mammalian cell membranes

Other head groups are also possible, giving the membranes different properties depending on the abundance of these distinct phospholipid types. Phosphatidylethanolamine affects the membrane curvature and fluidity due to its smaller head group and facilitates endocytosis and vesicle formation, whereas sphingomyelin increases membrane rigidity through numerous hydrogen bonds enabled by its saturated fatty acid chains. The latter also contributes to cell sorting, membrane organization and signaling by the formation of lipid rafts via interaction with cholesterol. Phosphatidylserine, on the other hand, influences the interactions between the membrane and its surroundings by possessing a negative charge at physiological pH. Phosphatidylcholine increases permeability due to its cylindrical shape. Although not a phospholipid, sphingosine is also an important player in the membrane as it influences signaling pathways and lipid interactions due to its long hydrophobic tail (Figure 6).[21]

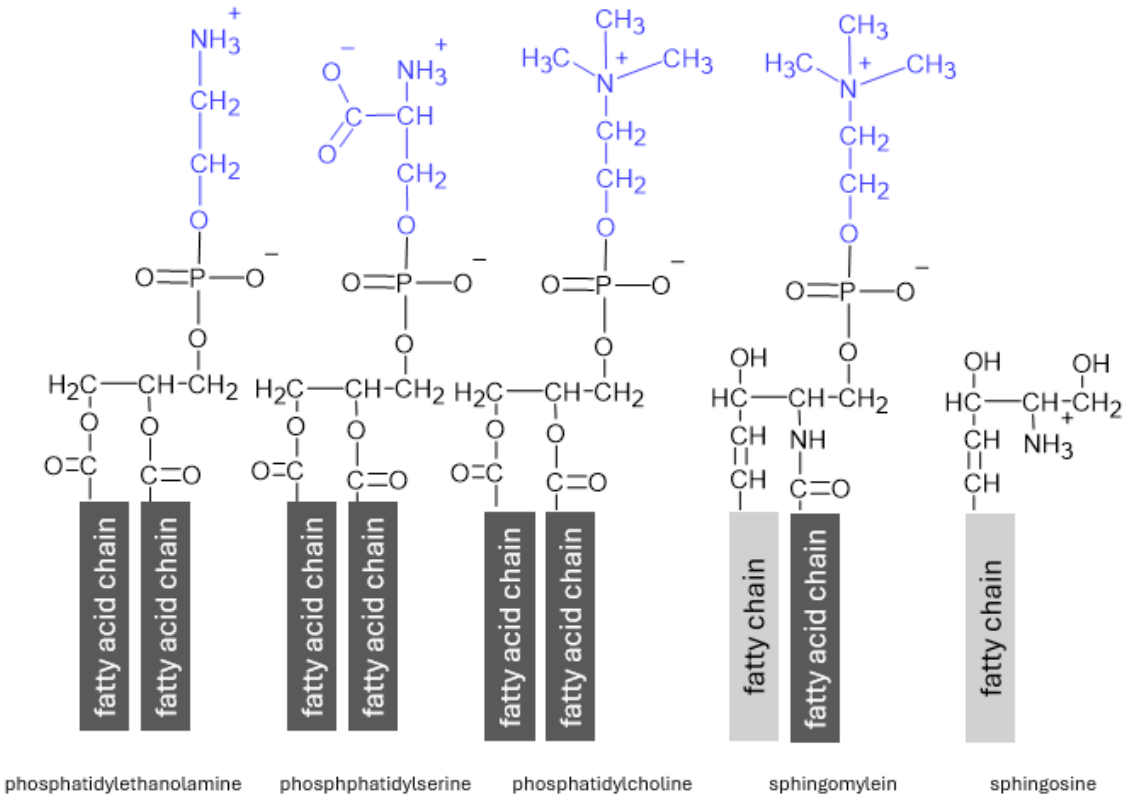

Figure 6 Different head groups of phospholipids

Phospholipids form bilayers spontaneously, which is due to their amphiphilic nature. In an aqueous environment, they arrange so that the hydrophilic heads face the aqueous side, whereas their hydrophobic tails face each other and in turn form a bilayer. This arrangement also gives membranes the ability to heal themselves. A tear in a membrane leads to a rearrangement of the phospholipids so that no hydrophobic tails are in an aqueous environment. Contrary to popular belief, a membrane is not a static structure; molecules within the membrane can diffuse freely within the plane of the lipid bilayer. As mentioned previously, fluidity is dependent on the composition of the lipid bilayer and the temperature. Not only can the head groups affect fluidity, but tails of phospholipids also have an influence as well. Shorter and unsaturated fatty acid chains with cis-double bonds make it harder for the lipids to stack together and therefore increase fluidity.[20]

Cholesterol also plays a role in membrane dynamics by inserting itself into the bilayer with the hydroxyl group in proximity to the polar head of the phospholipid, where the steroid-like rings immobilize regions of the hydrocarbon chains, making this region less susceptible to deformation and decreasing its permeability. Although cholesterol does not influence overall fluidity, it prevents hydrocarbon chains from crystallizing. Besides lateral diffusion, phospholipids can rotate and switch places with lipids on the other side of the bilayer, though the latter occurs rarely. One particular property of the plasma membrane is its asymmetry, not

only regarding the proteins present, but also in membrane composition, which is due to the distinct functions these components have on each side of the membrane, making the lipid flipping uncommon. Despite the fluidity of the membrane, designated areas with different lipids and protein compositions can aggregate to form lipid rafts. They assemble temporarily via protein-protein interactions, forming specialized membrane regions for a temporary purpose. Key membrane components, primarily located on the extracellular side, are glycolipids, which consist of sphingosine and sugar moieties connected by hydrogen bonds. Glycolipids contribute to membrane protection from harsh environments. Additionally, charged glycolipids such as gangliosides can alter the membrane's electrical properties.[21]

1.3.2. Membrane proteins

The cell membrane is an important platform for many biochemical reactions since its purpose is to mediate interactions with the extracellular space as well as protecting the cell from outer influences. Therefore, a plethora of proteins such as receptors inhabit the membrane. These usually consist of one or more regions that completely or partly reside in the membrane, and domains extending into the extra- or intracellular space. These proteins can either associate with membranes as single or multiple α-helices or as rolled-up β-sheets. However, it is not a necessity for proteins to be inserted into the membrane; they can be attached via a lipid chain (such as a fatty acid chain or a prenyl group) or an oligosaccharide linker or interact noncovalently with other membrane-bound proteins. The way a protein associates with the membrane reflects its purpose: Transmembrane proteins are proteins that serve a purpose on both sides of the membrane, such as cell surface receptors or transporters, and are most commonly in an α-helix conformation at the transmembrane domain. Extracellular domains usually interacts with ligands which upon binding often start a signaling cascade on the intracellular side.[20]

1.3.3. Membrane transport

Due to their hydrophobic interior, cellular membranes are impermeable for most polar molecules, which leads to a concentration gradient of ions within the cell compared to the extracellular space. This concentration gradient is a driver for passive diffusion through a membrane and will, given enough time, allow any molecule to diffuse through a protein-free lipid bilayer theoretically. The rate of diffusion, however, depends strongly on size, polarity and hydrophilicity. Smaller, hydrophobic and non-polar molecules diffuse more easily through a membrane than larger, hydrophilic and polar molecules (Figure 7).[20]

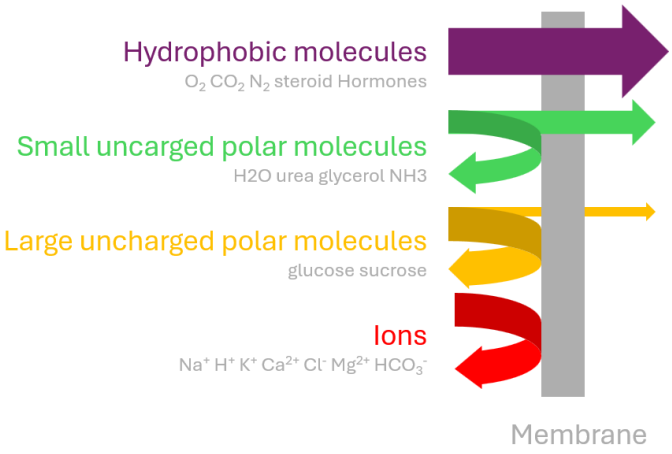

Figure 7 Permeability of different classes of molecules through a synthetic membrane

However, since cells need to transport ions and other impermeable substrates and metabolites across their membranes, specialized transport mechanisms have evolved. These can either move molecules along the concentration or electrochemical gradient or against it, which are regarded as passive and active respectively (Figure 8). Passive transport can occur via a channel or a transporter, whereas active transport is mediated via a transporter under the depletion of energy. These transporters have one or more specific binding sites for their substrates, which they aid across the membrane by undergoing conformational change. This transition occurs through an intermediate state, during which the substrate is inaccessible from either side of the membrane.[20]

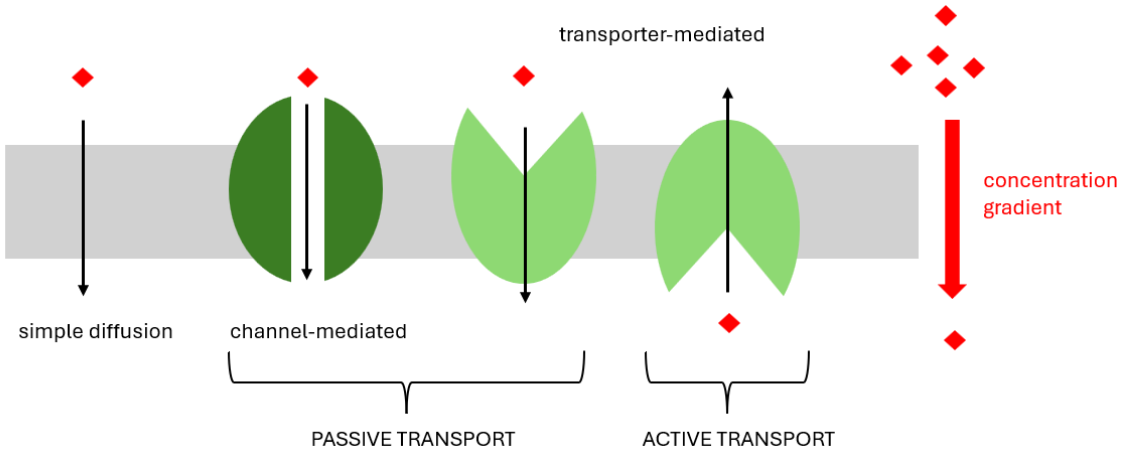

Figure 8 Forms of transport across a lipid bilayer

The rate of transport is dependent on the saturation of the transporter with its substrate and is also referred to as V_{max}, which shows the maximal rate of transport across the membrane when the enzyme is saturated with substrate. Each transporter also has a specific affinity for its substrate, K_M, which is the substrate concentration at which 50% of V_{max} is reached (Figure 9). Like enzymes, transporters can also be inhibited by competitive or non-competitive inhibitors.[20]

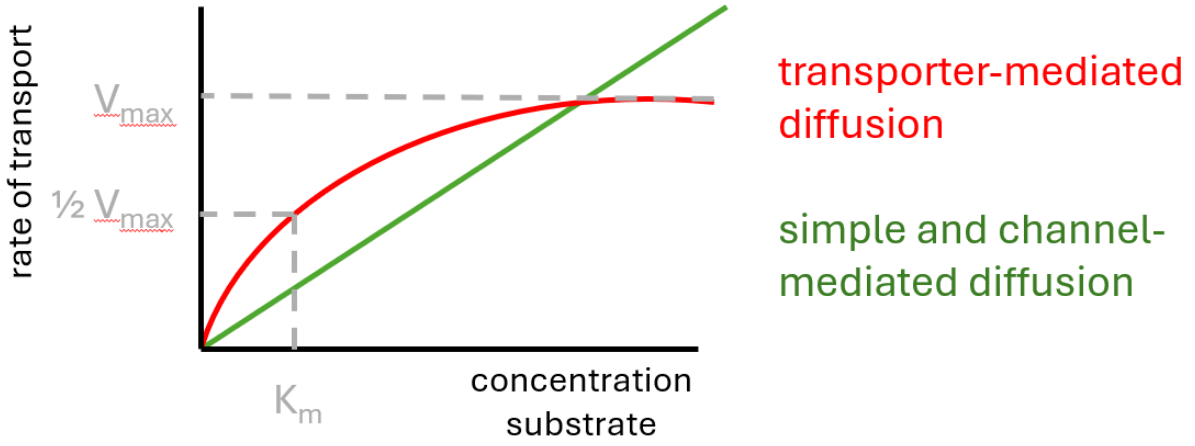

Figure 9 Kinetics of transporter-mediated diffusion versus simple diffusion

To move substrates against their concentration gradient, the transporter needs to be coupled to an energy source, which can happen in several ways. Coupled transporters use the energy released from moving one substrate along its concentration gradient to move another against its concentration gradient. They can be further distinguished into symporters, which move both substrates in the same direction, and antiporters, which import one and export the other substrate. ATP (adenosine triphosphate) driven pumps generate the required energy by the hydrolysis of ATP, whereas light- or redox-driven pumps use light or electrons as an energy source (Figure 10). Latter are mostly found in bacteria, archaea, mitochondria and chloroplasts.[20]

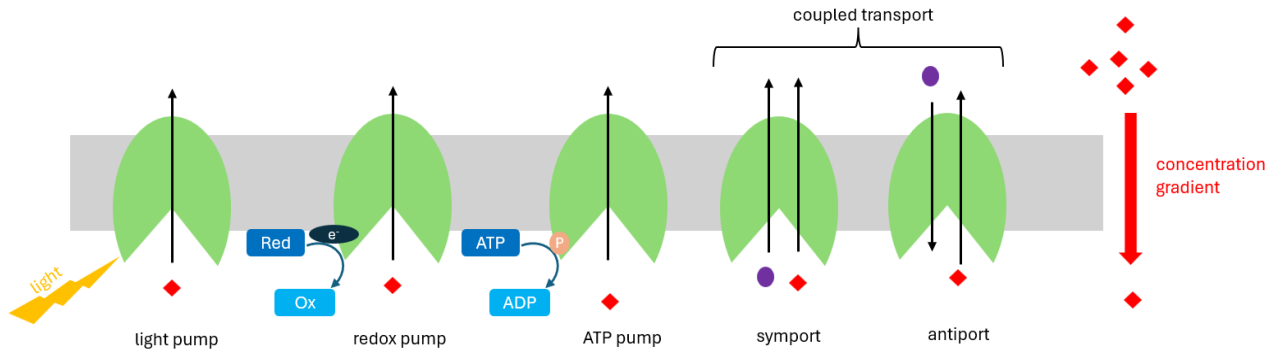

Figure 10 Types of active transporters and types of coupled transporters

While small molecules can be transported across the membrane via channels or transporters, larger molecules often rely on a cellular process called endocytosis (Figure 11). During this process, the substrate does not technically pass the membrane but is instead enclosed by the membrane and internalized within a vesicle, which happens via receptor mediation. Upon interaction, adaptor proteins are recruited, followed by the binding of a protein called clathrin, which starts to induce curvature in that part of the membrane. Dynamin assembles at the neck

of the forming bud, which, upon activation of the GTPase (guanosine triphosphatase) domain, starts cleaving off the vesicle. This is facilitated by bringing two non-cytosolic leaflets of the membrane in proximity. Adaptor proteins and clathrins dissociate from the newly formed vesicle. This vesicle can now transport the cargo to its intracellular destination. The receptors embedded in the vesicle membrane are either be recycled back into the cell membrane or degraded.[22]

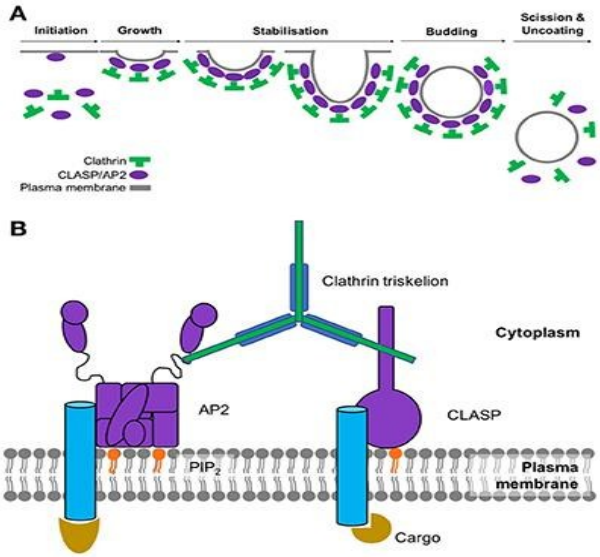

Figure 11 Schematic illustration of the process of endocytosis [22]

1.3.4. Uptake of peptides

As discussed in the previous chapter, there are several ways a molecule can enter a cell (Figure 12). The permeability of a given molecule can be quantified by determining its permeability coefficient (typically in cm/s), which describes the speed at which a molecule passes a membrane. This parameter is routinely assessed during the drug development process. For this, artificial lipid bilayers or cell monolayers from harvested from specific cell lines, which also allow transporter-mediated permeation, can be used as models. Peptides and proteins rarely pass through the membrane unaided, which poses challenges for medical applications and during the drug development process. Additionally, quantification of functional peptide or protein post-translocation through the membrane is particularly challenging. Hence, fluorescence-based methods or biological assays measuring the activity of the delivered peptide or protein are commonly used.[23]

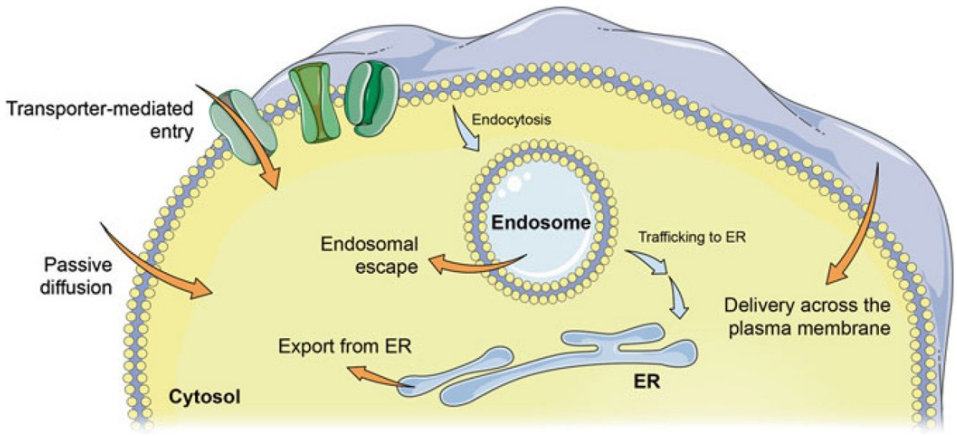

Figure 12 Schematic demonstration of entry ways for small molecules, peptides and proteins [23]

Cell-penetrating peptides, also known as peptide transduction domains, are a diverse class of peptides that can cross the cell membrane, the mechanism of which is still not fully understood. Representative members of this group are TAT (trans-activator of transcription) and penetratin, which have been found in naturally occurring proteins with proposed membrane permeability, such as homeoproteins.[24], [25] TAT is rich in arginine, whose guanidinium moieties allow delocalization of positive charge, which could lead to membrane permeability. However, permeability is still very low and typically very high concentrations (μM) of TAT are required for detectable translocation.[26], [27] Alteration of the physical properties of peptide cargos has been shown to increase permeability. Cyclic peptides as well as macrocyclic drugs are generally more polar than most small molecule drugs, and despite not complying with the rule of five (which is a guideline for small molecule drug design to enhance membrane permeability) [28], have been shown to be membrane-permeable if administrated orally, such as cyclosporin A.[29] Cyclisation and methylation of certain amides was proposed to improve membrane permeability for peptide drugs possibly by the formation of intramolecular hydrogen bonds in response to the low dielectric environment inside the membrane or by making the compounds more available for membrane transporters.[30], [31] The introduction of arginine residues with α-helices have also been proposed to improve permeability.[32] Although other membrane carrier systems, such as viruses, liposomes and other cell penetrating systems as mentioned above have been explored, [33], [34] the mechanism by which POMs facilitate membrane translocation is not yet confirmed to work by the same principle.

1.4. Targets and PET tracers of interest

1.4.1. CXCR4 and [^{68}Ga]Ga-Pentixafor

[^{68}Ga]Ga-Pentixafor is a CXCR4 (C-X-C chemokine receptor type 4) targeting PET (positron emission tomography) tracer, mainly used for the detection of myeloma and myeloproliferative neoplasms but also explored for the imaging of other pathologic processes.[35], [36] Its effectiveness in showing certain chronic infections and inflammatory conditions, such as

osteomyelitis and atherosclerosis, is also being explored.[37], [38] Pentixafor consists of a cyclic peptide structure and a DOTA (1,4,7,10-tetraazacyclododecane-1,4,7,10-tetraacetic acid) chelator to coordinate the gallium-68 radionuclide (Figure 13).

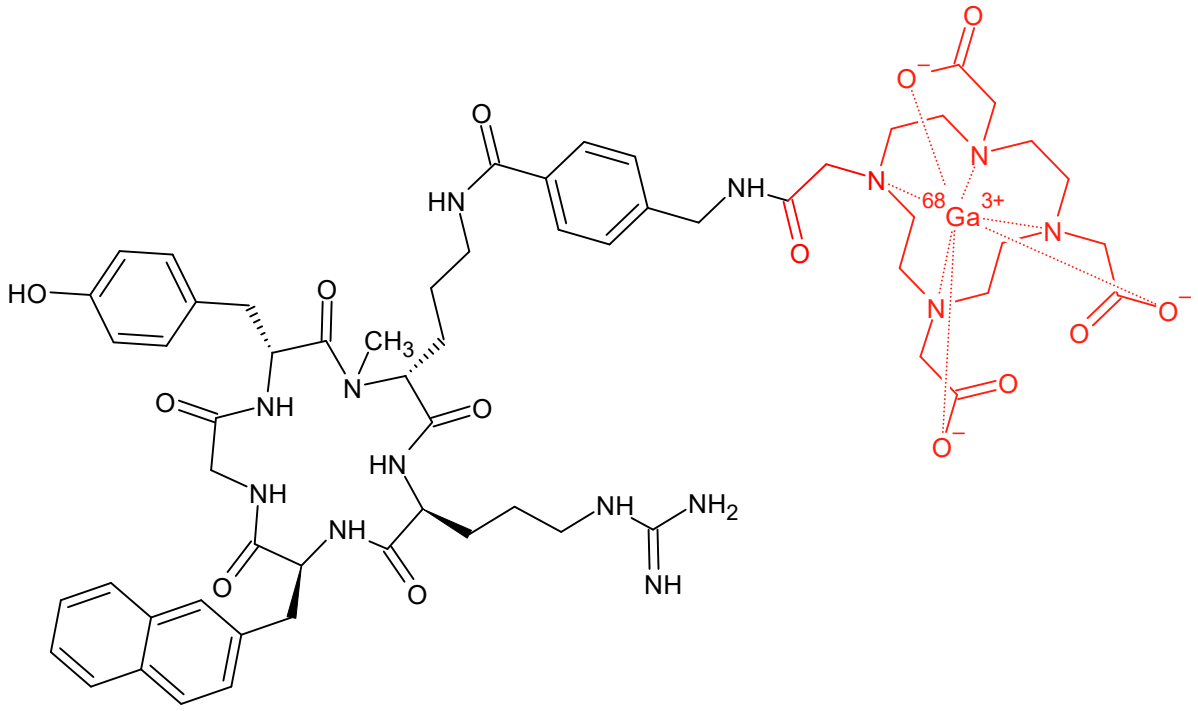

Figure 13 Structure of [^{68}Ga]Ga-Pentixafor

Consisting of a cyclic peptide structure (D-tyrosine, D-[N-methyl]-ornithine, D-arginine, naphthylalanine, glycine), a 4-AMBA (4-(aminomethyl)benzoic acid) linker and a DOTA (1,4,7,10-tetraazacyclododecane-1,4,7,10-tetraacetic acid) chelator coordinating gallium-68

Pentixafor binds to CXCR4 analogously to the endogenous ligand CXCL12 (C-X-C motif chemokine ligand 12), but does not activate the CXCL12-associated cascade, since the cyclic peptide moiety acts as an antagonist of CXCR4.[39] After internalization, the receptor is either recycled or degraded, whereas most of CXCR4 is degraded, hence most of the receptors that bound [^{68}Ga]Ga-Pentixafor tends to remain inside the cell.[40] Since Pentixafor is a charged, hydrophilic molecule, it cannot penetrate the cell without a membrane carrier or specific receptor interaction.[41]

CXCR4 is a chemokine receptor, which responds to a gradient of a directional chemokine called CXCL12. The CXCL12 axis influences intracellular calcium concentration, apoptosis inhibition, glucose metabolism and proliferation mechanisms and therefore plays a particular role in HIV (human immunodeficiency virus) infection and certain cancer types. CXCR4 is overexpressed in the kidney, lung, brain, prostate, breast, pancreas and ovarian cancer, as well as melanomas. It is an indicator of therapeutic resistance and is associated with poor prognosis.[41] In HIV infection, CXCR4 plays a role in CD4+ (cluster of differentiation 4 positive) T-cells as a co-receptor to the CD4 receptor and possibly facilitating viral fusion with

the target cell. Since the discovery of these connections, CXCR4 has been a target of interest for cancer imaging and treatment as well as for HIV treatment.[39]

CXCR4 is a G-protein-coupled receptor possessing seven transmembrane domains. Its endogenous ligand is the above-mentioned chemokine CXCL12 (also called SDF-1, stromal cell-derived factor 1α). Once CXCL12 binds to CXCR4, the G-protein dissociates and activates the following pathways (Figure 14).[41]

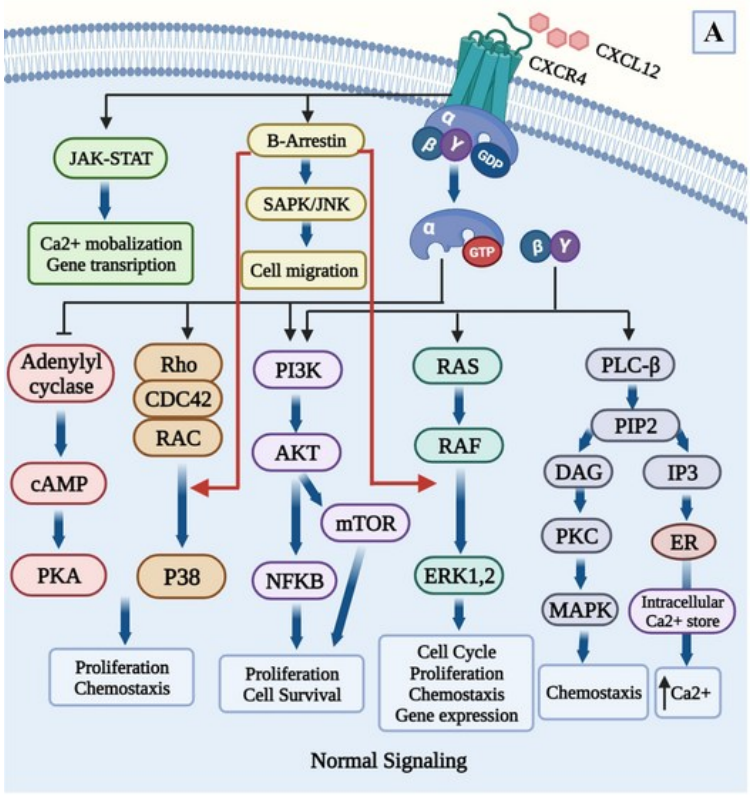

Figure 14 Overview of the signalling cascade initiated by CXCL12 binding to CXCR4 [41]

The G-protein dissociates into the βγ subunit, which activates the MAPK/ERK (mitogen-activated protein kinase/extracellular signal-regulated kinase) pathway. First, the GTPase Ras is activated, which functions as a molecular switch by exchanging GDP (guanosine diphosphate) for GTP (guanosine triphosphate), which in turn activates Raf. This then activates MEK1/2 (mitogen-activated protein kinase kinase) via phosphorylation. Since MEK1/2 is also a kinase, it in turn activates ERK1/2 (extracellular signal-regulated kinase) by phosphorylation. Activated/phosphorylated ERK1/2 translocates to the nucleus and activates transcription factors involved in cell proliferation and cell cycle progression.[42]

PI3K (phosphoinositide-3 kinase) is activated by both the α and βγ subunit. Since PI3K is a kinase, it phosphorylates PIP_2 (phosphatidylinositol-4,5-bisphosphate) to PIP_3 (phosphatidylinositol-3,4,5-triphosphate), which accumulates at the cell membrane. It activates PDK1 (PIP_3 dependent protein kinase 1) by binding to its PH (Pleckstrin homology) domain.

PIP_3 also recruits PKB (protein kinase B), to the cell membrane, where PIP_3 and PDK1 together activate PKB, which in turn activates proteins that inhibit apoptosis, stimulate cell growth and regulate glucose metabolism.[43]

PLC-β (phospholipase C-β) is activated by the βγ subunit of the G-protein. It hydrolyses PIP_2, which results in two messenger molecules namely DAG (diacylglycerol) and IP_3 (inositol-1,4,5-triphosphate). DAG further activates PKC (protein kinase C), which then activates MAPK. This then activates a series of kinases, as well as transcription factors as already outlined above.[44] IP_3 on the other hand interacts with receptors on the ER (endoplasmic reticulum) that cause an influx of Ca^{2+} into the cytoplasm, activating other kinase cascades that regulate gene expression, synaptic transmission, endocrine signaling, cell migration and cell division.[45]

Activated by the α subunit, RhoGEFs (guanine nucleotide exchange factors) activate Rho GTPases via the exchange of GDP for GTP, which in turn activate ROCK (Rho-associated kinases), that promote cell movement by activating proteins promoting actin-myosin contractility and stress fiber formation.[46]

The α subunit inhibits adenylyl cyclase, reducing the production of cAMP (cyclic adenosine monophosphate). Since cAMP is needed for the activation of PKA (protein kinase A) which inhibits actomyosin contractility, cell migration is promoted.[47]

Simultaneously, post G-protein dissociation, the receptor-substrate complex itself can also activate other pathways. It recruits the JAK (Janus kinase) 2 and 3, which activate STAT (signal transducer and activator of transcription) via phosphorylation. STAT dimerizes and translocates into the nucleus, where it binds to DNA and regulates genes involved in proliferation and inflammation.[48]

To desensitize the receptor, it is phosphorylated by GRKs (G-protein coupled receptor kinases) at the C-terminus, which are recruited post CXCR4 activation. This leads to the uncoupling of the G-proteins from the receptor and shut down CXCL12 induced signaling.[49] β-arrestin are recruited following desensitization. This association not only further desensitizes the receptor to new stimuli but also acts as an adaptor for clathrin-coated pits as well as AP-2 (adaptor protein 2), which aid endocytosis (Figure 15). β-arrestin also interferes with other already mentioned pathways, such as MAPK/ERK.[50]

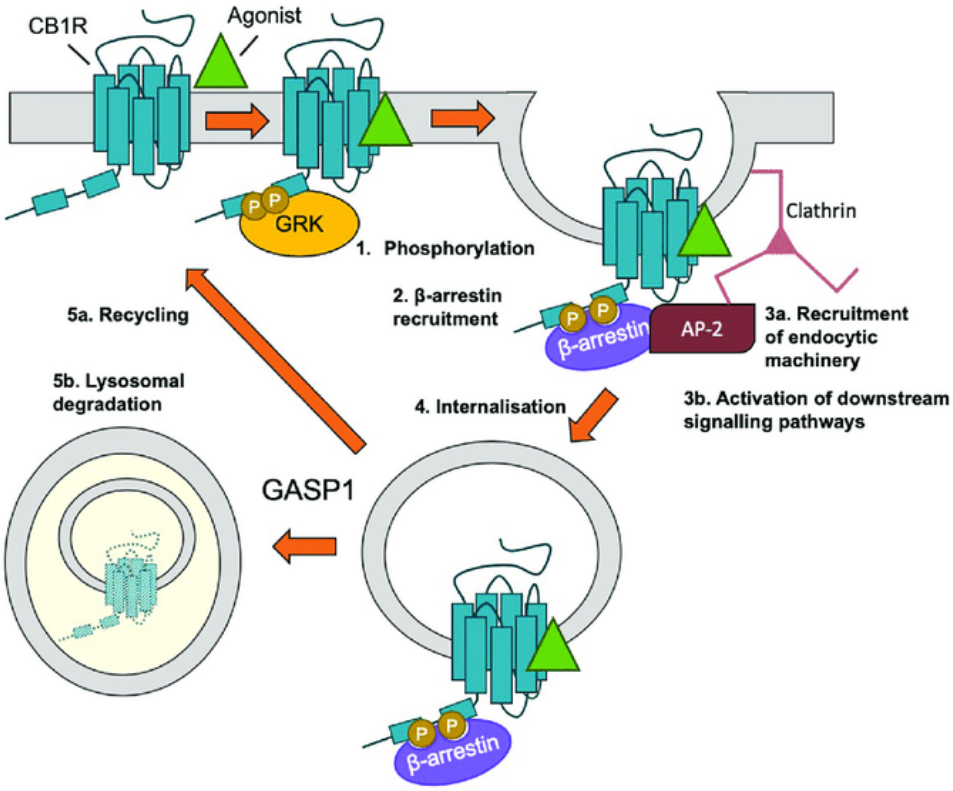

Figure 15 Endocytosis of agonist-bound GPCR via β-arrestin binding

After desensitization upon β-arrestin binding, β-arrestin also acts as an adaptor for the endocytic machinery, such as clathrin and AP-2. Post endocytosis, the receptor is either degraded or recycled [51]

1.4.2. PSMA and [^{68}Ga]Ga-PSMA-11

[^{68}Ga]Ga-PSMA-11, also known as gozetotide, is a PET radiotracer which consists of a chelator for gallium-68, a peptide moiety as well as an AHX (6-aminohexanoic acid) linker (Figure 16). Its purpose is to image PSMA (prostate-specific membrane antigen) overexpressing cells, most notably in prostate cancer.[52] However, PSMA is not only expressed in prostate cancer but also in other neoplasms such as renal cell carcinoma, glioblastoma, breast cancer, colorectal cancer, non-small cell lung cancer and pancreatic cancer. Importantly, PSMA has physiological expression also in specific healthy tissues such as the salivary glands, kidneys and small intestines.[53]

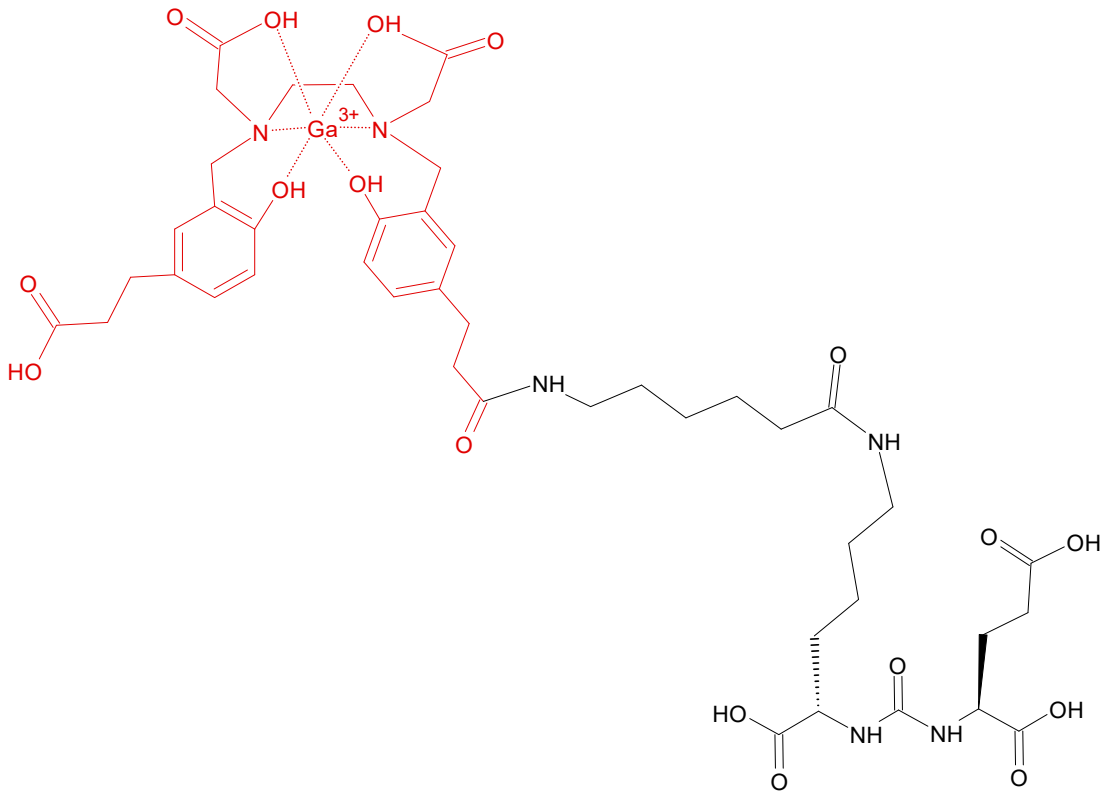

Figure 16 Structure of [^{68}Ga]Ga-PSMA-11

Consisting of a peptide structure (D-glutamine, urea, D-lysine), an AHX linker and a HBED-CC (N,N'-bis[2-hydroxy-5-(carboxyethyl)benzyl]ethylenediamine-N,N'-diacetic acid) chelator coordinating ^{68}Ga

PSMA acts as a transmembrane glycoprotein that cleaves glutamates from substrates. This free glutamate then activates glutamate receptors and serves as a metabolic substrate (Figure 17). It feeds into the TCA (tricarboxylic acid) cycle which results in energy production and activates mGluRs (metabotropic glutamate receptors), which in turn activate the PI3K pathway. As already mentioned, this pathway promotes cell growth and proliferation. Polyglutamated folates are transformed into their monoglutamated form via PSMA. This enhances folate uptake via transporters such as the RFC (reduced folate carrier), which in turn promotes proliferation, DNA synthesis and influences gene expression.[54]

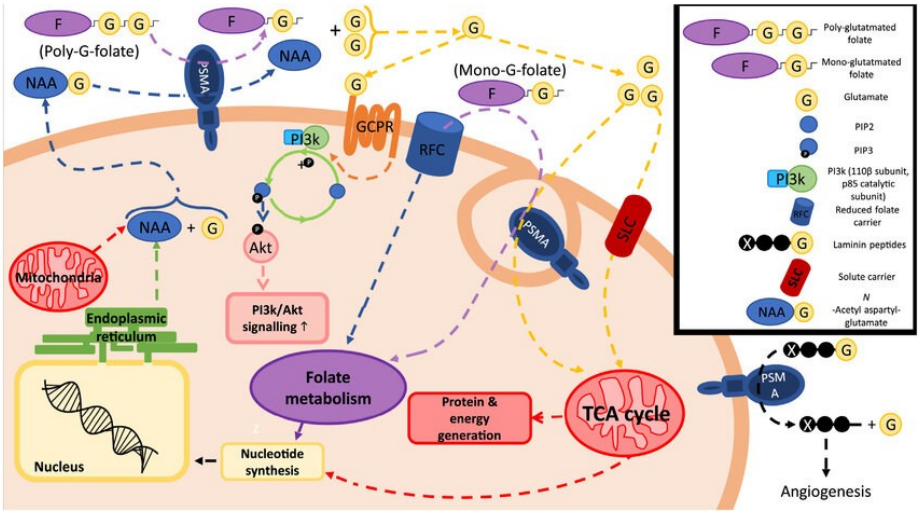

Figure 17 Illustration of the cellular function of PSMA [54]

PSMA also cleaves laminin-derived peptides into smaller fragments such as dipeptide LQ. These fragments activate endothelial cells to promote angiogenesis via integrin-mediated signal transduction, which promotes endothelial cell adhesion, migration and angiogenesis.[55], [56]

Binding PSMA targeting radiotracers accelerates the internalization process of this protein. Its main mode of action in cancer is associated with angiogenesis.[57], [58] PSMA is widely used as a target for prostate cancer diagnostics and therapy. Luthenium-177-labelled ligands have been shown to be effective in the treatment of castration-resistant prostate cancer.[59] Actinium-225-labelled ligands are considered as an additional treatment option in case of radiation resistance, since alpha emitting nuclides have a high linear energy transfer.[60] Additionally, PSMA inhibitors are being explored as therapeutic candidates.[61]

2. Experiments

2.1. Cell culture maintenance

2.1.1. Principle

Cell culture maintenance is one of the most important aspects when working with cells, as experimental outcomes are highly dependent on the vitality of the cells used. Different cell types often require specific conditions: some might need additives that others don't, some additives might even be mandatory for certain cell types, while detrimental to others. Certain cells need a surface to adhere to, which is provided by specifically treated plasticware such as flasks or dishes. During this master's thesis, only adherent cells were used.

Cell culture media usually contains a mixture of growth factors, hormones, proteins, trace elements, amino acids, vitamins and sugars, in addition to a buffering system, and often antibiotics. The buffering system, primarily CO_2 and bicarbonate, maintains the physiological pH (7.2-7.4 for mammalian cells) similarly to the mechanisms in eukaryotes. Therefore, a certain CO_2 content (between 5 and 10%) is maintained to ensure pH stability, in addition to 37°C temperature and a relative humidity of 90% to prevent medium evaporation.

To ensure nutrient availability and prevent the build-up of possibly toxic metabolites, the medium must be changed every 2-3 days. Cell cultures are grown in containers until they reach approximately 70% confluency. When this state is reached, cells are passaged, which means that they are detached from the surface using a trypsin or Accutase solution, which hydrolyses the peptide bonds in extracellular matrix proteins responsible for the adhesion of the cells to the surface. Cells are then resuspended in fresh medium and can either be seeded for experiments or further cultured. The fraction of the cell suspension needed to seed a new culture, the splitting factor, depends on the doubling time of the cell line, the surface area of the old and new culture vessels and when the culture should obtain confluency again. This fraction can be calculated using the following formula, where t is the time required to reach confluency, t_d is the doubling time, A_n/A_0 is the area of the new and old flask respectively and SF is the splitting factor.[62]

$$SF = \frac{1}{2^{t/t_d}} * \frac{A_n}{A_o}$$

To ensure that the cells remain healthy, work needs to be performed under sterile conditions. This is done by working in laminar flow hoods, where the air within is constantly drawn through specialized filters and redirected into the working space to purify the air. The air flow is unidirectional and laminar, which is either horizontal or vertical to the workbench. In vertical hoods, air is pushed out if the filter is above the working space, whereas in the horizontal model, the air flows from the back of the bench (Figure 18).[63]

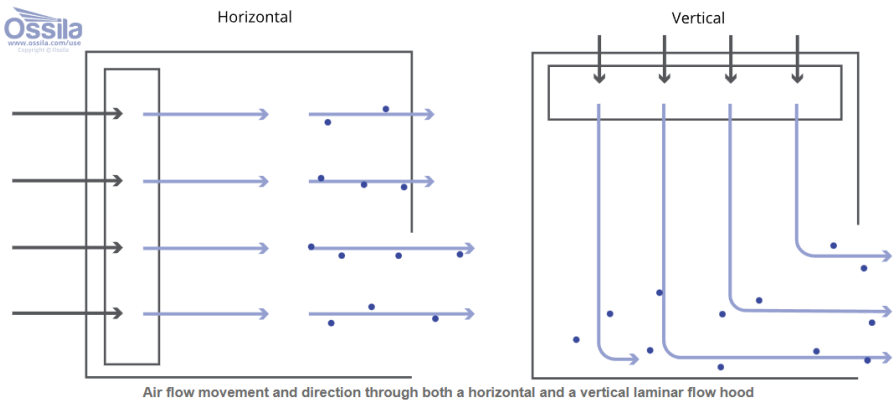

Figure 18 Air flow in horizontal (left) and vertical laminar flow hoods (right) [63]

A set of rules must be followed to ensure sterility in a laminar flow hood.

- Wearing gloves and sleeve protectors is mandatory
- The surface of anything that enters the laminar flow hood (including gloves and sleeve protectors) is disinfected with 70% ethanol prior to placing it into the hood
- Number of devices and materials in the hood should be as minimal as possible
- The workbench must be disinfected with ethanol before and after use and after spillage
- Packaged devices and materials are sterilized in the autoclave beforehand or are already bought sterilized
- Caps of bottles and flasks are put on the workbench facing upwards
- It is advised not to work with multiple cell lines in the hood at once to prevent cross contamination
- Working above the opening of containers should be avoided

Additionally, most cell cultures tolerate antibiotics in their media, such as penicillin and streptomycin, which provide additional protection against contamination. Though it is advised to use sparingly to reduce the risk of establishing resistances against antibiotics.[62] Some cell lines even show sensitivity towards antibiotics and do not grow with them present. It is also suspected that antibiotics modify the differentiation of cultured cells.[64]

In this master's thesis, the following mammalian cell lines were used:

- CHO-K1: A subclone of CHO (Chinese hamster ovary) cell line, which was obtained by a biopsy of an adult female Chinese hamster's ovary. These epithelial-like cells (Figure 19) can be used for recombinant protein production, in vitro cancer studies, toxicity screening and in drug discovery.[65], [66]

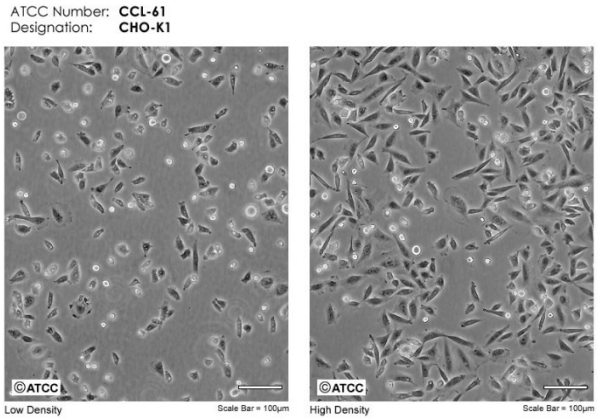

Figure 19 CHO-K1 cells at low (left) and high confluency (right) [66]

- HT29: An epithelial cell line that originated from a primary colorectal adenocarcinoma (Figure 20). The HT29 cells behave like mature intestinal cells, which makes them useful for gastrointestinal research. This cell line is used not only in cancer but also in drug and nutrition research.[67], [68]

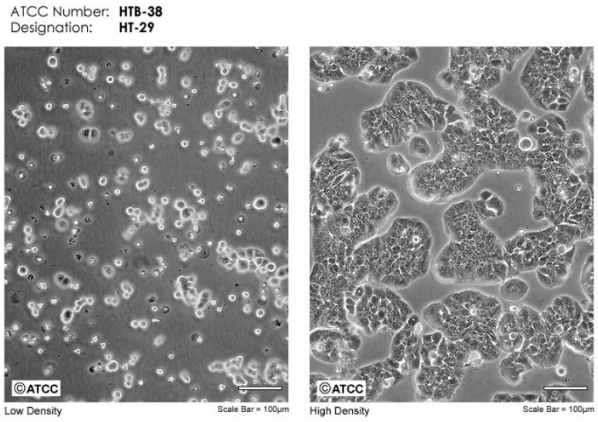

Figure 20 HT29 cells at low (left) and high confluency (right) [67]

- T47D: An estrogen receptor-positive epithelial cell line derived from an infiltrating ductal carcinoma in the breast (Figure 21). They are the mostly used in breast cancer research, but also to determine the effects of hormones or hormonally active substances on cells.[69], [70]

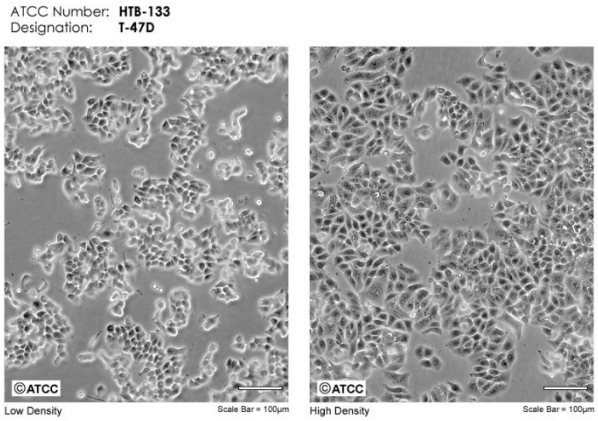

Figure 21 T47D cells at low (left) and high confluency (right) [69]

2.1.2. Chemicals, materials and devices

- Cell lines
    - CHO-K1 (ATCC - American Type Culture Collection)
    - CHO-K1 PSMA (CHO-K1 cell line transduced by Dr. Thomas Dilinger to express PSMA [71])
    - T47D (ATCC)
    - HT29 (ATCC)
- Reagent
    - Ham's F-12 Nutrient Mix (Gibco, Ref. 21765-029)
    - RPMI (Roswell Park Memorial Institute) 1640 medium (Gibco, Ref. 21875-034)
    - FBS (fetal bovine serum) (Gibco, Ref. A5256701)
    - Penicillin/Streptomycin (Gibco, Ref. 15140-122)
    - Puromycin (Gibco, Ref. A11138-03)
    - L-Glutamine (Sigma Aldrich, Cat. No. G7513)
    - DPBS (Dulbecco's phosphate-buffered saline) (Gibco, Ref. 14190-094)
    - Accutase® solution (Sigma Aldrich, Ref. 4400056840)
    - Trypan blue (Sigma Aldrich, Cat. No. T8154)
    - DMSO (dimethyl sulfoxide) (Thermo Scientific, Cat. No. 348441000)
    - Mycoplasma test reagents (MycoAlert® Mycoplasma Detection Kit, Lonza)
        - Positive control (Lonza, LT07-518)
        - Buffer (Lonza, LT27-220)
        - Reagent (Lonza, LT27-216)
        - Substrate (Lonza, LT27-224)
- Materials and devices
    - Cell culture flasks
        - 175 cm² (Thermo Fisher Scientific, Ref. 130191)
        - 75 cm² (Greiner Bio-One Cellstar®, Ref. 658 175)
        - 25 cm² (TPP, Ref. 90026)
    - Centrifuge tubes
        - 50 ml (Thermo Scientific, Ref. 339653)
        - 15 ml (Falcon, Ref. 352096)
    - White 96-well plates (Corning Costar ®, Ref. 3912)
    - Pipette boy (Integra pipetboy 2)
    - Sterile serological pipettes
        - 25 ml (Sarstedt, Ref. 86.1685.001)
        - 10 ml (Sarstedt, Ref. 86.1254.001)

        - 5 ml (Sarstedt, Ref. 86.1253.001)
    - Pipette tips (Eppendorf ep.T.I.P.S.®)
        - 1000 µL (Ref. 0030075250)
        - 200 µL (Ref. 0030075234)
        - 20 µL (Ref. 0030075226)
    - Plate reader (BioTek Synergy HTX multi-mode reader)
    - Cryogenic vials (Thermo Scientific, Ref. 5000-0020)
    - CoolCell® LX Cell Freezing Container (Corning)
    - Centrifuge (Hettich Rotanta 460 RC & Eppendorf 5424 R)
    - Microscope (Olympus CK2)
    - Cell counter (Luna™ Automated Cell Counter)
    - Incubator (Thermo Scientific Heracell 150i & Baker ReCO$_2$ver Plus)

2.1.3. Procedure

Four cell lines were used during this master's thesis: CHO-K1, CHO-K1 PSMA, HT29 and T47D. They were maintained at 37°C with 5% CO_2 and 90% RH (relative humidity) and in cell line-specific media mixtures (Table 1).

Table 1 Medium composition for each cell line

Cell line	Medium	Additives
CHO-K1	Nut Ham's 12	10% FBS 100 units/mL penicillin 100 µg/mL streptomycin
CHO-K1 PSMA	Nut Ham's 12	10% FBS 100 units/mL penicillin 100 µg/mL streptomycin 2.5 µL/mL puromycin
HT29	RPMI 1640	10% FBS 100 units/mL penicillin 100 µg/mL streptomycin
T47D	RPMI 1640	10% FBS 4 mM L-glutamine

The maintenance of the cells and the preparation for the experiments were performed in a laminar flow hood under sterile conditions. The medium was changed every 2-3 days. Cell cultures were maintained in flasks and were passaged upon reaching about 70% confluency.

To passage the cells, the medium was removed and the cells were washed using 5 mL DPBS, followed by the addition of 3.5 mL Accutase solution. The cells were incubated at 37°C, 5% CO_2 and 90% RH with the Accutase solution for 7 minutes, after which the reaction was stopped by the addition of 4.5 mL of medium. Any remaining attached cells were washed down by repeatedly pipetting the medium-Accutase mixture up and down. The resulting suspension was transferred to a Falcon tube and centrifuged at 482 RCF (relative centrifugal force) for 5 minutes at room temperature. The supernatant was removed and the cell pellet was resuspended in 1 mL cell line-specific medium. From this suspension, the culture was continued by using an appropriate fraction (Table 2) of the suspension to inoculate a new flask which will be confluent at a desired date, or - after determining the cell concentration - it was used to seed out for cell culture experiments.

Table 2 Splitting fractions

Days until confluency	Fraction of cell suspension taken (approximately 24 h doubling time, CHO-K1, CHO-K1 PSMA and HT29)	Fraction of cell suspension taken (approximately 48 h doubling time, T47D)
1	½	-
2	¼	½
3	1/8	-
4	1/16	¼
5	1/32	-
6	1/64	1/8

To determine the cell amount/concentration, 20 µL of the cell suspension was diluted 1:1 with trypan blue and counted in duplicate using the automated Luna cell counter after adjusting the contrast appropriately. If the cell count exceeded 1.5×10^7/mL, the suspension was further diluted. Cells were seeded out for experiments into the corresponding vessels to reach the desired cell amount after a specific time, based on the doubling time of the cell line and growth surface area of the vessel.

Low-passage cells were frozen in a freezing mixture of FBS and DMSO in a ratio of 9:1. The mixture was rapidly placed at -80°C in a Mr. Frosty freezing container, which allows controlled cooling at the rate of -1°C per minute.[72] After a few days, the vials were transferred to a liquid nitrogen tank at -190°C for long-term storage. Since cells can change with each passage, a new aliquot was thawed after reaching passage 40. Upon thawing, the cell suspension in the freezing medium was rapidly resuspended in fresh medium to minimize damage by DMSO.

To ensure that the cell cultures were not contaminated with mycoplasma, a mycoplasma test using a kit from Lonza [73] was performed every 4-6 weeks. For this, 1 mL of supernatant from the cell culture was collected. The supernatant was not taken directly after a medium change but was left on the cells for at least 24 h. The collected supernatant was centrifuged at 200 RCF for 5 min at room temperature to spin down any remaining cells. 50 µL of the centrifuged supernatant was transferred into a well of a white 96-well plate in duplicate, along with the positive control and the buffer as a negative control. 50 µL of reagent was added and after an incubation period of 5 min at room temperature, the luminescence was measured using a plate reader (reading A). Afterwards, 50 µL of substrate was added, followed by another incubation period of 10 min at room temperature. The luminescence was measured again (reading B). The ratio of reading A to reading B was used to estimate the possibility of mycoplasma contamination. Cultures with a value below 1.0 were considered negative.

2.2. Cytotoxicity experiments

The toxicity of the examined POMs was tested in the cell lines later used for other experiments, to ensure that the applied concentrations of POMs were not cytotoxic. Since some molybdenum-containing structures have previously demonstrated proliferative and estrogenic effects on the estrogen receptor-positive breast cancer cell line MCF-7 [2] the POMs of interest were additionally tested on the estrogen receptor-positive breast cancer cell line T47D.

2.2.1. Method

MTT (thiazolyl blue tetrazolium bromide) is taken up and enzymatically reduced in metabolically active cells to water-insoluble dark blue formazan crystals, which can be dissolved using DMSO, resulting in a purple solution (Figure 22). MTT can pass through the cellular and mitochondrial membrane presumably due to its lipophilicity and its positive charge. A reduction reaction in metabolically active cells leads to the formation of formazan, although the exact mechanism is not yet fully understood.[74]

Figure 22 Formazan structure (left) dissolved formazan crystals in DMSO (right)

Therefore, the intensity of the purple color after MTT treatment was used as a proxy for metabolic activity and was considered an indirect measure of cell viability in this master's thesis. In this assay, the viability of the cells was assessed after treatment with different POMs for 5 days. The resulting color intensity which reflects MTT reduction was plotted against the applied substance concentration, which typically results in an S-shaped curve. The inflexion point of this curve corresponds to the inhibitory concentration at which 50% of the cells exhibit diminished metabolic activity which often indicates cell death (IC_{50}). This information is important for planning further experiments to ensure that potential toxicity of POMs does not interfere with the experimental outcomes. However, this assay has several limitations, such as its low sensitivity, enzymatic degradation of MTT and potential MTT-induced cytotoxicity, which have been described to affect the reliability of the MTT assay. Also, it must be noted that the reduction of MTT to formazan represents the metabolic activity and does not necessarily correlate directly with cell viability.[74], [75] However, for the purposes of this master's thesis, the data obtained from the MTT assays were considered sufficient.

2.2.2. Chemicals, materials and devices

- Cell lines
  - CHO-K1 (ATCC)
  - T47D (ATCC)
  - HT29 (ATCC)
- Media as detailed in 2.1. Cell culture maintenance
- POMs
  - $GaMo_6$ (provided by Nadiia Gumerova, PhD.)
  - $GaMo_{12}$ (provided by Nadiia Gumerova, PhD.)
- Reagents
  - DPBS (Gibco, Ref. 14190-094)

- MTT (Sigma Aldrich, Ref. M5655)
- DMSO (Thermo Scientific, Cat. No. 348441000)

- Materials and devices
  - 96-well plate (Corning Costar®, Ref. 3598)
  - Plate reader (BioTek Synergy HTX multi-mode reader)
  - Incubator (Thermo Scientific Heracell 150i & Baker ReCO$_2$ver Plus)

2.2.3. Procedure

5000 cells per well were seeded in the central wells of a 96-well plate to reduce medium evaporation and allowed to adhere for 1 day. Subsequently, different POM concentrations - experimentally determined in prior screening experiments - were applied in triplicates (Figure 23). The cells were incubated with the POMs for 5 days at 37 °C, 5% CO_2 and 90% RH. On the final day, the medium was removed and replaced with 100 µL of MTT solution (5 mg/mL MTT stock in DPBS was diluted 1:7 in cell line-specific medium) per well. After a 4 h incubation at 37 °C, 5% CO_2 and 90% RH, the medium was carefully removed and replaced with 100 µL DMSO to dissolve the formazan crystals, resulting in a purple coloration. The absorbance of the resulting solution was determined by a plate reader at the wavelength of 550 nm, using 630 nm as a reference wavelength.

To calculate the IC_{50} values, the program GraphPrism was utilized, where the intensities were plotted against the logarithm of applied POM concentrations. The function dose-response (inhibition) was used either with the 3 parameter or 4 parameter model, whereas which one was chosen depended on the resulting R^2 as well as a subjective estimate which curve fits the values the best.

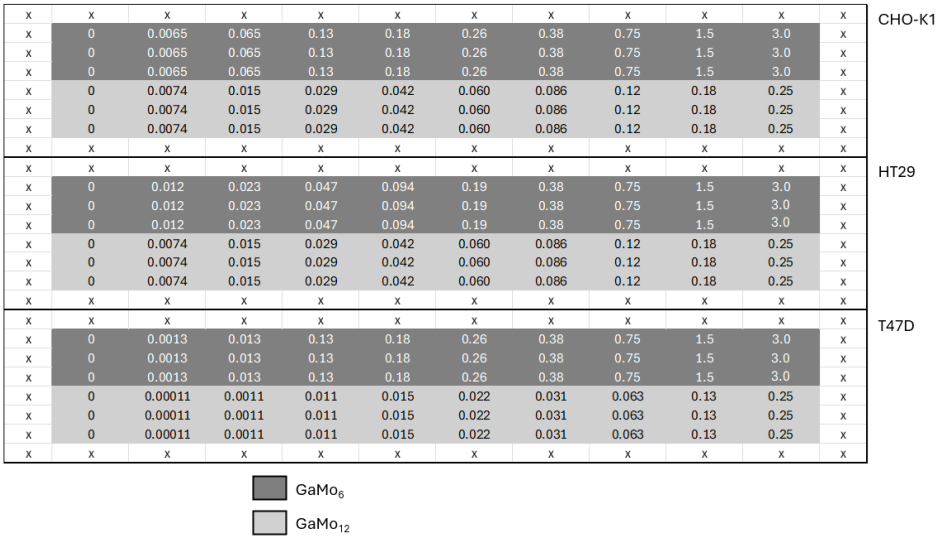

Figure 23 Applied concentrations of $GaMo_6$ and $GaMo_{12}$ to the cell lines CHO-K1, HT29 and T47D

2.2.4. Results

CHO-K1

The IC_{50} in CHO-K1 was determined to be 0.189 ± 0.037 mM (n = 9) for $GaMo_6$ and 0.131 ± 0.036 mM (n = 6) for $GaMo_{12}$. Both values were calculated using the four-parameter model for IC_{50} calculation in GraphPad Prism. While the inhibition curve for $GaMo_6$ reached a bottom plateau and formed a proper S-shaped curve, the curve for $GaMo_{12}$ did not (Figure 24).

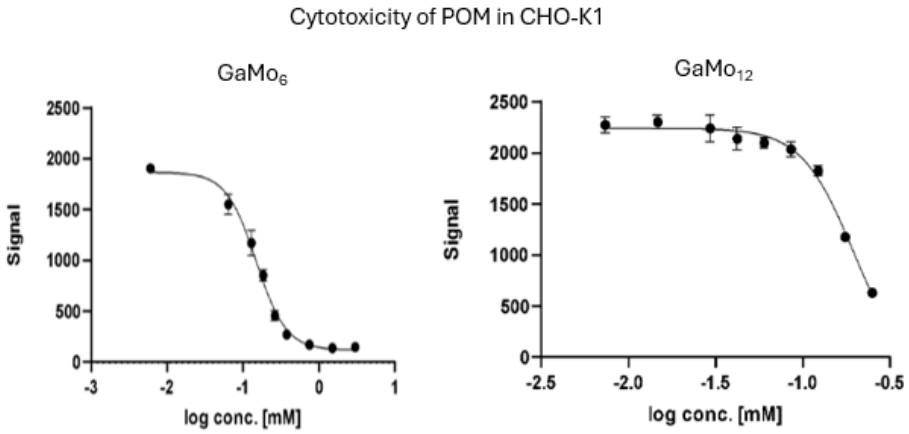

Figure 24 Representative inhibition curves of $GaMo_6$ and $GaMo_{12}$ in CHO-K1

HT29

The IC_{50} values in HT29 were 0.0618 ± 0.018 mM (n = 10) for $GaMo_6$ and 0.104 ± 0.021 mM (n = 5) for $GaMo_{12}$. Both were calculated using the 4-parameter method in GraphPad Prism. As with CHO-K1, $GaMo_{12}$ did not fully reach the bottom plateau, whereas the inhibition curve for $GaMo_6$ was properly S-shaped (Figure 25).

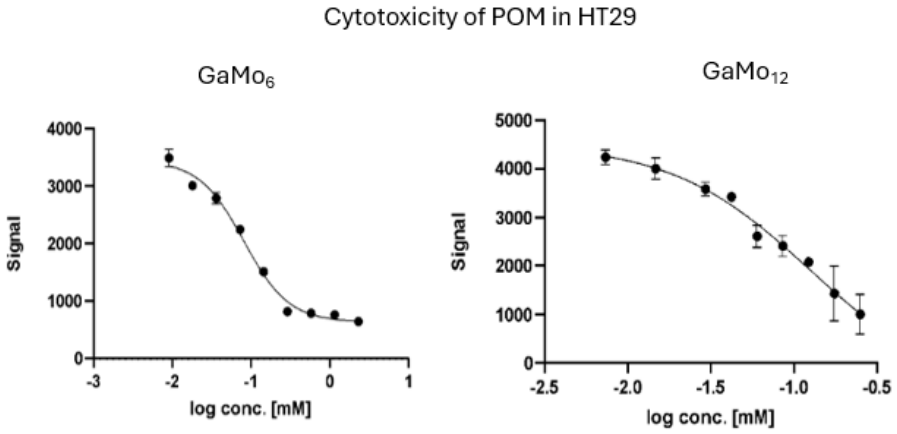

Figure 25 Representative inhibition curves of $GaMo_6$ and $GaMo_{12}$ in HT29

T47D

In T47D cells, the IC_{50} was 0.285 ± 0.079 mM (n = 4) for $GaMo_6$ and 0.0259 ± 0.0074 mM (n = 7) for $GaMo_{12}$. The IC_{50} for $GaMo_6$ was calculated using the four-parameter method, whereas the IC_{50} for $GaMo_{12}$ was obtained using the three-parameter method in GraphPad Prism. The curve for $GaMo_6$ is clearly S-shaped, while the curve for $GaMo_{12}$ is rather a prolonged S with a less steep slope, again not quite reaching the bottom plateau (Figure 26).

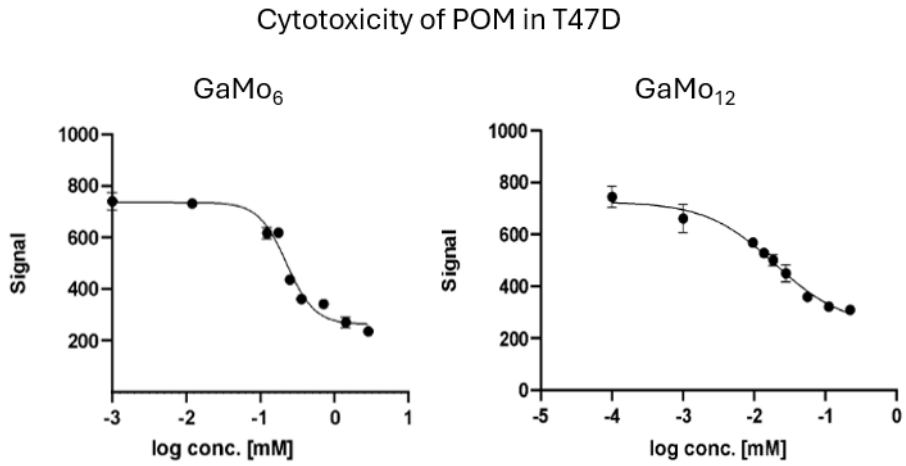

Figure 26 Representative inhibition curves of $GaMo_6$ and $GaMo_{12}$ in T47D

2.2.5. Discussion

The aim of these experiments was to ensure that the subsequent assays were conducted with POM concentrations below the IC_{50}. This was important to minimize interference from potential cytotoxic effects of the POMs. The following experiments using CHO-K1 and HT29 cells were therefore performed using a maximum concentration of 30 µM, which is bellow all determined IC_{50} values (Table 3) and ensures that adverse effects from the POMs of interest are not to be expected. For $GaMo_6$, T47D seems to be the least sensitive, followed by CHO-K1 and HT29, latter being the most sensitive. For $GaMo_{12}$, CHO-K1 is the least sensitive. T47D is the most sensitive to $GaMo_{12}$.

Table 3 IC50 results of POMs in the cell lines CHO-K1, HT29 and T47D

IC_{50} [mM]	CHO-K1	HT29	T47D
$GaMo_6$	189 ± 37.1	61.8 ± 17.7	285 ± 78.8
$GaMo_{12}$	131 ± 35.5	104 ± 21.1	25.9 ± 7.36

However, it should be noted that for $GaMo_{12}$ the bottom plateau of the IC_{50} curve was not reached due to solubility issues.

It has previously been shown that certain Mo-containing structures exhibit proliferative effects in some estrogen receptor-expressing cancer cell lines.[2] To assess potential effects, the cytotoxicity experiments were additionally conducted in T47D. However, no proliferative effects of $GaMo_6$ and $GaMo_{12}$ were detected in T47D. Although the published literature [2] observed these effects using an MTT assay as well, it should be noted that other assay types might be more suitable for the detection of proliferative effects in cells. Methods like flow cytometry, western blot or qPCR (qualitative polymerase chain reaction) could be considered for the analysis of proliferation-associated proteins to confirm the absence of proliferative effects. Since the cells were only treated with POM for 5 days, temporary or long-term effects might have been missed.

2.3. Synthesis of FITC-octaarginine

To bypass long delivery times of commercially available FITC-octaarginine, an in house-synthesis of this peptide was attempted.

2.3.1. Method

FITC-coupling

FITC is a commonly used fluorophore for peptide labelling. It absorbs light at 494 nm and emits fluorescence at 518 nm. When coupled to a peptide or a protein, the isothiocyanate group of FITC reacts with the N-terminal amine of the peptide (Figure 27).[76], [77]

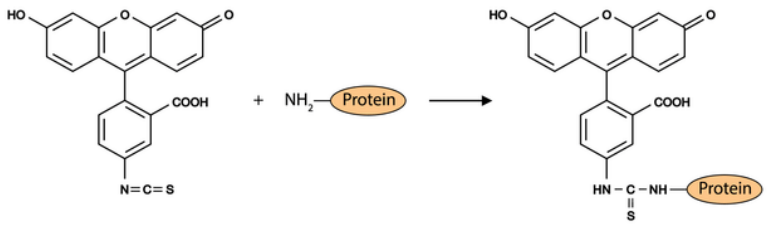

Figure 27 Reaction of FITC with a protein [77]

However, this reaction carries the risk of an unwanted cyclisation reaction between the thiourea group with the N-terminal amino acid, which leads to truncation of the peptide and the formation of a thiohydantoin (Figure 28). This is especially relevant for solid-phase peptide synthesis during the cleavage with TFA (trifluoroacetic acid). This can be prevented by the incorporation of a linker like AHX between the peptide and FITC.[78]

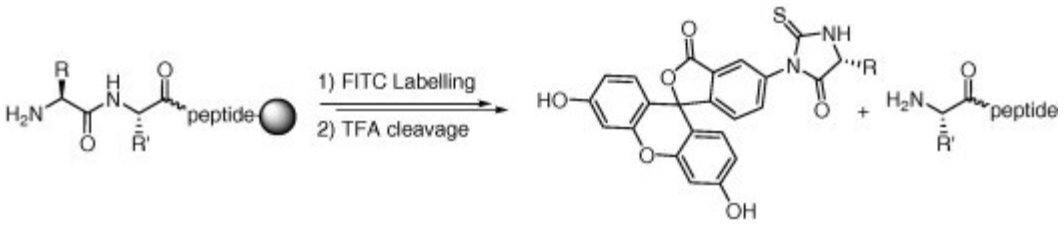

Figure 28 Unwanted cyclisation after FITC conjugation [76]

Chromatography

Chromatography is a chemical separation method which utilizes the different distribution coefficients of substances between a solid surface (stationary phase) and a solution (mobile phase). This distribution coefficient can depend on factors such as molecular size, affinity, charge or polarity. Chromatographic separation can be used either for analytical or preparative purposes. The separation process is typically visualized in a chromatogram, which shows a property (such as absorbance, conductivity or molar mass) of the eluent. When a substance is eluted from the column, it changes the measured property of the eluent and appears as a peak(Figure 29).[79]

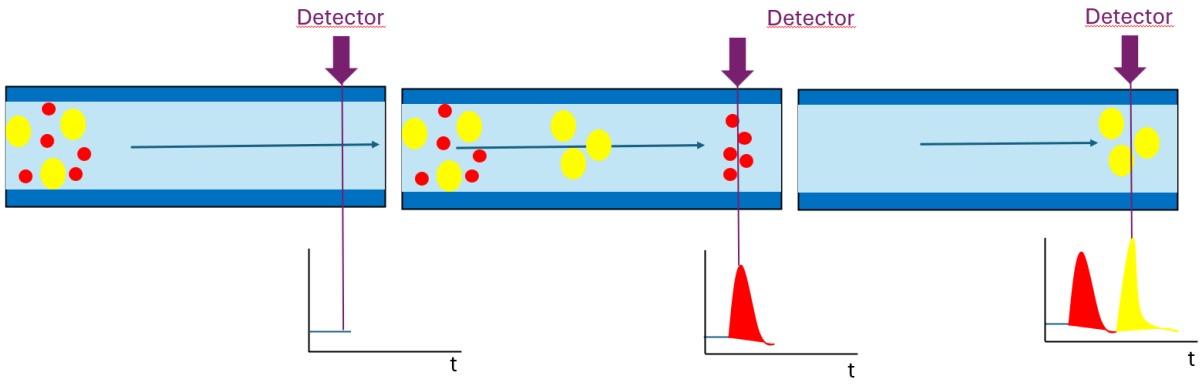

Figure 29 Schematic illustration of the principal behind chromatography

For quantification or proper purification, the peaks need to be sufficiently separated. The resolution of two peaks can be calculated using the formula below, where *t* is the retention time and *w* the peak width of analytes 1 and 2. A resolution greater than 1.5 is considered sufficient for separation.[80]

$$R = \frac{t_2 - t_1}{w_1 + w_2}$$

To ensure efficient separation of two or more components of a mixture, various parameters can be optimized. The mobile phase can either have a constant composition or can be applied as a gradient, where the composition changes over time. Additionally, a wide range of stationary phases is available, depending on the nature of the components to be

separated.[80] During these experiments, a LC-MS (liquid chromatography coupled with MS) was utilized.

Mass spectroscopy

In MS (mass spectroscopy), m/z (mass-to-charge ratios) of ions are detected, providing information about molecular weight and structure. For this, the sample is first ionized in a vacuum chamber to prevent collisions or interactions with air molecules. This results in charged fragments of the original molecule, which are then separated based on their mass-to-charge ratio. As ionized molecules travel through the apparatus, they are deflected by a magnetic field, which can be generated by a plethora of setups (Quadrupole, etc), which in turn act as a mass-to-charge filter. Ions that are either too light or too heavy are deflected too much or too little and collide with the apparatus wall, whereas ions with the selected correct m/z ratio will pass through until they reach the detector. By scanning through a wide range of magnetic field strengths, the corresponding m/z ratios and their signal intensities are recorded (Figure 30).[81]

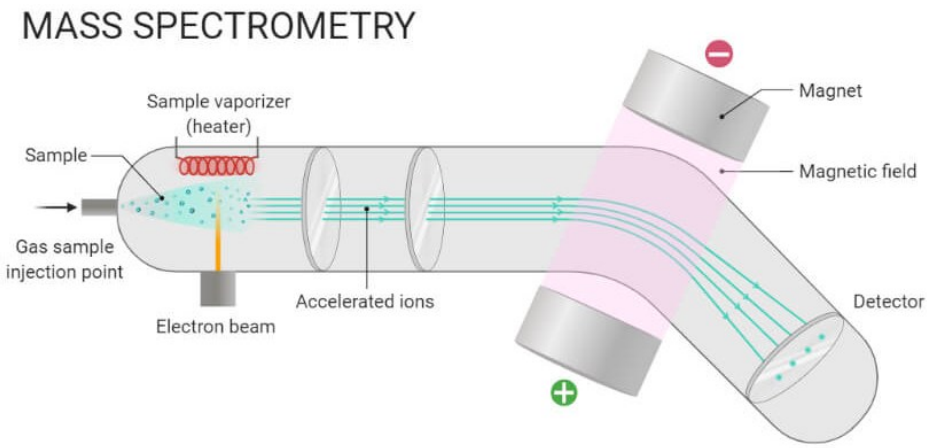

Figure 30 Basic principle of MS [82]

2.3.2. Devices and chemicals

- Reagents
  - Octaarginine (BaChem, Art. No. 4065816)
  - FITC (Merck, Ref. 46950)
  - DIPEA (*N,N*-diisopropylethylamin) (Sigma Aldrich, Ref. 496219)
- Shimadzu LCMS-2050
  - Column xBridge Shield RP18 2.5 µm 3.0 × 50 mm (Waters, SKU: 186006211)
  - Mobile phase
    - H_2O + 1% formic acid
    - ACN (acetonitril) + 1% formic acid

2.3.3. Procedure

Due to the high cost of FITC and octaarginine, the synthesis was attempted in a very small scale first. Stock solutions of FITC and octaarginine (each <1mg) were prepared in a mixture of 95% water and 5% ACN. A 1:1 mixture (v/v%) of the FITC and octaarginine stock solutions was prepared with a total volume of 1 mL and 2 µL of DIPEA was added. The reaction mixture was incubated at 4°C to inhibit possible reverse reactions. Reaction progress was monitored by LC-MS after 40, 90 and 150 minutes as well as on the next day. Another reaction was prepared from the same stock solutions and incubated overnight at room temperature. In another experimental approach approximately 1 mg octaarginine and 1 mg FITC were dissolved in 1 mL of 95% water and 5% ACN, treated with 2 µL DIPEA and kept at room temperature. The progress was assessed after 2 and 4 h using LC-MS. LC-MS analysis was performed using a concentration gradient of the mobile phase (Table 4), while the flow was kept consistent at 0.7 mL/min. Chromatograms were recorded for each of the starting materials as well as for the coupling reactions.

Table 4 Concentration gradient of mobile phase applied on the column

Time [min]	% H_2O (1% formic acid)	% ACN (1% formic acid)
0	95	5
2	95	5
13	10	90
16	10	90
18	95	5
19	95	5

The recorded chromatograms were filtered for m/z values of each starting material and the expected product, including ions of each (Table 5).

Table 5 Relevant m/z values for the starting materials and the desired product and their most probable multiply charged ions

Substance	M [g/mol]	Charge	Molecule	m/z
FITC	389	+1	$[M + H^+]^+$	390
		-1	$[M - H^+]^-$	388
Octaarginine	1267	+1	$[M + H^+]^+$	126
		+2	$[M + 2H^+]^{2+}$	635
		+3	$[M + 3H^+]^{3+}$	423
FITC-octaarginine	1656	+1	$[M + H^+]^+$	1657
		+2	$[M + 2H^+]^{2+}$	829
		+3	$[M + 3H^+]^{3+}$	553

2.3.4. Results

The chromatogram of the starting materials FITC (Figure 31 left) and octaarginine (Figure 31 right) showed an approximate retention time of 11.5 min for FITC and 0.75 min for octaarginine. FITC showed a more intense signal given the higher molecular concentration. The first reaction, using small amounts of each reactant under basic conditions and at 4 °C, was monitored after 40, 90, 150 minutes and overnight (Figure 32), however no product formed. Incubation overnight at 4 °C also did not lead to the formation of product, though it appears as if FITC was degraded. A reaction with the same concentrations kept at room temperature overnight (Figure 33) did only show a degradation of FITC and no product formation. A reaction with 1 mg of each reactant and were also incubated at room temperature for 4 hours (Figure 34), whereas a sample for mass spectroscopy was taken after 2 and after 4 hours. This setup also did not yield any detectable product.

FITC

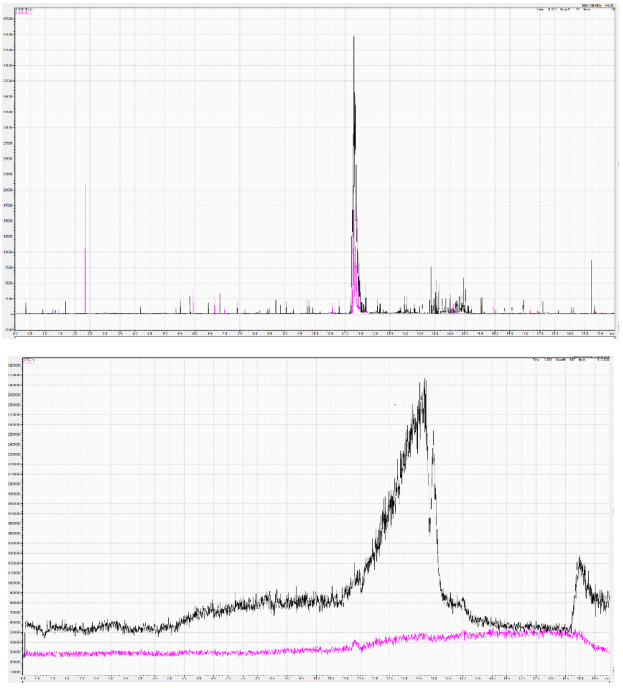

Legend: 390 (+) 388 (-)

Octaarginine

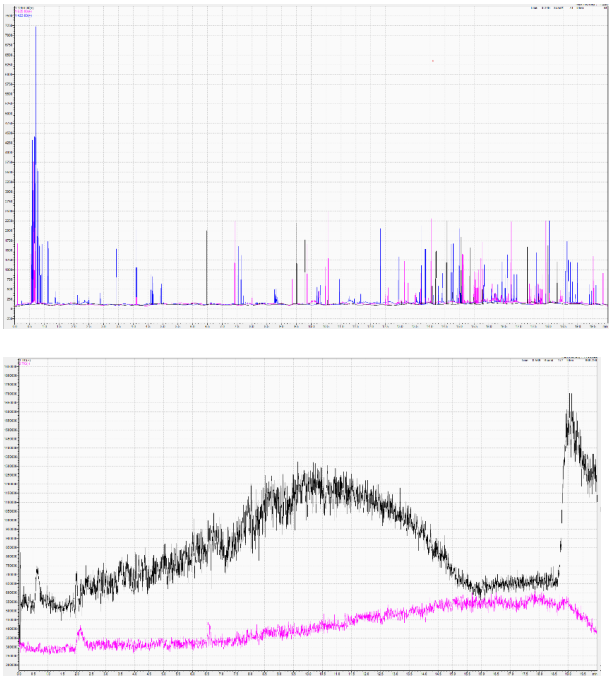

Legend: 1268 (+) 635 (+) 423 (+)

Figure 31 Chromatogram of octaarginine (right) and FITC (left), SIM (selected ion monitoring) plot (top) and TIC (total ion chromatogram) (bottom)

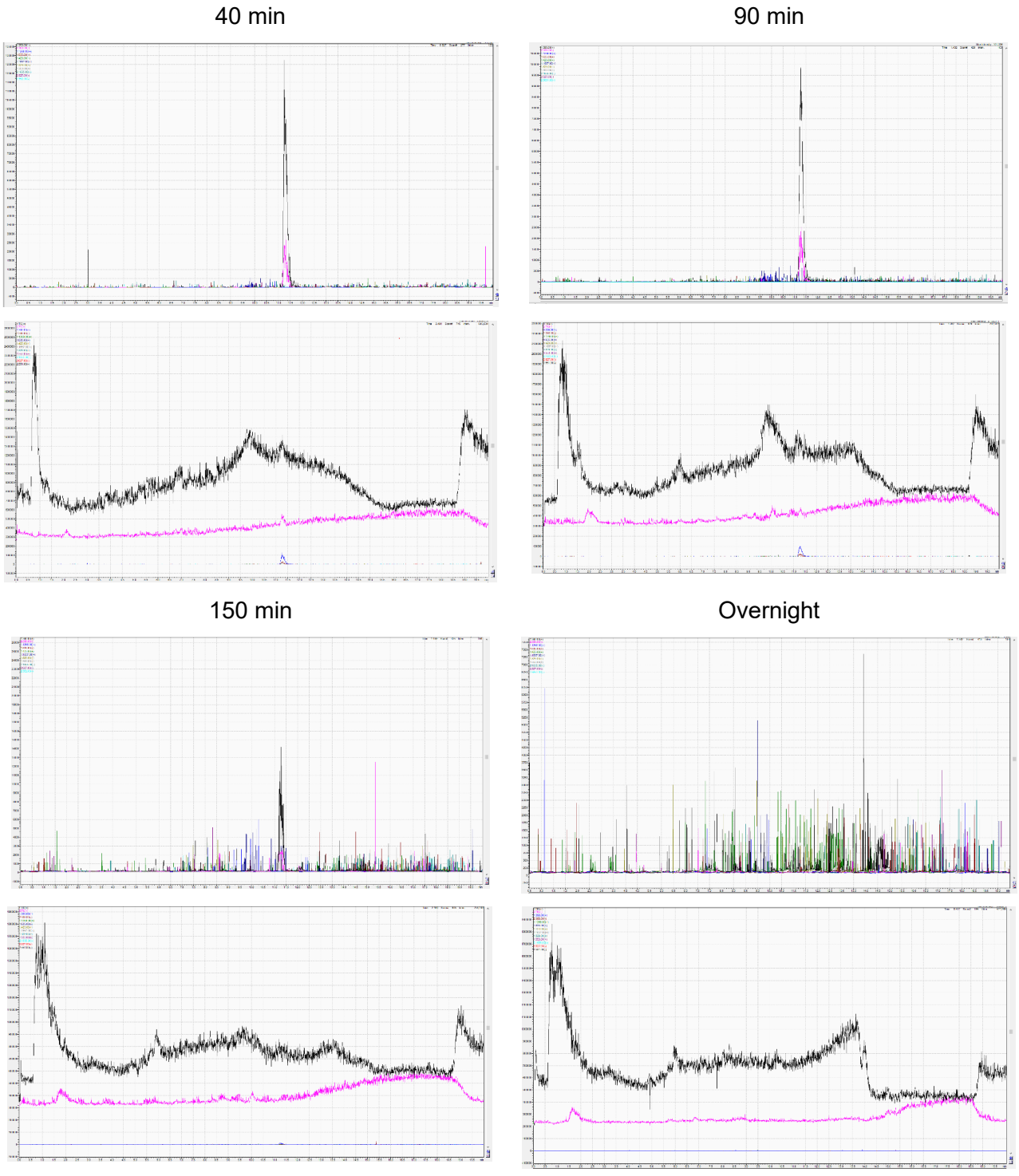

Figure 32 Chromatogram of FITC and octaargine in the presence of DIPEA after 40, 90, 130 minutes and overnight at 4 °C, SIM plot (top), TIC (bottom)

Overnight at room temperature

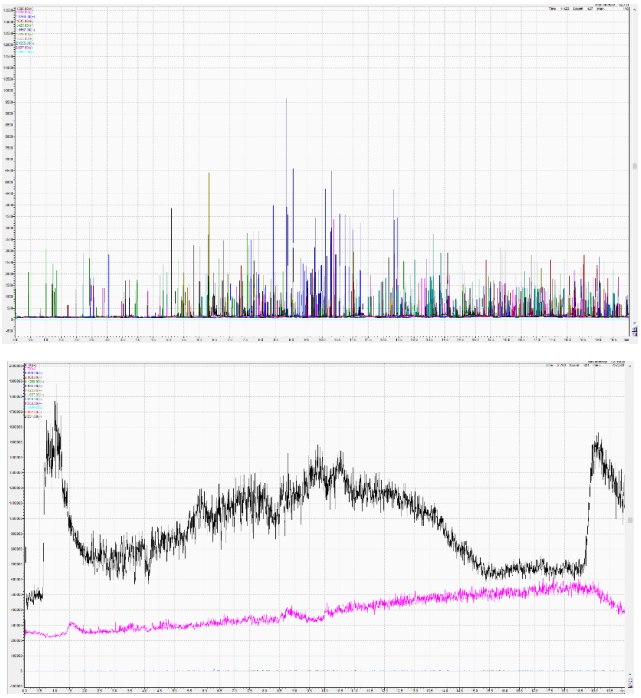

Legend: 390 (+) 388 (-) 1268 (+) 635 (+) 423 (+) 1657 (+) 829 (+) 553 (+)

Figure 33 Chromatogram of FITC and octaargine in the presence of DIPEA after overnight incubation at room temperature, SIM plot (top), TIC (bottom)

2 h room temperature

(higher concentration)

4 h room temperature

(higher concentration)

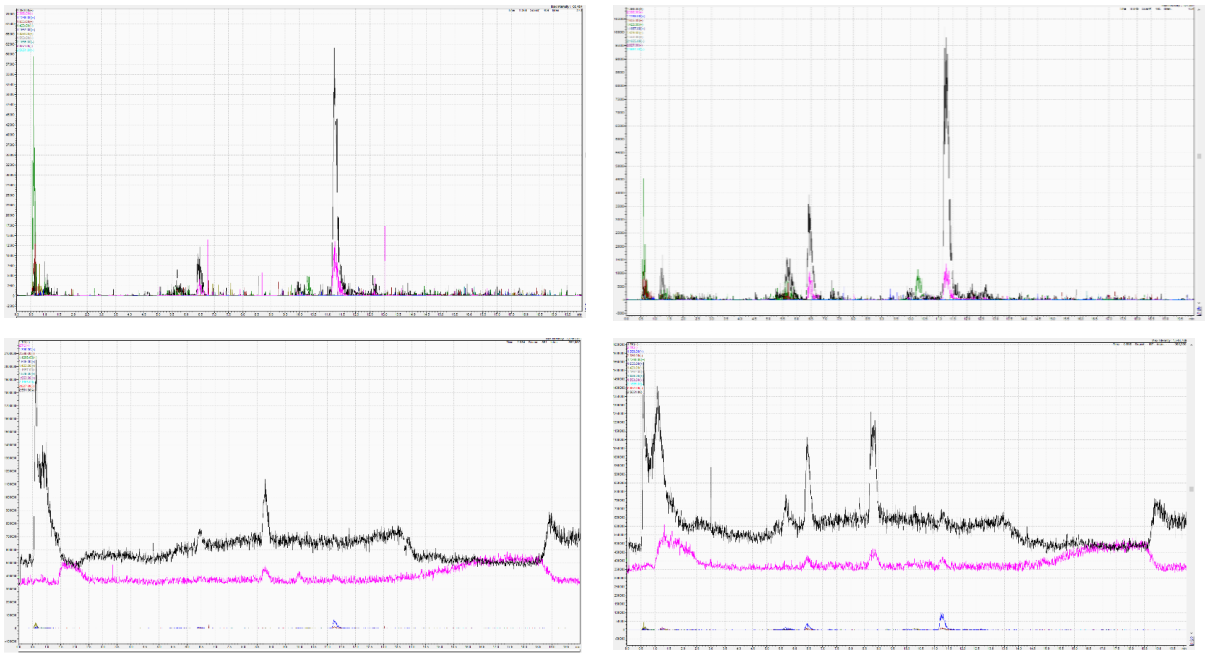

Legend: 390 (+) 388 (-) 1268 (+) 635 (+) 423 (+) 1657 (+) 829 (+) 553 (+)

Figure 34 Chromatogram of FITC and octaargine in the presence of DIPEA at higher concentrations incubated for 2 and 4 h at room temperature, SIM plot (top), TIC (bottom)

2.3.5. Discussion

The product was not isolated under the specified conditions. Neither the small scale nor the upscaled reaction setup led to improvement. The following optimizations could be attempted to perform this synthesis successfully.

- Increasing base concentration or switching to a different octaarginine salt, since a TFA salt was used it can be assumed that the amount of DIPEA used was not sufficient to create a basic enough environment for the reaction to occur
- Substituting DIPEA with other bases or using buffers instead [83]
- Altered temperatures and different solvents to improve reaction kinetics and solubility
- Adapting stochiometric ratios to prevent side reactions or incomplete labeling
- Desalting the peptide to remove possible interfering ions such as TFA (trifluoroacetic acid) [84]
- Using an AHX-linker to reduce steric hindrance

As it was not the focus of this thesis as well as due to time constraints, the in-house synthesis of FITC-octaarginine was not pursued any further.

2.4. Fluorescence experiments

To determine the membrane carrier properties of POMs, cells were incubated with FITC-labelled protamine and octaarginine together with the POMs, followed by fluorescence microscopy to determine the uptake and peptide localization under POM utilization.

2.4.1. Method

Fluorescence is a phenomenon whereby a substance emits light of a longer wavelength than the one used for its excitation. This is due to the loss of energy through molecular vibration as the molecule returns to its ground state post-excitation (Figure 35). This phenomenon is exploited in microscopy, where fluorescently labelled proteins in cells can be visualized by excitation using light with a wavelength suitable for the fluorophore.

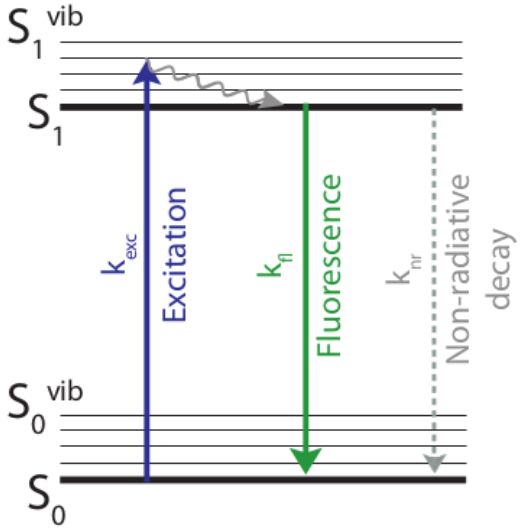

Figure 35 Schematic illustration of fluorescence [85]

A fluorescence microscope (Figure 36 left) consists of a light source, an excitation and emission filter, a dichroic mirror, an objective and an ocular. The excitation filter ensures that the specimen is illuminated only with light at the wavelength suitable for the used fluorophore. The dichroic mirror reflects the light from the source toward the specimen while allowing emitted light to pass through to the ocular as it has different reflective and transmissive properties at different wavelengths.[20] This technique has been further refined to enable sectional view of one layer within cell or tissue samples using confocal microscopy (Figure 36 right). In this method, the excitation light is only focused onto a single focal plane within the specimen. The resulting emitted light is then again focused to pass through a pinhole positioned in front of the detector. Out-of-focus light is hereby largely excluded from detection, which reduces the background signal and increases spatial resolution (Figure 37).[86]

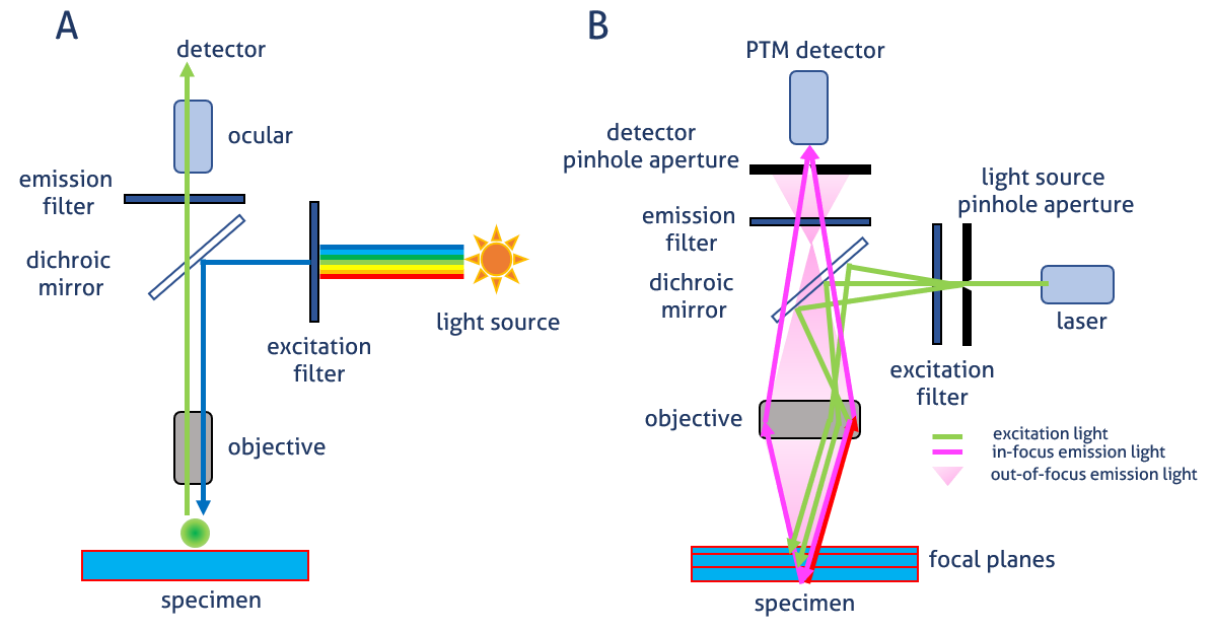

Figure 36 Schematic illustration and comparison between widefield (A) and confocal microscopy (B) [87]

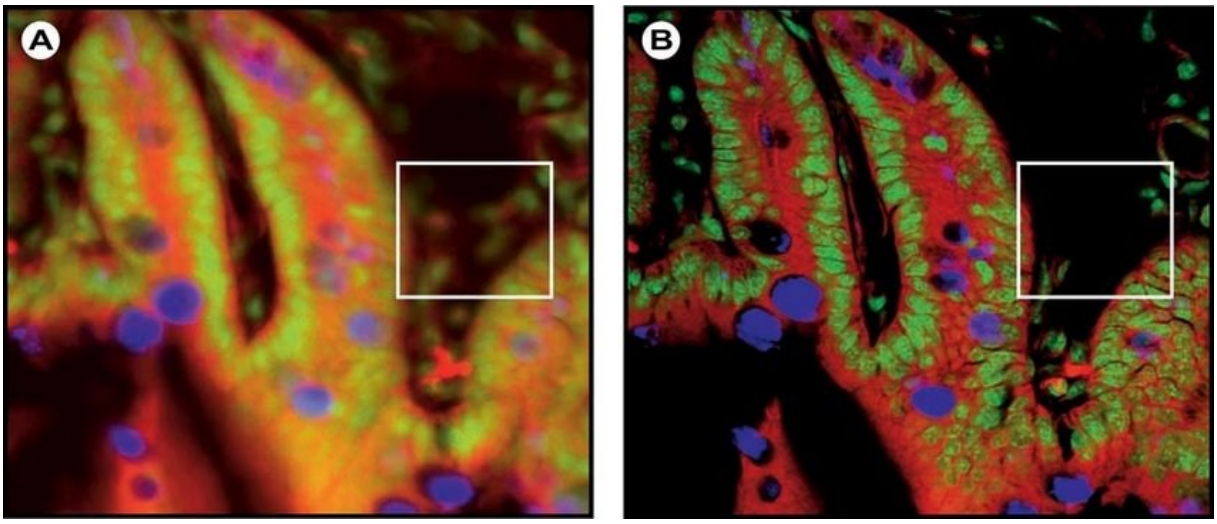

Figure 37 Images of triple-labelled cell aggregate obtained using widefield (A) and confocal (B) fluorescent microscopy [88]

Typical fluorescent probes include DAPI (4',6-diamidino-2-phenylindol), FITC, GFP (green fluorescent protein) and many others, each with characteristic excitation and emission wavelengths allowing for simultaneous labelling of multiple targets within one experiment. There are different approaches to label a target protein with a fluorescent probe. It is possible to genetically modify cells to express the protein of interest together with e.g. GFP, although the addition of GFP may potentially impair the function of that protein. Another approach uses specific antibodies, either directly fluorescently labelled or indirectly using a primary and secondary antibody, where the secondary antibody is coupled to a fluorophore and binds primary antibody, which has bound to the target first. If the target is expressed intracellularly, additional permeabilization of the cell is necessary to allow antibodies to enter. Fluorescence

microscopy can also be used to determine the uptake and intracellular localization of proteins, peptides or other molecules,[89] which was also the main application of fluorescence microscopy in this master's thesis. For this, two fluorescently labelled peptides were applied to cells (with and without the membrane carriers present) under different conditions to see if the peptides penetrate the cell and if so, where they accumulate.

2.4.2. Chemicals, materials and devices

- Cell line
  - CHO-K1 cells (ATCC)
- POMs
  - $GaMo_6$ (provided by Nadiia Gumerova, PhD.)
  - $GaMo_{12}$ (provided by Nadiia Gumerova, PhD.)
  - $SiMoW_{11}$ (provided by Nadiia Gumerova, PhD.)
- FITC-labelled peptides
  - FITC-protamine (KamulinBiotechCo. Ltd, Cat No.# R-R-0265)
  - FITC-octaarginine (Biomatik, Ref. SP240838 188557)
- Solutions
  - Nut-Ham's F-12 nutrient mix (Gibco, Ref. 21765-029)
  - HBSS (Hank's balanced salt solution) (Gibco, Ref. 14175-095)
  - Heparin 1000 IU/mL (Gilvasan, Ref. 3909981)
  - Paraformaldehyde 4% solution
  - PBS (phosphate-buffered saline) (Morphisto, Ref. 11237.00500, 1:10)
  - DAPI (Sigma Aldrich, Ref. M6900), 2µg/ml in PBS
  - DPBS (Gibco, Ref. 14190-094)
  - Fluoromount-G (Invitrogen/Thermo Fisher, Ref. 00-4958-02)
  - Triton X-100 (Sigma Aldrich, Ref. 282103)
- Materials and devices
  - 4-chamber slides (Lab-Tek® II, Ref. 154526)
  - Digital orbital shaker (Heathrow Scientific)
  - Fluorescence microscope (Olympus BX53)

2.4.3. Procedure

The following protocol, based on the work of Barba-Bon *et al.*, [1] was performed to determine the uptake behavior of two FITC-labelled peptides, octaarginine and protamine, in the presence of three POMs. $SiMoW_{11}$ already demonstrated membrane carrier properties [1] and was used as a positive control, whereas the carrier properties of $GaMo_6$ and $GaMo_{12}$ were evaluated.

A 4-chamber slide was seeded with approximately 5,000 CHO-K1 cells per chamber and grown under standard growth conditions for this cell line, as described in “cell culture maintenance”. After an incubation time of 48 h, which yields 20,000 cells per chamber, the experiment was initiated. The medium was exchanged for Ham’s F-12 nutrient mix medium without additives. POM solutions with the concentration of 125 µM in water were freshly prepared for each experiment to ensure that POM did not degrade. The FITC-protamine and -octaarginine solution of 400 µM in water was also prepared freshly for each experiment. The exact molar concentration of FITC-protamine was calculated since the manufacturers did not specify this parameter. 40 µL of either a POM solution or water was added to each chamber, followed by shaking at 100 rpm for 5 min at room temperature. Afterwards, 5 µL of the respective FITC-labelled peptide (protamine or octaarginine) was added to each chamber, followed by 5-minute shaking step at 100 rpm at room temperature. The cells were incubated at 37 °C, 5% CO_2 and 90% RH for 1 h. After incubation, the medium was removed and cells were washed twice with 0.5 mL HBSS containing 100 µg/mL heparin and two times with 0.5 mL PBS. Afterwards, the cells were fixated with 0.5 mL 4% paraformaldehyde solution at 4 °C for 20 minutes, followed by two PBS washes (0.5 mL). Cell nuclei were stained using 0.5 mL of a 2 µg/mL DAPI solution for 10 min at room temperature followed by two final PBS washes. After the walls of the chamber slides were removed, one drop of mounting solution Fluoromount-G was added. The entire slide was covered with a coverslip while taking care to avoid generation or entrapment of air bubbles between the slide and the cover slip. The mounting solution was left to dry overnight. After drying, imaging was performed using a fluorescence microscope (Olympus BX53). For the imaging of the nuclei staining, the DAPI filter was used; for imaging of the FITC-labelled peptides a filter for FITC was used. To perform imaging of the FITC-peptides, different settings for exposure time and ISO were necessary as outlined in the “Results” section. For DAPI imaging, an exposure time of 100 ms and ISO 100 were consistently used.

Since the uptake was difficult to detect, several adaptations were made to the protocol described above. Initially, FITC-protamine was used for protocol optimization and troubleshooting:

- Variation of FITC-labelled peptide concentration
  Final FITC-protamine concentrations of 4 µM, 8 µM, 32 µM, 60 µM, 200 µM and 400 µM were tested. For FITC-octaarginine, only 4 and 8 µM were examined due to the limited amount of FITC-octaarginine available.
- Variation of incubation time and temperature
  For both labelled peptides, the incubation times of 1 h and 2 h at 37°C, 5% CO_2 and 90% RH, as well as overnight incubation at 4 °C under atmospheric conditions, were tested.

- Modified heparin amount

  FITC-protamine uptake was examined after washing with HBSS either without heparin or with 1000 µg/mL heparin, which corresponds to ten times increase as compared to the original protocol.
- Incubation in DPBS instead of medium

  To assess the influence of the phenol red in the medium, cells were incubated in DPBS for 1 h at 37 °C, 5% CO_2 and 90% RH with a final concentration of 10 µM POM and 200 µM FITC-protamine.
- Pre-incubation of POM and peptide mixture

  To ensure proper interaction between POM and FITC-protamine, 0.5 ml of additive-free medium was mixed with FITC-protamine and POM at final concentrations of 200 µM and 10 µM, respectively. After mixing for 5 minutes, the solution was added to the cells.
- Permeabilization using Triton X-100

  Since none of the previous adaptations yielded higher signals, a permeabilization of the cells prior to incubation with POM and FITC-protamine was performed. Cells were treated with a 0.2% Triton X-100 in PBS for 10 minutes at room temperature prior to incubation with FITC-protamine and POM at final concentrations of 200 µM and 10 µM, respectively.

2.4.4. Results

FITC-Protamine

During the initial experiments for the assessment of the carrier properties of $SiMoW_{11}$, $GaMo_6$ and $GaMo_{12}$ for FITC-protamine, only weak uptake of the peptide was observed, both in the presence (Figure 38B-D) and absence (Figure 38A) of a membrane carrier (POM). A strong background signal, which could not be eliminated, posed further difficulties for assessment of uptake as well as for the comparison between the experiments. For the imaging of FITC-protamine, exposure time of 5 s and an ISO 1600 were necessary. As described in the “Procedure” section, further modifications were made to the protocol to optimize imaging. As $SiMoW_{11}$ was already established to act as a membrane carrier,[1] these optimizations were carried out using this silicium-containing POM as a positive control.

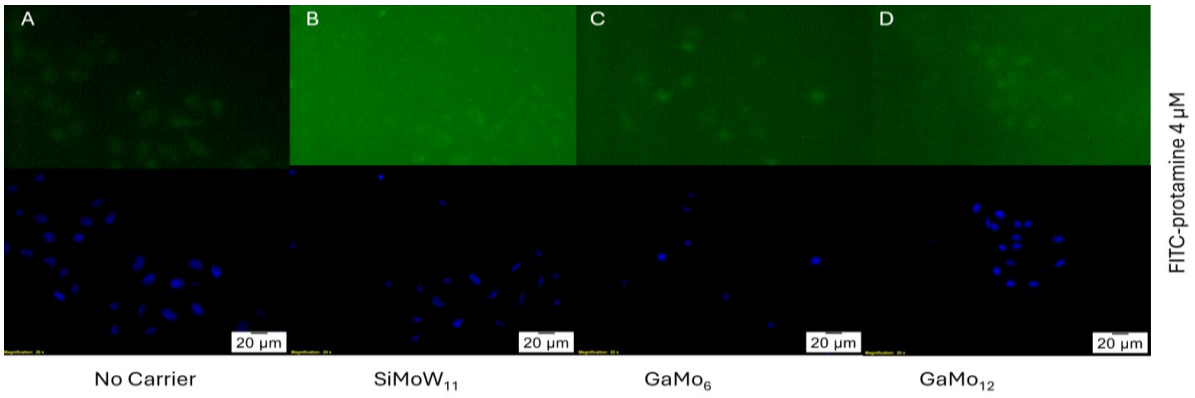

Figure 38 Uptake of FITC-protamine in the presence of different POMs

Uptake of FITC-protamine at 4 µM in the presence of 10 µM $SiMoW_{11}$ (B), $GaMo_6$ (C) and $GaMo_{12}$ (D) and in the absence of POMs (A). The cells were incubated for 1 h at 37°C, 5% CO_2 and 90% RH. FITC-protamine was imaged with an exposure time of 5 s and ISO1600, whereas DAPI was imaged at 100 ms and ISO 100. Magnification: 200-fold.

Uptake of FITC-protamine at varying concentrations and extended incubation time was compared between cells incubated with $SiMoW_{11}$ (Figure 39) and without membrane carrier (Figure 40). In these experiments, a strong background signal was observed again. Since it was not possible to perform background correction, an objective comparison between the two conditions (with and without) was difficult. The required exposure time remained particularly high at 3.5 s, prompting further experiments with increased FITC-protamine concentrations.

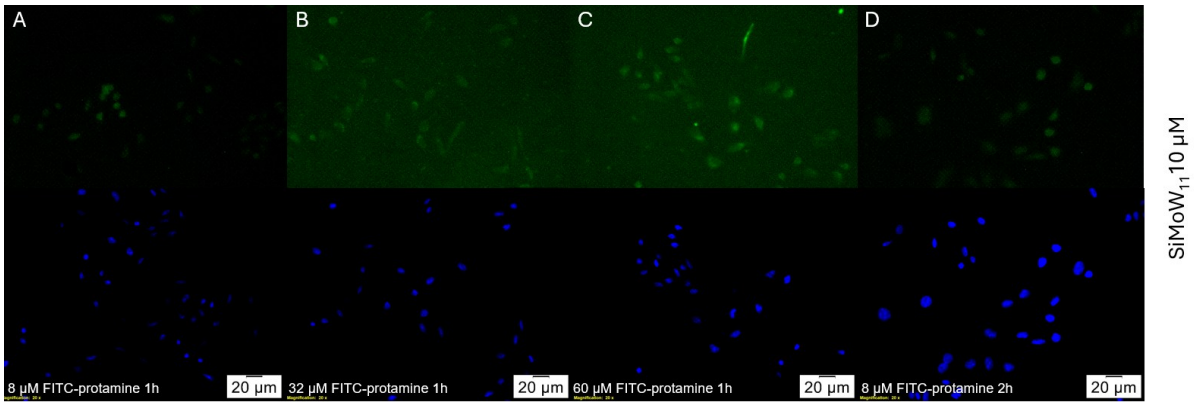

Figure 39 Uptake of FITC-protamine at different concentrations in the presence of 10 µM $SiMoW_{11}$

Uptake of FITC-protamine at 8 (A), 32 (B),60 µM (C) final concentration after 1 h incubation at 37 °C, 5% CO_2 and 90% RH and uptake of 8 µM FITC-protamine for 2 h under the same conditions (D), in the presence of 10 µM $SiMoW_{11}$. FITC-protamine was imaged with an exposure time of 3.5 s and ISO 1600, whereas DAPI was imaged at 100 ms and ISO 100. Magnification: 200-fold.

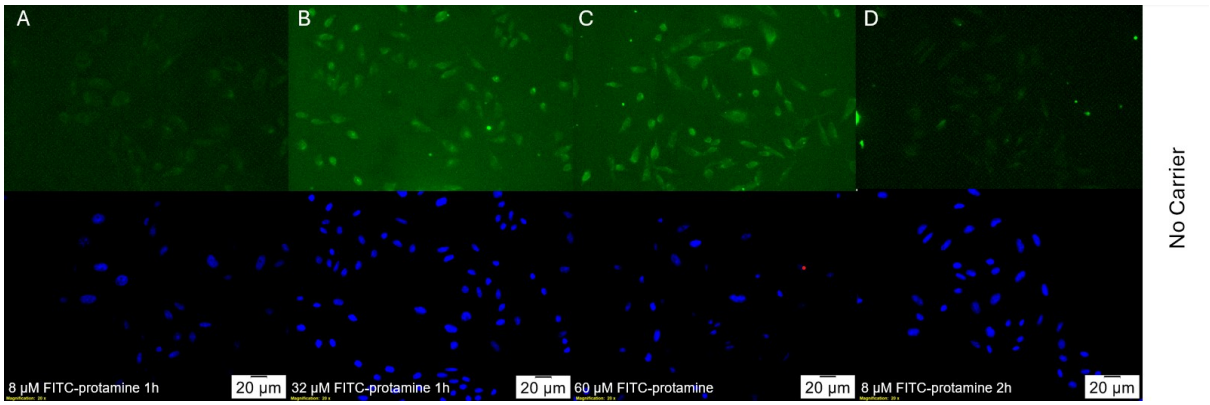

Figure 40 Uptake of FITC-protamine at different concentrations without membrane carrier

Uptake of FITC-protamine in 8 (A), 32 (B), 60 µM (C) final concentration after 1 h incubation at 37 °C, 5% CO_2 and 90% RH and uptake of 8 µM FITC-protamine for 2 h under the same conditions (D), in the absence of any membrane carriers. FITC-protamine was imaged with an exposure time of 3.5 s and ISO 1600, whereas DAPI was imaged at 100 ms and ISO 100. Magnification: 200-fold.

The FITC-protamine concentration was further increased to 200 (Figure 41A and Figure 42A) and 400 µM (Figure 41B and Figure 42B), which indeed reduced the required exposure time to 714 ms. However, a signal intensity remained insufficient to assess the membrane carrier properties of $SiMoW_{11}$. While the background was visibly reduced at 400 µM FITC-protamine, it still posed an issue at 200 µM. An attempt to reduce the background signal involved increasing the heparin concentration in the HBSS to 1000 µg/mL (Figure 41C and Figure 42C), which however did not lead to a reduced background as anticipated. To evaluate the influence of phenol red present in the medium, the incubation was performed in DPBS instead (Figure 41D and Figure 42D), which decreased the background, but also the visibility of FITC-protamine uptake.

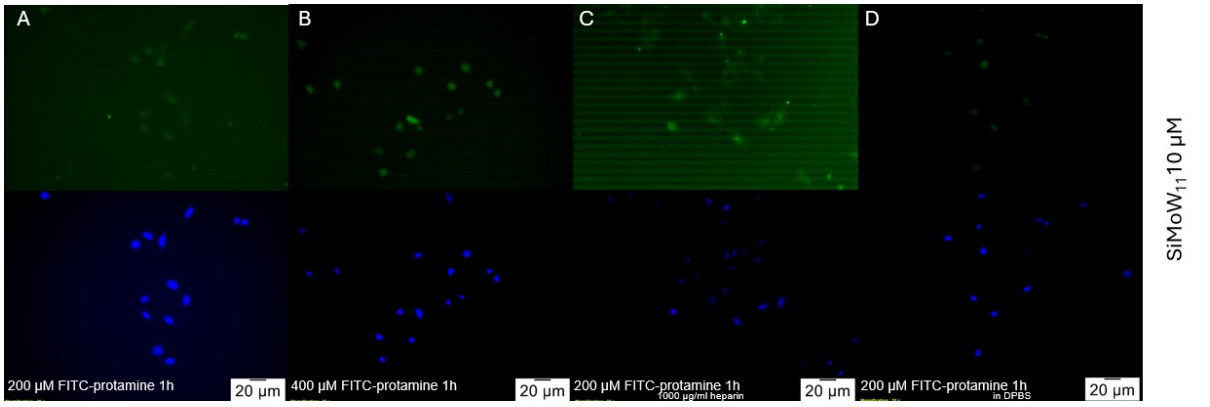

Figure 41 FITC-protamine uptake at higher concentrations, with increased heparin concentration and incubated in DPBS in the presence of 10 µM $SiMoW_{11}$

Uptake of FITC-protamine at 200 (A) and 400 µM (B) after 1 h at 37 °C, 5% CO_2 and 90% RH in the presence of 10 µM $SiMoW_{11}$. Uptake when washed with Hank's balanced salt solution with 1000 µg/mL heparin after 200 µM FITC-protamine incubation for 1 h at 37 °C, 5% CO_2 and 90% RH in the presence of 10 µM $SiMoW_{11}$ (C).Uptake after incubation with of 200 µM FITC-protamine in DPBS instead of Ham's F-12 nutrient mix under the same conditions and in the presence of 10 µM $SiMoW_{11}$

(D). FITC-protamine was imaged at an exposure time of 714 ms and ISO 100, whereas DAPI was imaged at 100 ms and ISO 100. Magnification: 200-fold.

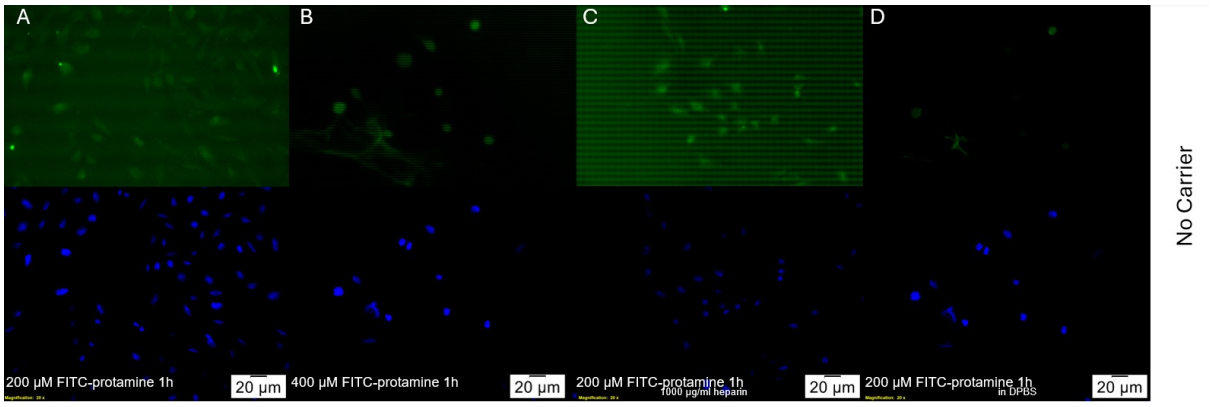

Figure 42 FITC-protamine uptake at higher concentrations, with increased heparin concentration and incubated in DPBS in the absence of a membrane carrier

Uptake of FITC-protamine at 200 (A) and 400 µM (B) after 1 h at 37 °C, 5% CO_2 and 90% RH in the absence of membrane carrier. Uptake when washed with Hank's balanced salt solution with 1000 mg/mL heparin after 200 µM FITC-protamine incubation for 1 h at 37 °C, 5% CO_2 and 90% RH in the absence of membrane carrier (C). Uptake after incubation with 200 µM FITC-protamine at in DPBS instead of Ham's F-12 nutrient mix after 1 h at 37 °C, 5% CO_2 and 90% RH in the absence of membrane carrier (D). FITC-protamine was imaged at an exposure time of 714 ms and ISO 100, whereas DAPI was imaged at 100 ms and ISO 100. Magnification: 200-fold.

A 0.2% Triton X-100 solution was used to determine whether FITC-protamine could be detected in cells after permeabilization. A comparison between incubation with $SiMoW_{11}$ (Figure 43A) and without it (Figure 44A) was hampered by a high background signal in the no carrier sample. Nonetheless, it can be assumed that permeabilization of the cells facilitated the internalization of FITC-protamine, though the exact difference between the presence and absence of carrier cannot be determined. To further investigate the influence of heparin, cells were washed with HBBS without heparin (Figure 43B and Figure 44B), which increased signal intensity, but not sufficiently to make a notable difference compared the other experimental conditions. Additionally, there is no visible difference between the uptake with and without carrier present. To allow for a better interaction between the peptide and $SiMoW_{11}$, the POM was preincubated with FITC-protamine before the addition to the cells, which resulted in even worse visibility of the uptake (Figure 43C and Figure 44C)

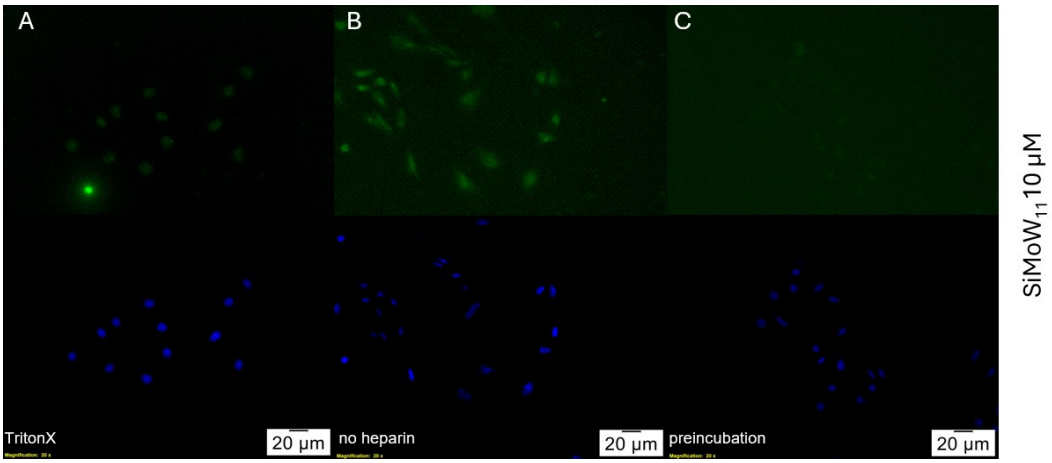

Figure 43 Uptake of FITC-protamine after permeabilization, in the absence of heparin and following preincubation with $SiMoW_{11}$

Uptake of FITC-protamine at 200 µM after permeabilization with 0.2% Triton X-100 (A) following 1 h incubation at 37 °C, 5% CO_2 and 90% RH in the presence of 10 µM $SiMoW_{11}$. Influence on uptake when cells were washed with Hank's balanced salt solution without heparin following incubation with 200 µM FITC-protamine for 1 h under the same conditions in the presence of 10 µM $SiMoW_{11}$ (B). 1 h incubation under the same conditions with a mixture of Ham's F-12 nutrient mix with 200 µM FITC-protamine and 10 µM $SiMoW_{11}$ that was prepared in advance (5 min incubation) (C). FITC-protamine was imaged with an exposure time of 1 s (A and B), 1.2 s (C) and ISO 100, whereas DAPI was imaged at 100 ms and ISO 100. Magnification: 200-fold.

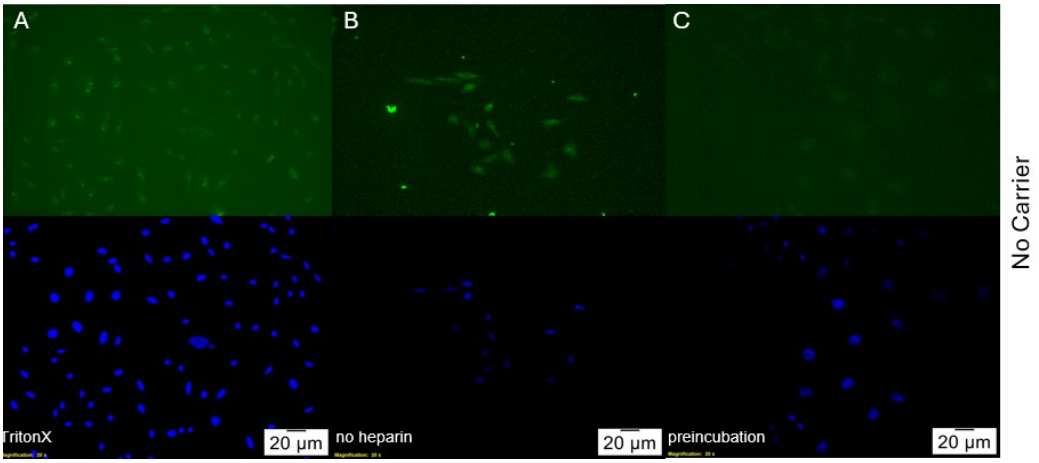

Figure 44 Uptake of FITC-protamine after permeabilization, in the absence of heparin and following preincubation with water

Uptake of FITC-protamine at 200 µM after permeabilization with 0.2% Triton X-100 (A) following 1 h incubation at 37 °C, 5% CO_2 and 90% RH in the absence of membrane carrier. Influence on uptake when cells were washed with Hank's balanced salt solution without heparin following incubation with 200 µM FITC-protamine for 1 h under the same conditions in the absence of membrane carrier (B). 1h incubation under the same conditions with a mixture of Ham's F-12 nutrient mix with 200 µM FITC-protamine and water that was prepared in advance (5 min incubation) (C). FITC-protamine was imaged with an exposure time of 1 s (A and B), 1.2 s (C) and ISO 100, whereas DAPI was imaged at 100 ms and ISO 100. Magnification: 200-fold.

Cells were also incubated overnight at 4°C with 4 and 100 µM FITC-protamine in the presence of $SiMoW_{11}$ (Figure 45A and B) and in the absence of a membrane carrier (Figure 45C and D), which did not lead to an improved signal visibility. Despite the differences in background intensity, no clear difference can be determined between the $SiMoW_{11}$ present and absent.

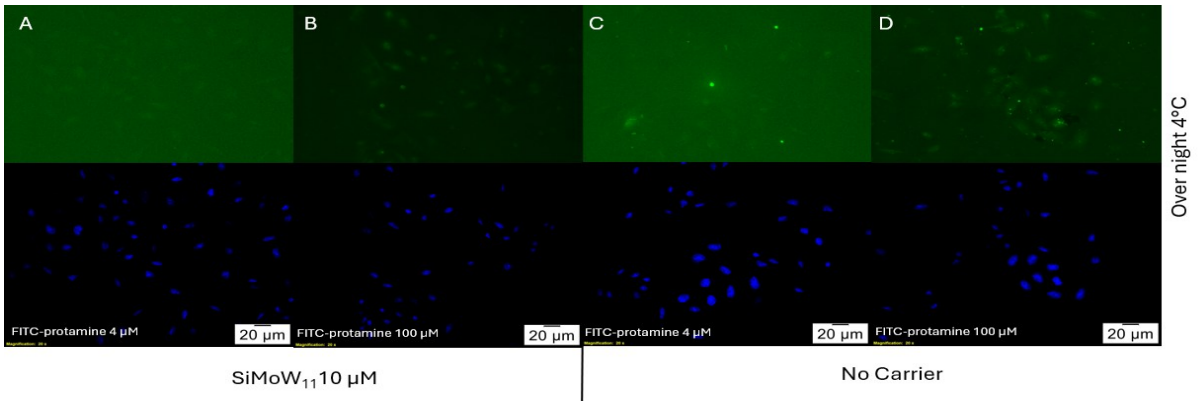

Figure 45 Uptake of FITC-protamine after overnight incubation

Uptake of 4 and 100 µM FITC-protamine in the presence of 10 µM $SiMoW_{11}$ (A and B) and without membrane carrier present (C and D) after overnight incubation at 4 °C. FITC-protamine was imaged with an exposure time of 1 s and ISO 100, whereas DAPI was imaged at 100 ms and ISO 100. Magnification: 200-fold.

FITC-octaarginine

FITC-labelled octaarginine was applied to CHO-K1 cells in combination with the previously examined POMs. The cells with no carrier, $GaMo_6$ and $GaMo_{12}$ (Figure 46A, C and D) present seem to show peptide uptake of similar intensity, whereas $SiMoW_{11}$ shows a decrease in uptake compared to the no-carrier condition (Figure 46A and B). Besides reduced internalization into the nucleus, $SiMoW_{11}$ seems to worsen peptide uptake overall. However, since the background color could not be adjusted and different imaging settings were necessary to detect the signal, comparing intensities between the experiments where uptake was visible was difficult.

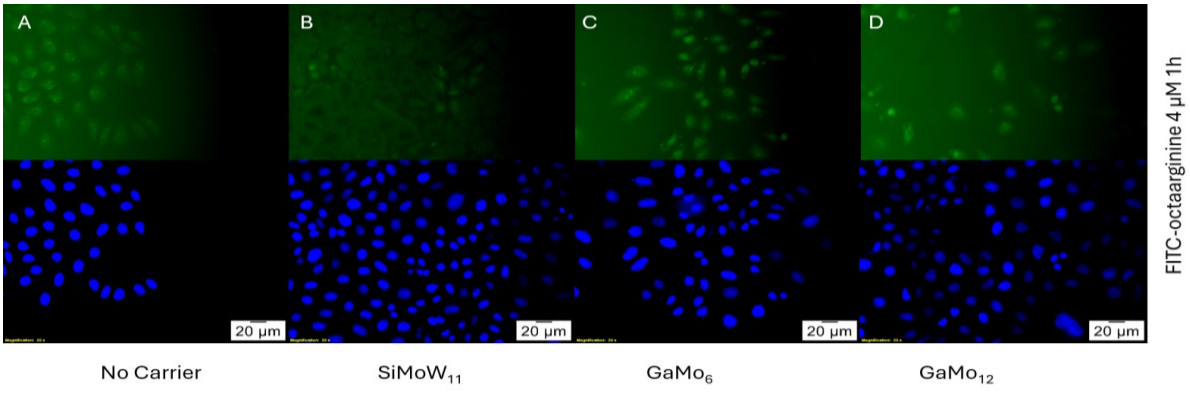

Figure 46 Uptake of FITC-octaarginine in the presence of different POMs

Uptake was imaged after incubating CHO-K1 cells with 4 µM FITC-octaarginine and no carrier present (A), or 10 µM $SiMoW_{11}$ (B), $GaMo_6$ (C) or $GaMo_{12}$ (D) at 37°C, 5% CO_2 and 90% RH for 1 h. FITC-octaarginine was imaged with an exposure time of 714 ms and ISO 100 (A, C and D) or ISO 1600 (B), whereas DAPI was imaged at 100 ms and ISO 100. Magnification: 200-fold.

To increase signal visibility, the FITC-octaarginine incubation time (Figure 47) and concentration (Figure 48) were increased in the following experiments. As in the previous experiment, uptake was again visible in the absence of a carrier and with $GaMo_6$ or $GaMo_{12}$

(Figure 47A, C and D) present, whereas $SiMoW_{11}$ (Figure 47B) showed the lowest peptide uptake (indicative by the higher exposure time necessary) and a rather membranous accumulation as compared to the other POMs. It was noted that background intensity increased with incubation time. Since the background again could not be removed, no assumptions could be made about differences in signal intensity in the conditions where uptake was observed.

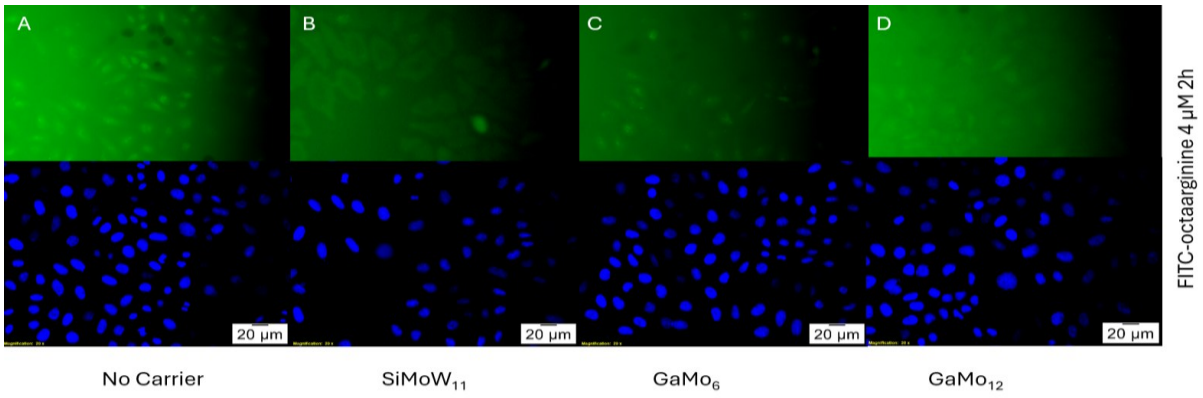

Figure 47 Uptake of FITC-octaarginine in the presence of different POMs after extended incubation

Uptake was imaged after incubating CHO-K1 cells with 4 µM FITC-octaarginine and no carrier present (A), or 10 µM $SiMoW_{11}$ (B) , $GaMo_6$ (C) or $GaMo_{12}$ (D) at 37°C, 5% CO_2 and 90% RH for 2 h. FITC-octaarginine was imaged with an exposure time of 714 ms and ISO 100 (A, C and D) or ISO 1600 (B), whereas DAPI was imaged at 100 ms and ISO 100. Magnification: 200-fold.

When increasing the FITC-octaarginine concentration to 8 µM, a more distinct difference can be observed, at least between $GaMo_6$ (Figure 48C) and $GaMo_{12}$ (Figure 48D), the former seemingly enhancing peptide uptake compared to the latter. In contrast, $SiMoW_{11}$ (Figure 48B) showed the lowest uptake, taking the imaging settings into account. However, it must be noted that the background signal was again strong and could not be removed, which posed issues especially for the imaging of cells without a membrane carrier present (Figure 48A). Here, the exposure time had to be reduced to 300 ms to avoid overexposure, whereas the other conditions were imaged with an exposure time of 714 ms. Therefore, except for the assumption that $GaMo_6$ could possess better membrane carrier properties than $GaMo_{12}$ under those conditions, no further conclusions could be drawn from this experiment.

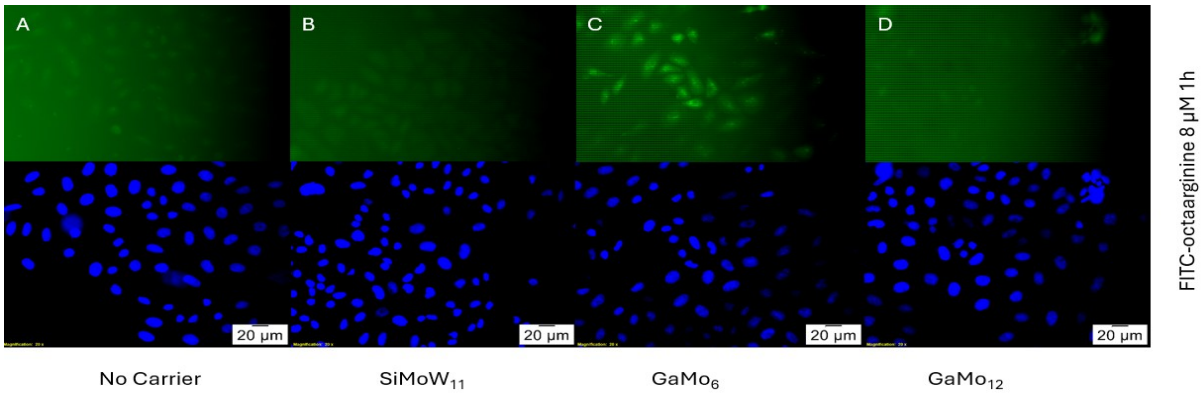

Figure 48 Uptake of FITC-octaarginine in the presence of different POMs at a higher peptide concentration

Uptake was imaged after incubating CHO-K1 cells with 8 µM FITC-octaarginine and no carrier present (A), or 10 µM $SiMoW_{11}$ (B) , $GaMo_6$ (C) or $GaMo_{12}$ (D) at 37°C, 5% CO_2 and 90% RH for 1 h. FITC-octaarginine was imaged with an exposure time of 300 ms (A) or 714 ms (B, C and D) and ISO 100 (A, C and D) or ISO 1600 (B), whereas DAPI was imaged at 100 ms and ISO 100. Magnification: 200-fold.

When incubated overnight, uptake was only observed in the absence of a membrane carrier (Figure 49A). The background signal in the experiments with the POMs present was very high (Figure 49B, C and D). However, there are dark spots visible where the cells could be, indicating that there might be even more FITC-octaarginine present in the surrounding than inside the cells. However, due to the low contrast, these remain only assumptions.

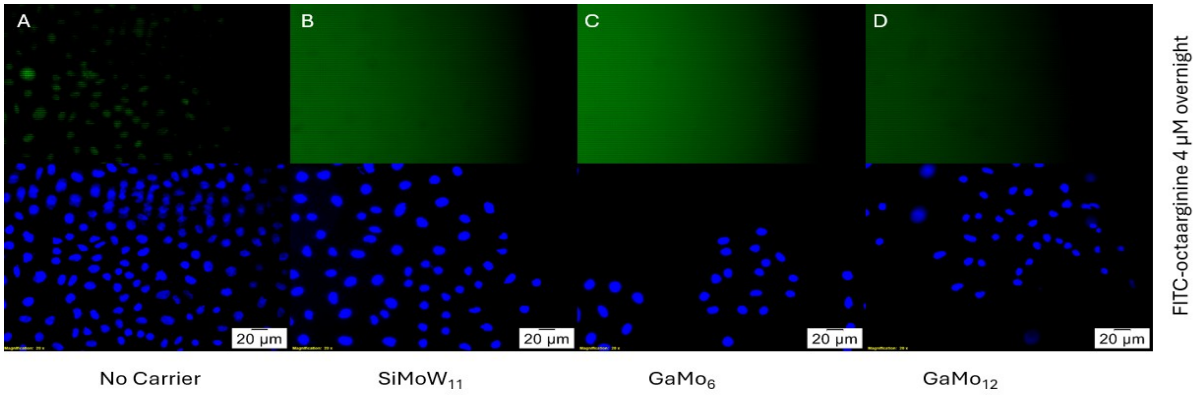

Figure 49 Uptake of FITC-octaarginine in the presence of different POMs after overnight incubation

Uptake was imaged after incubating CHO-K1 cells with 8 µM FITC-octaarginine and no carrier present (A), or 10 µM $SiMoW_{11}$ (B), $GaMo_6$ (C) or $GaMo_{12}$ (D) overnight at 4 °C. FITC-octaarginine was imaged with an exposure time of 285 ms and ISO 100, whereas DAPI was imaged at 100 ms and ISO 100. Magnification: 200-fold.

2.4.5. Discussion

As it was previously shown that certain POMs can act as membrane carriers for specific peptides [1], the aim of these experiments was to determine the carrier properties of the novel POMs, in comparison to a previously established membrane carrier $SiMoW_{11}$.[1] This property was tested with two FITC-labelled peptides. Protamine was chosen due to its commercial

availability, as well as octaarginine, which had previously been used in published fluorescence experiments.[1]

Even though $SiMoW_{11}$ showed membrane carrier activity for protamine on artificial membranes,[1] this behavior towards FITC-protamine was not observed in the experiments carried out during this master's thesis. Neither different incubation conditions (higher peptide concentration, switching out medium for DPBS, longer incubation times, different incubation temperatures), nor adaptations to the protocol (increasing and removing heparin from washing solution, pre-incubation of POM and peptide mixture, permeabilization with Triton X-100), improved the fluorescence signal to a degree that would make it possible to reliably assess differences in uptake. A high background signal, which could not be removed with any of the previously mentioned protocol adaptations, further decreased the reliability of subjective uptake assessment. The high background signal could have been caused by not removed unreacted FITC in the used FITC-peptide.[90] Therefore, no assumptions could be made about the uptake behavior of FITC-protamine in the presence of $SiMoW_{11}$, $GaMo_6$ and $GaMo_{12}$.

While the signal intensity was higher when using FITC-octaarginine, interpretation of uptake was still complicated by a persistent, non-removable background signal, which worsened with both longer incubation time and higher FITC-octaarginine concentration. While a slight improvement in uptake was observed at 8 µM FITC-octaarginine concentration in the presence of $GaMo_6$ as compared to $GaMo_{12}$, the only consistently observed behaviour was a decrease in signal when FITC-octaarginine was applied together with $SiMoW_{11}$, compared to experiments without carrier or with the other POMs, which contradicts previous results where $SiMoW_{11}$ was established to act as a membrane carrier for FITC-octaarginine specifically.[1] Since this experiment was only performed once (n = 1) due to limited amount of FITC-octaarginine, these findings require further validation.

To answer the question, whether the examined POMs can act as membrane carriers for FITC-protamine and FITC-octaarginine, it is suggested to repeat the experiments with different equipment or alternative detection methods. Difficulties arose when attempting to replicate the results from a previous publication, in which $SiMoW_{11}$ was shown to facilitate the uptake of FITC-octaarginine.[1] In contrast, this was not observed in the present work and the data even suggest that $SiMoW_{11}$ might hinder uptake of FITC-octaarginine under the employed experimental conditions. Several differences in experimental setup should be noted between this master's thesis and the mentioned publication. First, better results were obtained when live cells were imaged using a confocal microscope as compared to fixed cells [1]; however, a confocal microscope was not available during this thesis. Second, it was not specified whether the FITC-octaarginine used in the published study contained an AHX-linker, while FITC-octaarginine used in this thesis included AHX-linker. Since an AHX-linker spaces out FITC and

the peptide, it could interfere with the membrane-peptide or membrane-POM-peptide interaction and therefore also influence internalization.[91] Third, adhesion of FITC-labelled peptides to plasticware could contribute to the high background present. Similar explanations may also explain the lack of uptake seen with FITC-protamine. While the published study did not evaluate carrier abilities of POMs for FITC-protamine using fluorescence studies, experiments with synthetic membranes have shown carrier properties of $SiMoW_1$ for unlabeled protamine. Overall, these findings highlight the need for further investigation before definitive conclusions can be drawn. As already mentioned, repeating the experiments using live-cell fluorescence microscopy may help resolve some of the issues discussed.

An alternative approach would be to use a different method, such as FACS (fluorescence activated cell sorting), which additionally enables quantitative analysis of peptide uptake. This technique can sort cells according to the presence of fluorescent labels but can also quantify the intensity of fluorescence within the cells. A proposed workflow would involve incubating adherent cells with FITC-labelled peptides and POMs as done during these fluorescence microscopy experiments, followed by a washing step, cell detachment and resuspension, followed by a flow cytometry analysis. Comparing POM-treated and untreated cells would allow a quantifiable comparison between the two conditions and eliminate the subjectivity inherent for interpretation of fluorescence microscopy images. However, cell detachment might influence the amount of peptide that is attached to the membrane. Furthermore, FACS cannot distinguish between membrane-bound and internalized peptide.

2.5. LigandTracer® experiments

To obtain kinetic data of the process of POM facilitated PET tracer internalization, uptake experiments with LigandTracer® technology were conducted.

2.5.1. Method

LigandTracer® is a device that allows the collection of kinetic data on ligand-cell interactions. The device continuously measures the activity in a section of the dish as it rotates, recording the background signal (the area where no cells are present) and the signal in the area containing cells (Figure 50). This method enables real-time, non-invasive monitoring of ligand binding to living cells, allowing for the analysis of binding kinetics, affinity as well as changes in internalization and membrane binding with increasing concentrations.[92]

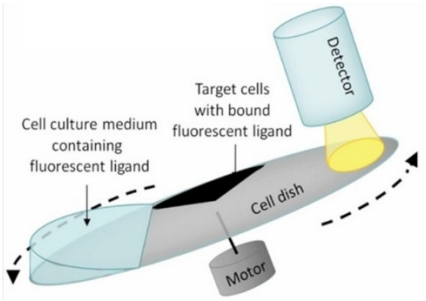

Figure 50 LigandTracer® methodology [93]

Different types of LigandTracers® are available (Figure 51). Yellow, White and Grey detect radiation, whereas LigandTracer® Green detects fluorescence. High- and low-energy gamma photons are detected using LigandTracer® Yellow and Grey, respectively, whereas LigandTracer® White detects beta particles.[92]

Figure 51 Different types of LigandTracer® [92]

2.5.2. Chemicals, materials and devices

- Cell line
  - HT29 (ATCC)
- POM
  - $SiMoW_{11}$ (provided by Nadiia Gumerova, PhD.)
- PET tracer
  - Pentixafor (ABX Advanced Biochemical Compounds, 9916.0000.050 or from intern production; [^{68}Ga]Ga-Pentixafor is then generated in house from these precursers)
- Medium
  - Ham's F-12 nutrient mix (Gibco, Ref. 21765-029)
- Devices
  - Petri dish 100 × 20 mm (Cellstar, ref. 6640160)
  - LigandTracer® Yellow (Ridgeview Instruments
  - LigandTracer® White (Ridgeview Instruments)

2.5.3. Procedure

The day before the experiment, 250,000 cells in 3 mL were seeded onto a part of a 100 × 12 mm cell culture dish. The dish was kept in the incubator at an angle of approximately 30° to ensure that the cells grow only on one area of the dish (Figure 52a).

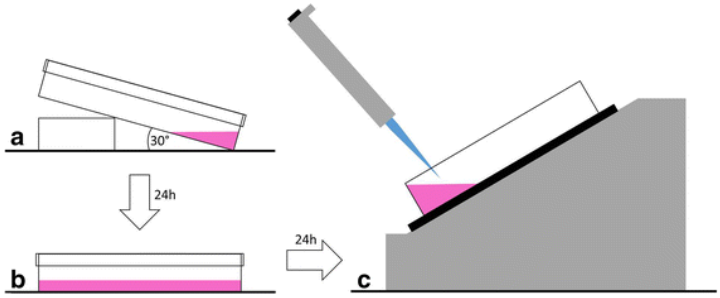

Figure 52 Cell culture dish preparation for LigandTracer® experiment. In the publication, as opposed to this thesis, cells were seeded two days prior to an experiment [94]

The HT29 cells were kept in the medium outlined in "2.1 Cell culture maintenance". On the day of the experiment, the medium was replaced by 3 mL Ham's F-12 nutrient mix without any additives. LigandTracer® White and Yellow were used for these experiments. Although LigandTracer® Yellow measures high-energy gamma photons, since gallium-68 produces 511 keV gamma ray photons upon electron annihilation, this device was also available for this experiment.[99] After inserting the dish into the LigandTracer® device, the background activity was recorded for approximately 5 min. [^{68}Ga]Ga-Pentixafor and $SiMoW_{11}$ (freshly prepared) were added in increasing concentrations (Table 6 and Table 7) and the activity was always measured for approximately 5 min.

2.5.4. Results

The first experiment performed using LigandTracer® White was started with lower concentrations of [^{68}Ga]Ga-Pentixafor. After the 4th addition of the radiotracer (final concentration 30 nM), a slightly higher increase in binding to the cells as compared to the plastic surface could be observed. Increasing the concentration of [^{68}Ga]Ga-Pentixafor to 100 nM (5th addition) led to an increase in cell-associated activity and showed a slight curvature. However, the binding to the plastic in the background region of the dish was extremely high. Additions of $SiMoW_{11}$ (100-10,000 nM final concentration, Table 6) did not further influence the curvature (Figure 53).

The second experiment using LigandTracer® Yellow was started directly with the addition of higher concentrations of [^{68}Ga]Ga-Pentixafor (Table 7). However, in this case, no difference between binding of the PET tracer to the cells *vs.* to the plastic surface of the cell culture dish was observed, nor was any effect of the addition of $SiMoW_{11}$ detected (Figure 54).

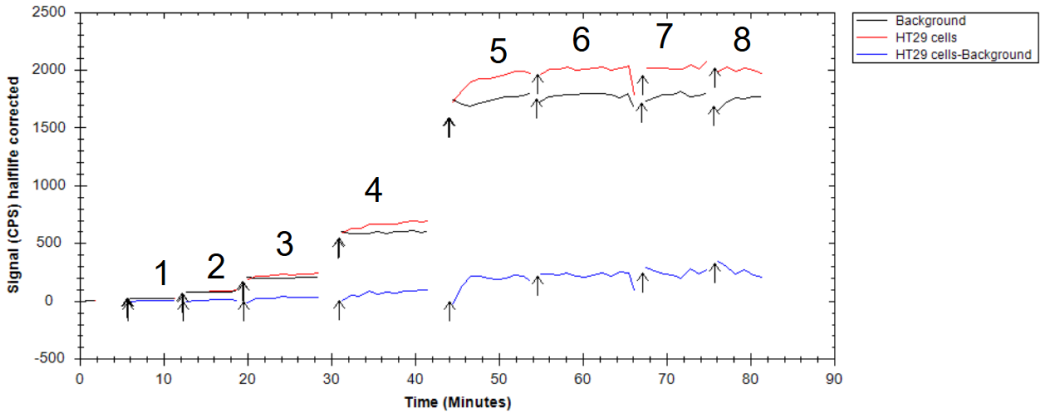

Figure 53 Binding curves of [^{68}Ga]Ga-Pentixafor to HT29 cells

Measured using LigandTracer® White after eight additions of [^{68}Ga]Ga-Pentixafor or $SiMoW_{11}$ (see Table 8). Half-life-corrected signal in CPS (counts per second) is plotted against time (min).Binding to HT29 cells (red line) is compared to background binding (no cells, black line) and HT29 binding corrected for background binding (blue line).

Table 6 Final concentrations of [^{68}Ga]Ga-Pentixafor and $SiMoW_{11}$ after each addition (related to Figure 53)

Addition	Final [^{68}Ga]Ga-Pentixafor concentration [nM]	Final $SiMoW_{11}$ concentration[nM]
1	1	0
2	4	0
3	10	0
4	30	0
5	100	0
6	100	100
7	100	1,000
8	100	10,000

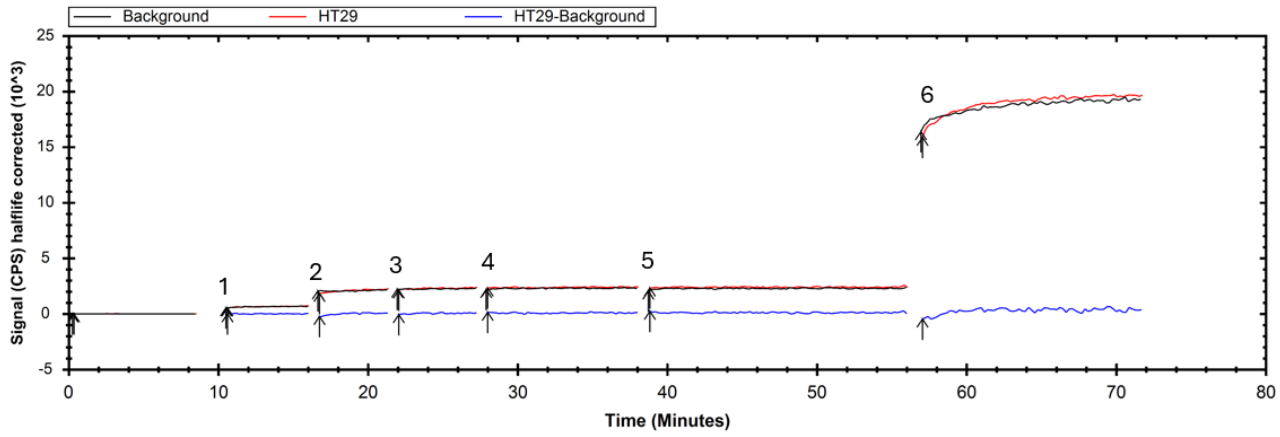

Figure 54 Binding curves of [^{68}Ga]Ga-Pentixafor to HT29 cells

Measured using LigandTracer® Yellow after six additions of [^{68}Ga]Ga-Pentixafor or $SiMoW_{11}$ (see Table 9). Half-life-corrected signal in CPS (counts per second) is plotted against time (min). Binding to HT29 cells (red line) is compared to background binding (no cells, black line) and HT29 binding corrected for background binding (blue line).

Table 7 Final concentrations of [^{68}Ga]Ga-Pentixafor and $SiMoW_{11}$ after each addition (related to Figure 54)

Addition	Final [^{68}Ga]Ga-Pentixafor concentration [nM]	Final $SiMoW_{11}$ concentration [nM]
1	30	0
2	100	0
3	100	100
4	100	1,000
5	100	10,000
6	1,000	10,000

2.5.5. Discussion

The addition of [^{68}Ga]Ga-Pentixafor to the cells generally did not sufficiently increase cell-associated activity as compared to the background. This was observed in both experiments performed using two different LigandTracer® devices. Importantly, the addition of POM $SiMoW_{11}$ did not cause any change in cell-associated activity. The background activity was extremely high, likely due to the binding and adhesion of [^{68}Ga]Ga-Pentixafor to the dish surface. This has previously been observed with other peptide-based and lipophilic PET tracers. Attempts have been made in the past to solve this issue (addition of Tween-20 to the radiotracer solution, coating of the dish, etc.); however, these were not very successful (unpublished). Due to this, and since the tracer binding to plastic does not interfere with conventional uptake experiments performed in well plates, no further attempts were made to address the adhesion to the dish surface and well plate uptake experiments were performed instead.

2.6. Conventional well plate uptake experiments with PET tracers

To determine internalization and membrane binding amounts of different PET tracers in conjunction with $SiMoW_{11}$, $GaMo_6$ and $GaMo_{12}$ in comparison to without POM present, a conventional uptake assay with different cell lines under different conditions was performed.

2.6.1. Method

A PET tracer is a molecule that interacts with a receptor of interest and is labelled with a positron-emitting radionuclide. Commonly used PET nuclides include fluorine-18, carbon-11, gallium-68 and zirconium-89. Those labelled molecules are administered to a patient, where they bind to tissues of interest, typically pathological tissues characterized by changes that the biomolecules selectively associate with (e.g. cancer, inflammatory processes).[35], [36], [37], [38], [52] While PET tracers are currently used primarily for diagnostics, some PET nuclides have also therapeutic potential. A diagnostic PET tracer is often paired with a therapeutic SPECT agent in a theragnostic approach.[95]

The uptake assay employed here is based on internalization studies. The amount of surface-bound [^{68}Ga]Ga-NJMP1 was evaluated using an acidic glycine wash like the one used in this master's thesis.[96] An acidic glycine wash is mild enough to avoid damaging cells when used properly, but strong enough to sufficiently disrupt the non-covalent interactions between the PET tracer and the receptor. The investigation of luthenium-177-labelled somatostatin receptor ligands involved removing the membrane-bound fraction with acidic glycine, followed by cell lysis with NaOH to determine the amount of internalized substance.[97]

2.6.2. Chemicals and devices

- Cell lines
    - CHO-K1 (ATCC)
    - CHO-K1 PSMA (transduced by Dr. Thomas Dilinger [71])
    - HT29 (ATCC)
- POMs
    - $SiMoW_{11}$ (provided by Nadiia Gumerova, PhD.)
    - $GaMo_6$ (provided by Nadiia Gumerova, PhD.)
    - $GaMo_{12}$ (provided by Nadiia Gumerova, PhD.)
- PET tracers
    - [^{68}Ga]Ga-Pentixafor (ABX advanced biochemical compounds, 9916.0000.050 or from intern production)
    - [^{68}Ga]Ga-PSMA-11 (Novartis, Locametz 25 µg)
- Inhibitors

    - 2-PMPA (2-(phosphonomethyl)pentanedioic acid) (Sigma Aldrich, Ref. SML1612-5mg)
    - CXCR4 Antagonist 1 (AMD3100) (Merck, Ref. 239820-5mg)
- Solutions
    - Ham's F-12 Nutrient mix (Gibco, Ref. 21765-029)
    - Acidic glycine solution (0.05 M glycine, 0.1 M NaCl, pH 2.9)
    - NaOH (0.1M)
    - DPBS (Gibco, Cat. No. 14190144)
- Materials and devices
    - 12-well plates (TPP, Ref. 92412)
    - Dose calibrator (Veenstra, VDC-505)
    - Gamma counter (Perkin Elmer, 2480 Wizard²)
    - Eppendorf tubes 2.0 ml (Eppendorf, Cat. No. 0030121686)
    - Eppendorf tubes 1.5 ml low binding (Eppendorf, Cat. No. 0030108132)

2.6.3. Procedure

To determine the amount of internalized and membrane-bound radiolabeled PET tracers relative to the applied dosage, a cell uptake assay was performed. 12-well plates were seeded out to obtain approximately 360,000 cells per well on the day of the experiment. The cells were prepared the weekend before the experiments, resulting in an incubation period of 2-6 days. They were cultivated under cell line-specific growth conditions and counted in triplicate as detailed in "2.1 Cell culture maintenance". The medium in each well was replaced with 0.5 mL Ham's F-12 nutrient mix without additives. POMs ($SiMoW_{11}$, $GaMo_6$ and $GaMo_{12}$, stock solutions 250 µM in water, freshly prepared each day) were added to achieve final concentrations of 10 and 30 µM. Pure water served as a vehicle control. Subsequently, the respective inhibitor was added leading to a 10 µM final concentration of 2-PMPA or AMD3100 (from a 2 mM stock solution in water, stored at 4°C for several months), the former inhibiting PSMA and the latter inhibiting CXCR4. For vehicle control, the corresponding amount of bi-distilled water was added to the cells. [^{68}Ga]Ga-Pentixafor or [^{68}Ga]Ga-PSMA-11, produced for clinical use in the Division of Nuclear medicine of the General Hospital Vienna, were diluted 1:10 with MQ-H_2O. The PET tracer was then added, resulting in 10 nM final concentration. Cells were incubated for 2 hours at either 37°C (5% CO_2, 90% RH) or 4°C (ambient conditions), after which three fractions were collected (Figure 55). The first fraction consisted of the supernatant and two subsequent DPBS washes with 0.5 mL each. To obtain the membrane-bound fraction, the cells were washed twice with 0.5 mL ice-cold acidic glycine solution for 5 minutes on ice. Finally, the internalized fraction was obtained by lysing the cells with 0.5 mL 0.1 M NaOH solution for 10 minutes at 37°C, with two subsequent washes with 0.5 mL 0.1 M NaOH solution. The radioactivity of each fraction and of the standards was quantified using a

gamma counter. These experiments were performed n = 3 in triplicate under various experimental conditions (Table 8). The PET-tracers [^{68}Ga]Ga PSMA-11 and [^{68}Ga]Ga-Pentixafor were tested using both target-negative and target-positive cell lines. For [^{68}Ga]Ga-PSMA-11, CHO-K1 (PSMA-negative) and CHO-K1 PSMA (PSMA-positive) cell lines were used, whereas for [^{68}Ga]Ga-Pentixafor, CHO-K1 (CXCR4-negative) and HT29 (CXCR4-positive) cells were used. POMs $SiMoW_{11}$, $GaMo_6$, and $GaMo_{12}$ were tested at 10 and 30 µM final concentrations. Experiments were conducted at both 4°C and 37°C.

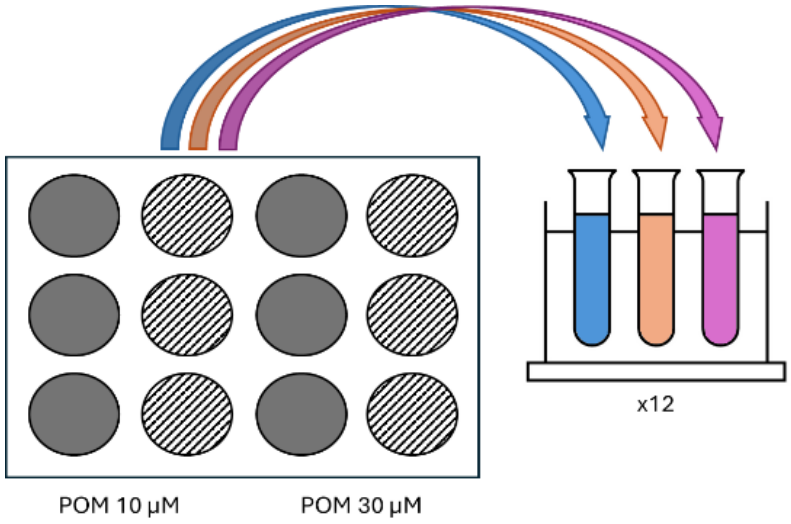

Figure 55 Scheme of cell uptake experiment
Filled and striped wells represent the cells in absence or presence of an inhibitor, respectively. From each well, three fractions were collected, blue representing the supernatant fraction, orange representing the membrane bound fraction and purple representing the internalized fraction.

Table 8 Overview of tested conditions

Tracer	Cell lines		Temperatures		POMs	POM concentrations [µM]			Inhibitior [µM]	
	positive	negative								
[^{68}Ga]Ga-Pentixafor	HT29	CHO-K1	37°C	4°C	$SiMo_{11}$, $GaMo_6$, $GaMo_{12}$	0	10	30	10	0
[^{68}Ga]Ga-PSMA-11	CHO-K1 PSMA	CHO-K1	37°C	4°C	$SiMo_{11}$, $GaMo_6$, $GaMo_{12}$	0	10	30	10	0

2.6.4. Calculations and statistical analysis

The data measured by gamma counter consisted of activity values for each collected fraction as well as the standards expressed in CPM (counts per minute). If necessary, the activity values were decay-corrected using the formula below:

$$N_c = \frac{N_m}{e^{\frac{\ln(2)}{t_{1/2}} * t}}$$

N_c … decay-corrected activity

N_m … measured activity

$t_{1/2}$ … half-life of the radionuclide (gallium-68 = 67.71 min)

t … time elapsed since reference measurement (in min)

The decay-corrected activity was then normalized to a cell count of 500,000 using the following formula:

$$N_n = \frac{N_c * 500{,}000}{C}$$

N_n … normalized activity

N_c … decay-corrected activity

C … actual cell count of an experiment

To express uptake as %AD/5.0e^5 cells (percentage of applied dose per 500,000 cells) following equation was used:

$$\% \frac{AD}{5.0e^5 cells} = \frac{N_n}{N_s} * 100$$

%AD/5.0e^5 cells … percentage of applied dose per 500,000 cells

N_n … normalized activity

N_s … activity of the standard (representing 100% applied dose)

Each experiment was performed in triplicate and outliers within triplicates were identified using the Z-test. The Shapiro-Wilk test was used for testing for normal distribution. Of each experiment, the average, standard deviation and variance of the adherent and internalized tracers were calculated. Since all experiments were repeated at least three times, inter-experimental replicates for each experiment were also checked for outliers using the Z-test. Their normal distribution was assessed using the Shapiro-Wilk test and homogeneity of variance was determined with an F-test. As most of the datasets were normally distributed, statistical significance was tested using two tailed, unpaired t-tests, although some datasets showed uptake below the detection limit (blocking conditions) with an averages of almost zero. For the experiments where the distribution was not calculatable, it was assumed that they are normally distributed.

Using two tailed, unpaired t-tests, the following comparisons were made:

- POM versus no carrier: Within each experiment, it was tested whether the presence of POM significantly altered the uptake compared to cells incubated with no carrier present (vehicle control) either at 37°C or at 4°C. Both values obtained under blocked and non-blocked conditions were compared to the respective no-carrier controls.
- Total versus blocked condition: Determination whether the uptake is significantly different when the target receptor was inhibited. The total membrane binding/internalization in presence of a POM was compared to the membrane binding/internalization in the presence of a POM and the respective inhibitor.
- 10 µM versus 30 µM POM: It was tested whether increasing POM concentration significantly affects the uptake. Comparisons were made between 10 µM and 30 µM for each POM and under blocked and non-blocked conditions separately.

The levels of significance were defined as not significant *ns* ($p > 0.05$) significant * ($p < 0.05$), highly significant ** ($p < 0.01$) and very highly significant *** ($p < 0.001$)

These calculations and statistical analyses were performed using R, and the respective code can be seen in the Appendix under “6.3 Calculation and statistical evaluation of cell uptake experiments”.

2.6.5. Results

The determined uptake values are shown in the appendix. The results of the statistical evaluation of these results are shown below.

[^{68}Ga]Ga-Pentixafor

The addition of POMs, particularly $SiMoW_{11}$ and $GaMo_{12}$, affected the membrane binding and internalization of [^{68}Ga]Ga-Pentixafor in both tested cell lines, CHO-K1 and HT29, and at both temperatures (Figure 56 - Figure 63). The results were statistically examined using t-tests (

Table 9 -Table 11). The results are discussed in more detail below.

The rates of internalization and membrane binding of [^{68}Ga]Ga-Pentixafor in HT29 and CHO-K1, both at 37 °C and 4 °C each, in the presence of $SiMoW_{11}$, $GaMo_6$ and $GaMo_{12}$ were statistically compared to those of the corresponding no-carrier control using a two-tailed unpaired t-test: comparisons were made separately for not inhibited and inhibited conditions (

Table 9). In HT29 cells at 37 °C, $SiMoW_{11}$ significantly increased tracer internalization at both tested concentrations, regardless of target inhibition, whereas $GaMo_{12}$ led to a significant increase in internalization only under not inhibited conditions, again at both concentrations. Regarding membrane binding behavior, $SiMoW_{11}$ and $GaMo_{12}$ both caused a significant decrease at 30 µM in the absence of CXCR4 inhibitor AMD3100. In HT29 at 4 °C only $SiMoW_{11}$

led to a significant increase in non-inhibited tracer internalization at a concentration of 30 µM, whereas no significant differences in membrane binding were observed. In CHO-K1 at 37 °C $SiMoW_{11}$ significantly increased tracer internalization at both 10 and 30 µM under inhibited conditions, whereas under non-inhibited conditions, a significant increase was observed only at 30 µM. Additionally, $SiMoW_{11}$ at 10 µM significantly increased membrane binding in the presence of the CXCR4 inhibitor. In CHO-K1 at 4 °C, internalization was not significantly affected by any POM, whereas membrane binding significantly increased in the presence of $GaMo_{12}$ and $SiMoW_{11}$ at 30 µM as compared to the no-carrier control under blocked conditions.

Table 9 Statistical comparison between no carrier and POM mediated internalization (int) and membrane binding (mb) of [^{68}Ga]Ga-Pentixafor

Cell line		HT29								CHO-K1							
Temperature [°C]		37				4				37				4			
Fraction		int		mb		int		mb		int		mb		int		mb	
Inhibition		no	yes	no	yes	no	yes	no	yes	no	yes	no	yes	no	yes	no	yes
$SiMoW_{11}$	10 µM	↑(*)	↑(*)	ns	ns	ns	ns	ns	ns	ns	↑(*)	ns	↑(**)	ns	ns	ns	ns
	30 µM	↑(**)	↑(*)	↓ (*)	ns	↑(*)	ns	ns	ns	↑(*)	↑(*)	ns	ns	ns	ns	ns	↑(*)
$GaMo_6$	10 µM	ns	ns	ns	ns	ns	ns	ns	ns	ns	ns	ns	ns	ns	ns	ns	ns
	30 µM	ns	ns	↓(***)	ns	ns	ns	ns	ns	ns	ns	ns	ns	ns	ns	ns	ns
$GaMo_{12}$	10 µM	↑(*)	ns	ns	ns	ns	ns	ns	ns	ns	ns	ns	ns	ns	ns	ns	ns
	30 µM	↑(*)	ns	ns	ns	ns	ns	ns	ns	ns	ns	ns	ns	ns	ns	ns	↑(*)

ns ($p > 0.05$)
** ($p < 0.05$)*
*** ($p < 0.01$)*
**** ($p < 0.001$)*
↑/↓ increase/decrease

It was also evaluated if inhibiting CXCR4 significantly influenced both membrane binding and internalization of the tracer (Table 10). In HT29 at 37 °C, blocking the target led to a statistically significant decrease of tracer internalization in the absence of POMs and with $GaMo_6$ at 10 µM, whereas in the presence of $SiMoW_{11}$ at 10 µM internalization increased significantly under blocked conditions. A significant decrease in membrane binding between non-blocked and blocked conditions was observed not only in the no-carrier control but also in the presence of $SiMoW_{11}$ (at 30 µM), $GaMo_6$ (at both tested concentrations), $GaMo_{12}$ (at both tested concentrations). The only significant effect of target inhibition on internalization at 4 °C in HT29 was in the no-carrier control, where inhibition led to a decrease. For membrane binding, a significant decrease in tracer binding was seen in the no-carrier control and with $GaMo_6$ at 30 µM as well as in the no carrier control. In CHO-K1 at 37 °C, the only statistically significant differences between blocked and non-blocked conditions were observed with $SiMoW_{11}$ at 10 µM and 30 µM, where CXCR4 inhibition led to increased internalization. Differences in membrane binding were not found statistically significant. At 4 °C, no statistically significant differences between blocked and non-blocked conditions were observed in either the internalized nor the membrane-bound fraction.

Table 10 Statistical comparison between inhibited and not inhibited internalization (int) and membrane binding (mb) of [^{68}Ga]Ga-Pentixafor

Cell line		HT29				CHO-K1			
Temperature [°C]		37		4		37		4	
Fraction		int	mb	int	mb	int	mb	int	mb
$SiMoW_{11}$	10 µM	↑ (*)	ns	ns	ns	↑ (*)	ns	ns	ns
	30 µM	ns	↓ (*)	ns	ns	↑ (*)	ns	ns	ns
$GaMo_6$	10 µM	↓ (*)	↓ (*)	ns	ns	ns	ns	ns	ns
	30 µM	ns	↓ (*)	ns	↓ (*)	ns	ns	ns	ns
$GaMo_{12}$	10 µM	ns	↓ (*)	ns	ns	ns	ns	ns	ns
	30 µM	ns	↓ (*)	ns	ns	ns	ns	ns	ns
NC		↓ (*)	↓ (*)	↓ (*)	↓ (**)	ns	ns	ns	ns

ns ($p > 0.05$)

** ($p < 0.05$)*

*** ($p < 0.01$)*

**** ($p < 0.001$)*

↑/↓ increase/decrease

To evaluate the effect of POM concentration on tracer internalization and membrane binding, these values were also statistically analyzed (Table 11). An increased concentration of $SiMoW_{11}$ significantly increased tracer internalization under non-inhibited conditions in HT29 at 37 °C, whereas in contrast, increasing concentrations of $GaMo_6$ and $GaMo_{12}$ did not cause significant changes. Regarding membrane binding, only $GaMo_6$ in the absence of CXCR4 inhibitor showed a significant concentration-dependent decrease. In HT29 at 4 °C as well as CHO-K1 at 37 °C and 4 °C no significant differences were observed between 10 µM and 30 µM for any POM in either internalization or membrane binding, regardless of CXCR4 inhibition.

Table 11 Statistical comparison between 10 µM and 30 µM of applied POM in terms of internalization (int) and membrane binding (mb) of [^{68}Ga]Ga-Pentixafor

Cell line	HT29								CHO-K1							
Temperature [°C]	37				4				37				4			
Fraction	int		mb		int		mb		int		mb		int		mb	
Inhibition	no	yes	no	yes	no	yes	no	yes	no	yes	no	yes	no	yes	no	yes
$SiMoW_{11}$	↑ (*)	ns	ns	ns	ns	ns	ns	ns	ns	ns	ns	ns	ns	ns	ns	ns
$GaMo_6$	ns	ns	↓ (*)	ns	ns	ns	ns	ns	ns	ns	ns	ns	ns	ns	ns	ns
$GaMo_{12}$	ns	ns	ns	ns	ns	ns	ns	ns	ns	ns	ns	ns	ns	ns	ns	ns

ns ($p > 0.05$)

** ($p < 0.05$)*

*** ($p < 0.01$)*

**** ($p < 0.001$)*

↑/↓ increase/decrease

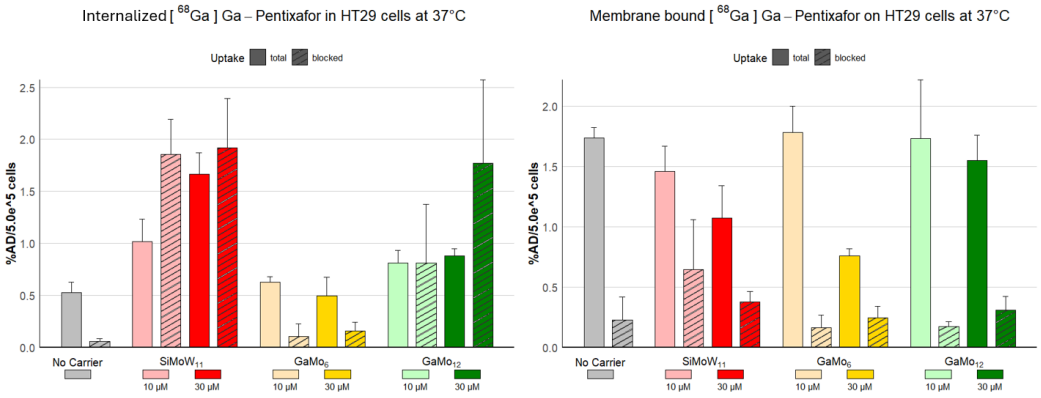

Figure 56 internalized and membrane bound percentage of applied dosage (%AD) of [^{68}Ga]Ga-Pentixafor in HT29 cells at 37 °C

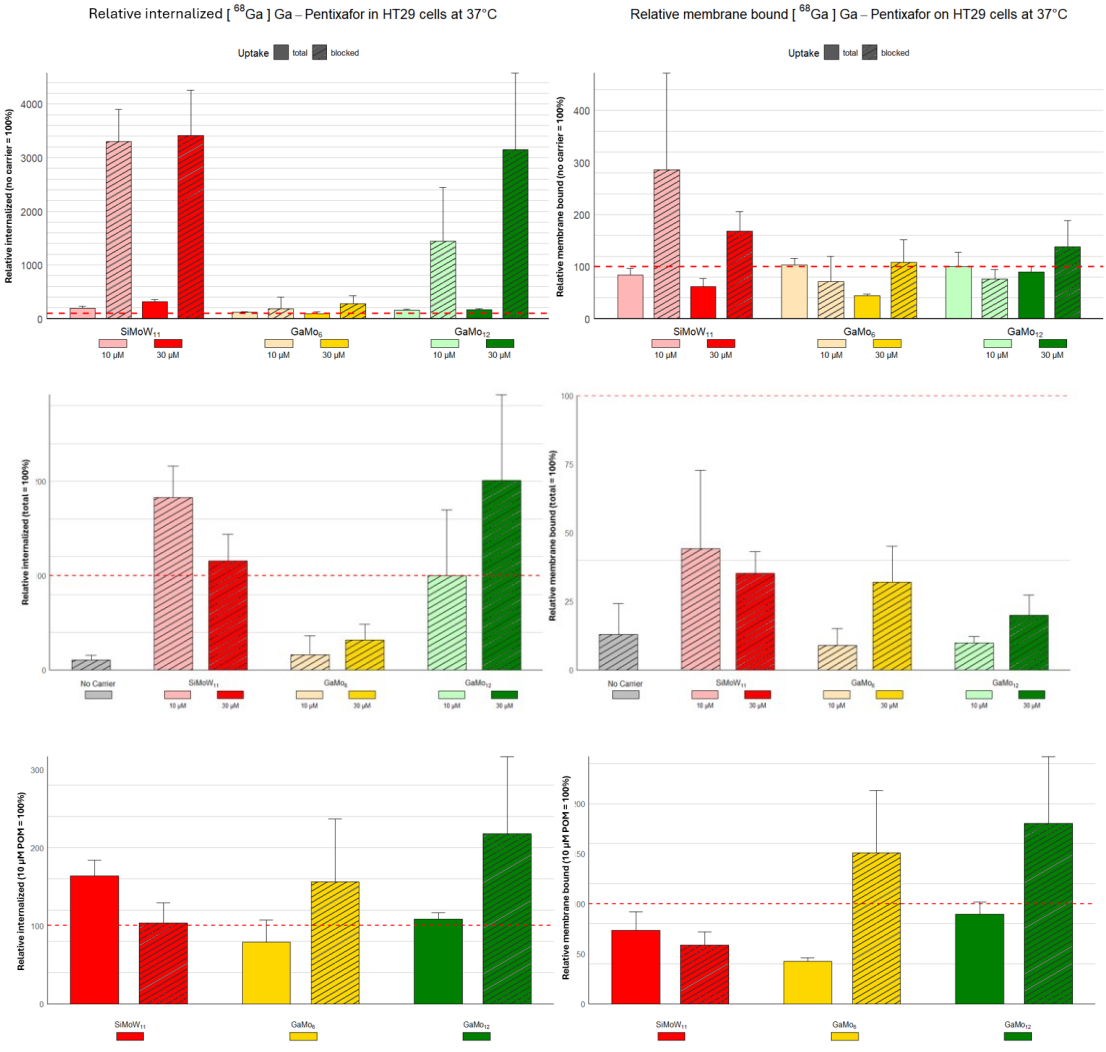

Figure 57 Relative membrane-bound and internalized fractions of [^{68}Ga]Ga–Pentixafor in HT29 at 37 °C

Top row: Uptake and blocked fractions normalized shown relative to their respective "No carrier" values (= 100 %)

Middle row: Blocked fractions normalized to the respective total uptake (= 100 %)

Bottom row: Uptake at 30 µM normalized to uptake at 10 µM (= 100 %)

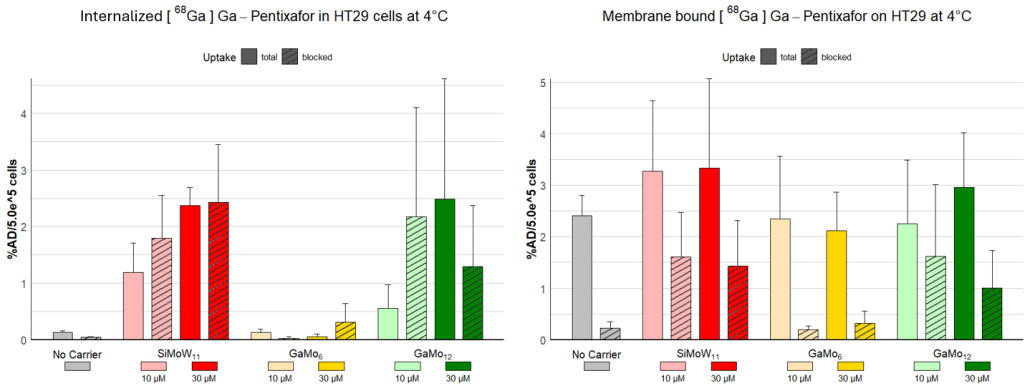

Figure 58 Membrane bound and internalized percentage of applied dosage (%AD) of [^{68}Ga]Ga-Pentixafor in HT29 cells at 4 °C

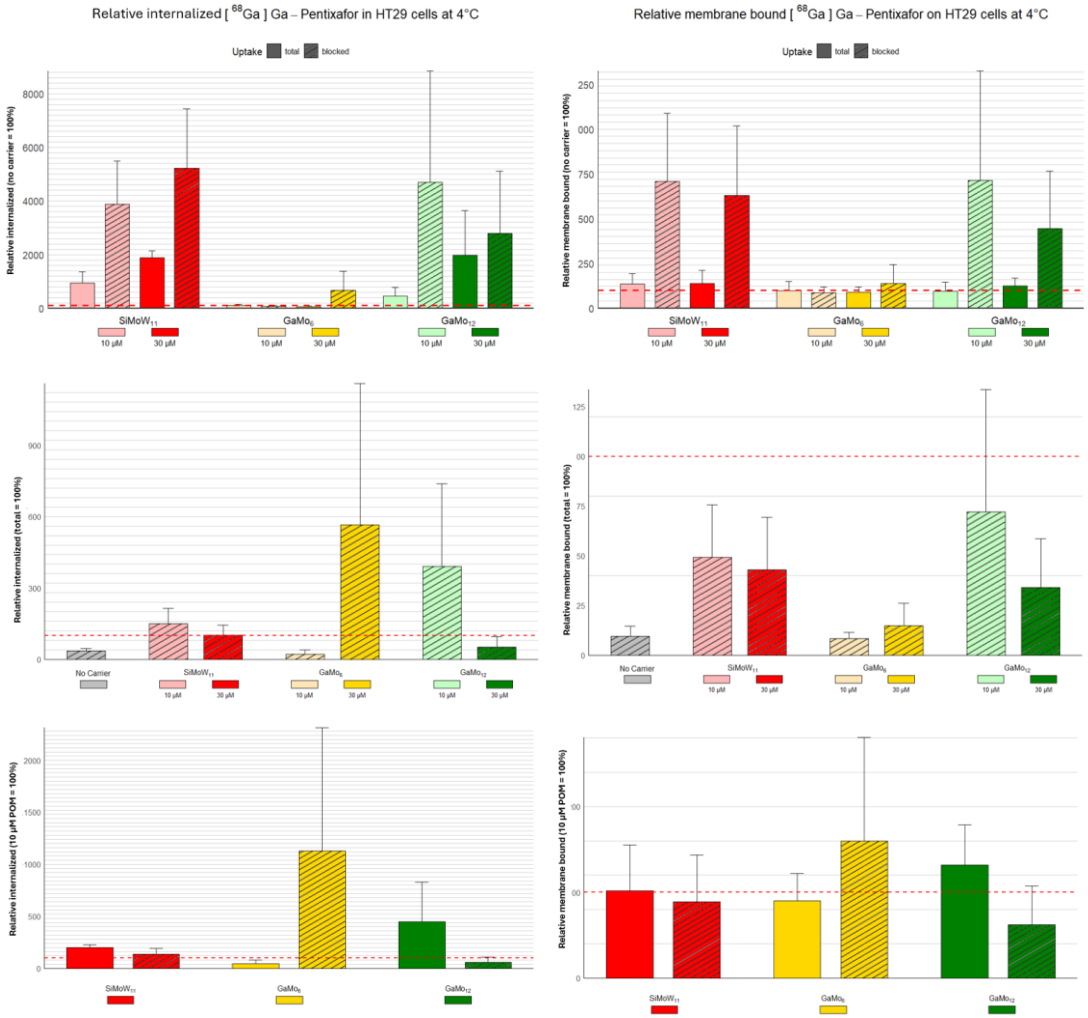

Figure 59 Relative membrane-bound and internalized fractions of [^{68}Ga]Ga–Pentixafor in HT29 cells at 4 °C

Top row: Uptake and blocked fractions normalized shown relative to their respective "No carrier" values (= 100 %)
Middle row: Blocked fractions normalized to the respective total uptake (= 100 %)

Bottom row: Uptake at 30 µM normalized to uptake at 10 µM (= 100 %)

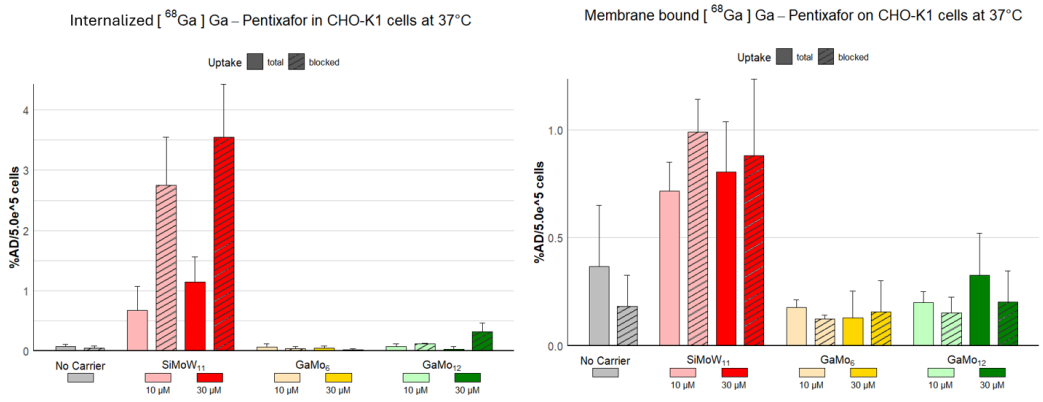

Figure 60 Membrane bound and internalized percentage of applied dosage (%AD) of [^{68}Ga]Ga-Pentixafor in CHO-K1 cells at 37 °C

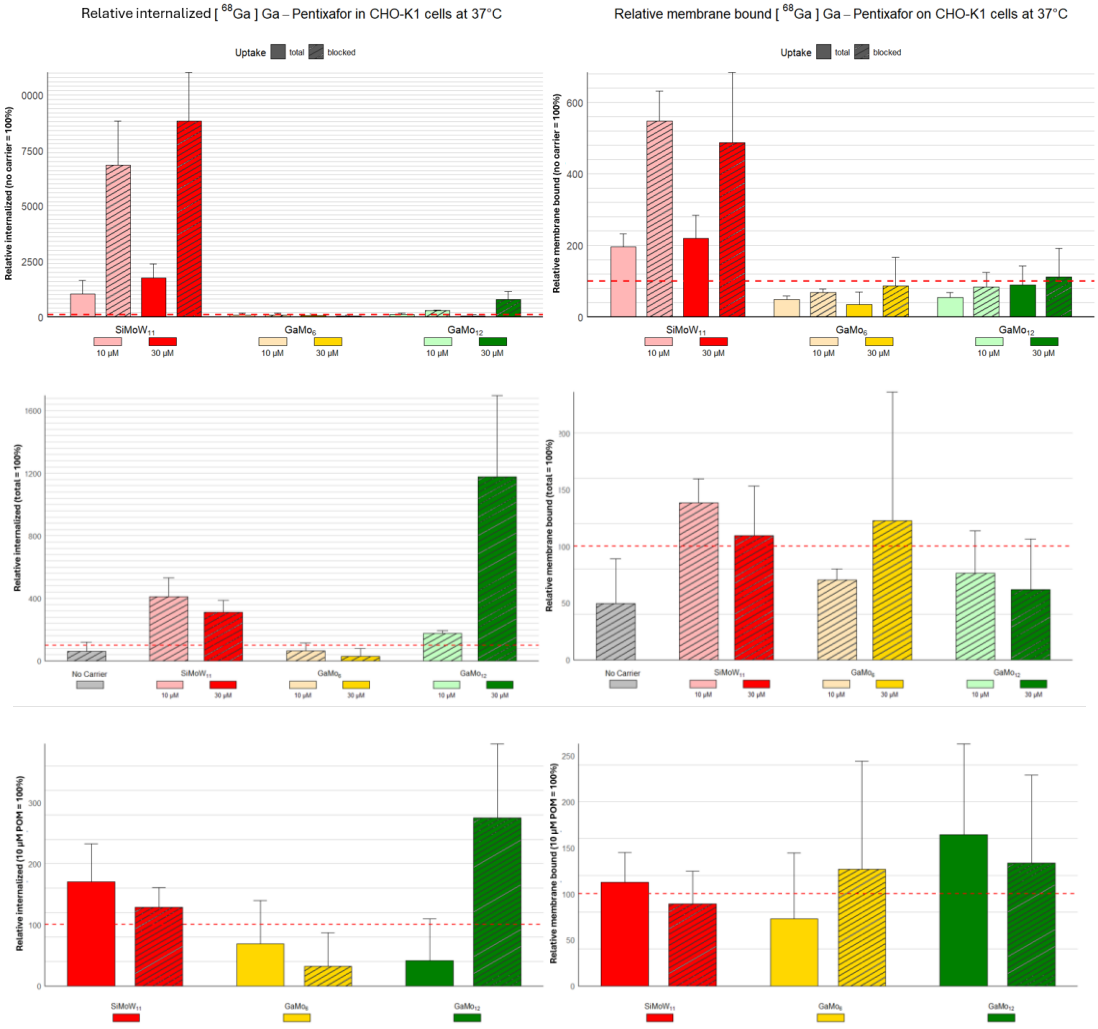

Figure 61 Relative membrane-bound and internalized fractions of [^{68}Ga]Ga–Pentixafor in CHO–K1 cells at 37 °C

Top row: Uptake and blocked fractions normalized shown relative to their respective "No carrier" values (= 100 %)

Middle row: Blocked fractions normalized to the respective total uptake (= 100 %)

Bottom row: Uptake at 30 µM normalized to uptake at 10 µM (= 100 %)

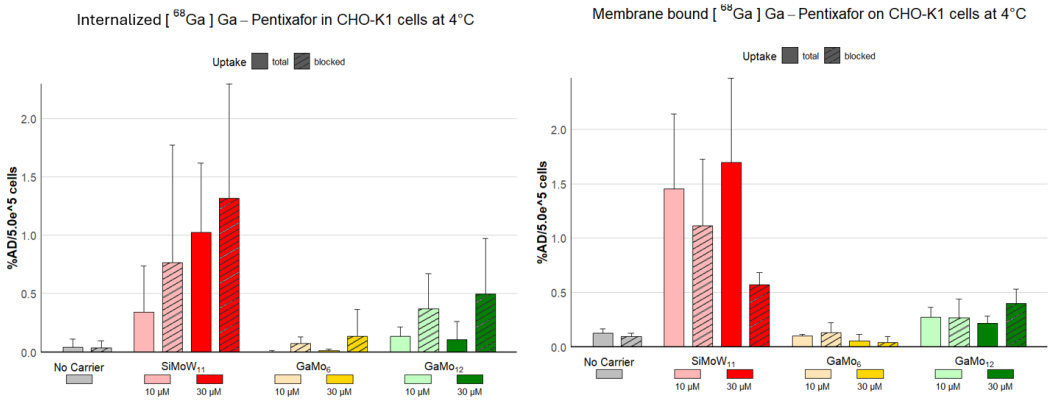

Figure 62 Membrane bound and internalized percentage of applied dosage (%AD) of [^{68}Ga]Ga-Pentixafor in CHO-K1 cells at 4 °C

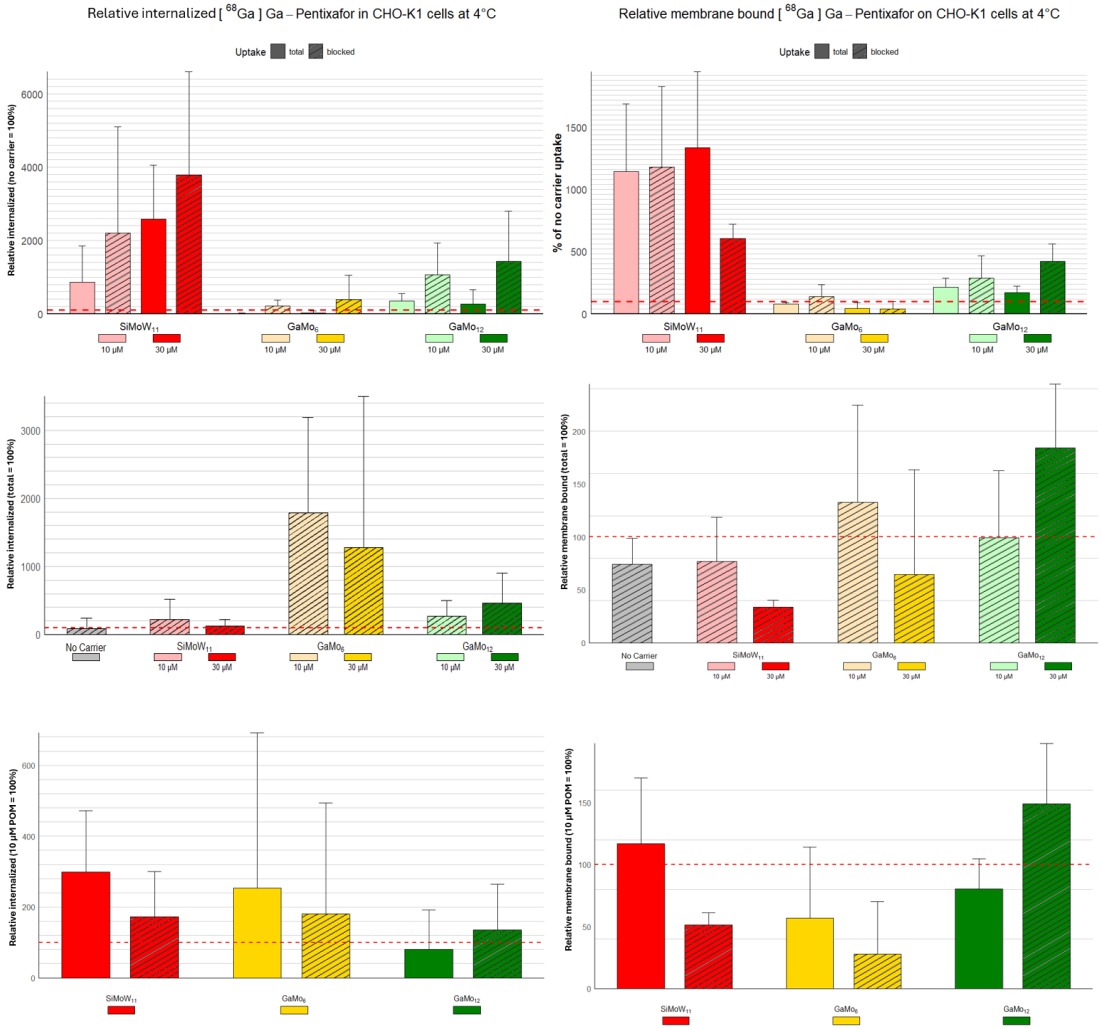

Figure 63 Relative membrane-bound and internalized fractions of [^{68}Ga]Ga–Pentixafor in CHO–K1 cells at 4 °C

Top row: Uptake and blocked fractions normalized shown relative to their respective "No carrier" values (= 100 %)

Middle row: Blocked fractions normalized to the respective total uptake (= 100 %)

Bottom row: Uptake at 30 µM normalized to uptake at 10 µM (= 100 %)

[^{68}Ga]Ga-PSMA-11

The influence of the POMs $SiMoW_{11}$, $GaMo_6$ and $GaMo_{12}$ on the internalization and membrane binding of [^{68}Ga]Ga-PSMA-11 in CHO-K1 PSMA and CHO-K1 cells at 37 °C and 4 °C was determined (Figure 64 - Figure 71) and statistically evaluated (Table 12 - Table 14). The results are discussed in more detail below.

The rates of internalization and membrane binding of [^{68}Ga]Ga-PSMA-11 in CHO-K1 PSMA and CHO-K1, both at 37 °C and 4 °C, in the presence of $SiMoW_{11}$, $GaMo_6$ and $GaMo_{12}$ were statistically compared to those of the corresponding no-carrier control using a two-tailed unpaired t-test: comparisons were made separately for non-blocked and blocked conditions (Table 12). In CHO-K1 PSMA cells incubated at 37 °C, $SiMoW_{11}$ and $GaMo_{12}$ showed significantly reduced internalization at both concentrations, but only when PSMA was not inhibited. Decreases in membrane binding were also observed in the presence of $SiMoW_{11}$ and $GaMo_{12}$ at both concentrations without receptor blocking. In CHO-K1 PSMA at 4 °C, no significant differences in internalization were observed. However, $GaMo_{12}$ at 10 µM showed under blocked conditions a significant decrease in membrane binding. In CHO-K1 at 37 °C it was found that while membrane binding was not significantly affected by any of the POMs, internalization was altered by all three. $SiMoW_{11}$ and $GaMo_{12}$ led to a significant decrease in internalization under both blocked and non-blocked conditions and at both tested concentrations. $GaMo_6$ significantly reduced internalization under blocked conditions at 10 µM and at 30 µM in both blocked and not blocked conditions. In CHO-K1 at 4 °C no significant differences were observed between the no-carrier control and any of the POMs for either internalization or membrane binding.

Table 12 Statistical comparison between no carrier and POM mediated internalization (int) and membrane binding (mb) of [^{68}Ga]Ga-PSMA-11, concentrations of POM in µM

Cell line		CHO-K1 PSMA								CHO-K1							
Temperature [°C]		37				4				37				4			
Fraction		int		mb		int		mb		int		mb		int		mb	
Inhibition		no	yes	no	yes	no	yes	no	yes	no	yes	no	yes	no	yes	no	yes
$SiMoW_{11}$	10 µM	↓(*)	ns	↓(*)	ns	ns	ns	ns	ns	↓(***)	↓(*)	ns	ns	ns	ns	ns	ns
	30 µM	↓(*)	ns	↓(*)	ns	ns	ns	ns	ns	↓ (**)	↓(**)	ns	ns	ns	ns	ns	ns
$GaMo_6$	10 µM	ns	ns	ns	ns	ns	ns	ns	ns	ns	↓(**)	ns	ns	ns	ns	ns	ns
	30 µM	ns	ns	ns	ns	ns	ns	ns	ns	↓ (***)	↓ (**)	ns	ns	ns	ns	ns	ns
$GaMo_{12}$	10 µM	↓ (*)	ns	↓ (*)	ns	ns	ns	ns	↓(*)	↓(***)	↓ (**)	ns	ns	ns	ns	ns	ns
	30 µM	↓(**)	ns	↓(**)	ns	ns	ns	ns	ns	↓(**)	↓(**)	ns	ns	ns	ns	ns	ns

ns ($p > 0.05$)

** ($p < 0.05$)*

*** ($p < 0.01$)*

**** ($p < 0.001$)*

↑/↓ increase/decrease

To determine the effect of target inhibition on the internalization and membrane binding of [^{68}Ga]Ga-PSMA-11, values were compared between blocked and non-blocked conditions for each POM at different concentrations (Table 13). Regarding internalization, a significant reduction upon target inhibition in CHO-K1 PSMA at 37 °C was observed in the no-carrier control, and with $GaMo_6$ and $SiMoW_{11}$ at 10 µM in. A significant decrease in membrane binding under blocked conditions was observed for the no-carrier control and with $GaMo_6$ at 10 µM. No significant differences were observed between total and blocked conditions in either the internalized or membrane-bound fractions in CHO-K1 PSMA at 4 °C. In CHO-K1 at 37 °C, inhibiting PSMA resulted in a significant reduction in internalization in the no-carrier control. Additionally, $GaMo_6$ at 10 µM significantly reduced both membrane binding and internalization of [^{68}Ga]Ga-PSMA-11. Furthermore, no significant differences were found when comparing blocked to non-blocked conditions in CHO-K1 at 4 °C.

Table 13 Statistical comparison between inhibited and not inhibited internalization (int) and membrane binding (mb) of [^{68}Ga]Ga-PSMA-11

Cell line		CHO-K1 PSMA				CHO-K1			
Temperature [°C]		37		4		37		4	
		int	mb	int	mb	int	mb	int	mb
$SiMoW_{11}$	10 µM	↓ (**)	ns	ns	ns	ns	ns	ns	ns
	30 µM	ns	ns	ns	ns	ns	ns	ns	ns
$GaMo_6$	10 µM	↓ (*)	↓ (*)	ns	ns	↓(*)	↓(*)	ns	ns
	30 µM	ns	ns	ns	ns	ns	ns	ns	ns
$GaMo_{12}$	10 µM	ns	ns	ns	ns	ns	ns	ns	ns
	30 µM	ns	ns	ns	ns	ns	ns	ns	ns
NC		↓ (**)	↓ (*)	ns	ns	↓(***)	ns	ns	ns

ns ($p > 0.05$)
** ($p < 0.05$)*
*** ($p < 0.01$)*
**** ($p < 0.001$)*
↑/↓ increase/decrease

The effect of POM concentrations was also assessed (Table 14). In CHO-K1 PSMA at 37 °C only the increase of $SiMoW_{11}$ concentration from 10 µM to 30 µM led to a significant reduction of [^{68}Ga]Ga-PSMA-11 internalization under non-blocked conditions. A significant decrease in membrane binding was observed for $GaMo_6$ without target inhibition going from 10 µM to 30 µM. At 4°C in CHO-K1 PSMA however, increasing the concentration of POMs also did not significantly influence either fraction. In CHO-K1 at 37 °C a higher concentration of $SiMoW_{11}$ significantly reduced internalization of [^{68}Ga]Ga-PSMA-11 under blocked and non-blocked conditions, while $GaMo_6$ had a significantly decreasing effect in the absence of 2-PMPA. However, membrane binding was not significantly changed by an increased POM concentration. At 4°C in CHO-K1, no significant differences between 10 µM and 30 µM POM were determined.

Table 14 Statistical comparison between 10 µM and 30 µM of applied POM in terms of internalization (int) and membrane binding (mb) of [^{68}Ga]Ga-PSMA-11

Cell line	CHO-K1 PSMA								CHO-K1							
Temperature [°C]	37				4				37				4			
Fraction	int		mb		int		mb		int		mb		int		mb	
Inhibition	no	yes	no	yes	no	yes	no	yes	no	yes	no	yes	no	yes	no	yes
$SiMoW_{11}$	↓(*)	ns	ns	ns	ns	ns	ns	ns	↓(**)	↓(**)	ns	ns	ns	ns	ns	ns
$GaMo_6$	ns	ns	↓(*)	ns	ns	ns	ns	ns	↓(*)	ns	ns	ns	ns	ns	ns	ns
$GaMo_{12}$	ns	ns	ns	ns	ns	ns	ns	ns	ns	ns	ns	ns	ns	ns	ns	ns

ns ($p > 0.05$)

** ($p < 0.05$)*

*** ($p < 0.01$)*

**** ($p < 0.001$)*

↑/↓ increase/decrease

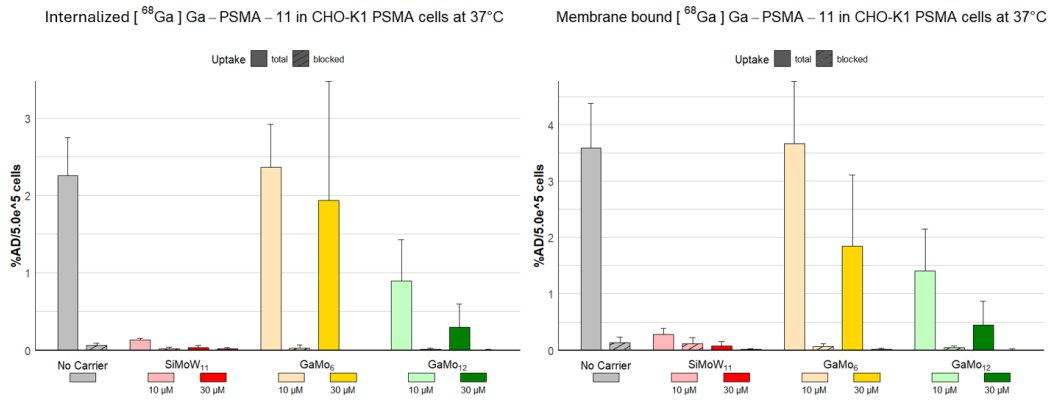

Figure 64 Membrane bound and internalized percentage of applied dosage (%AD) of [^{68}Ga]Ga-PSMA-11 in CHO-K1 PSMA cells at 37 °C

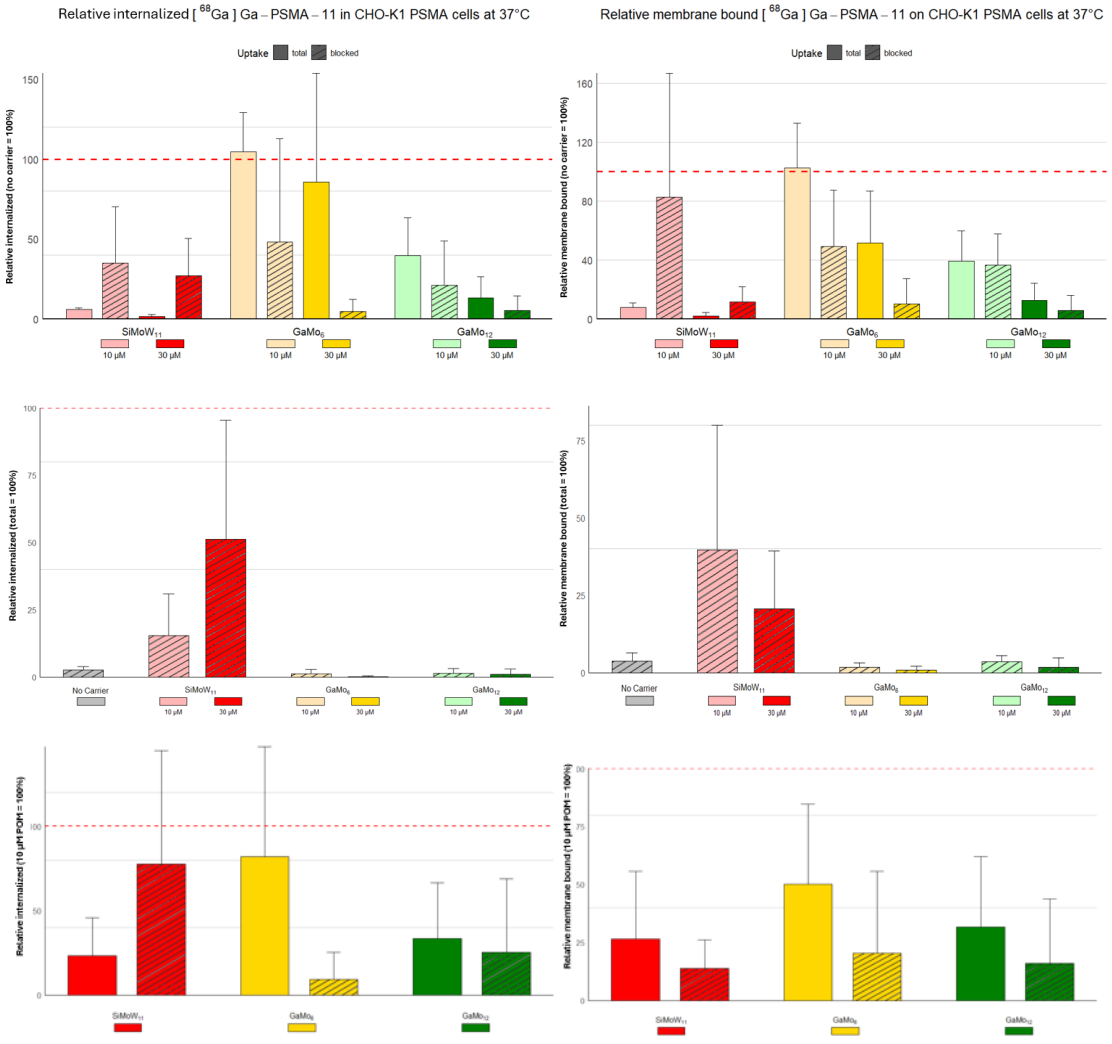

Figure 65 Relative membrane-bound and internalized fractions of [^{68}Ga]Ga–PSMA-11 in CHO–K1 PSMA cells at 37 °C

Top row: Uptake and blocked fractions normalized shown relative to their respective "No carrier" values (= 100 %)

Middle row: Blocked fractions normalized to the respective total uptake (= 100 %)

Bottom row: Uptake at 30 µM normalized to uptake at 10 µM (= 100 %)

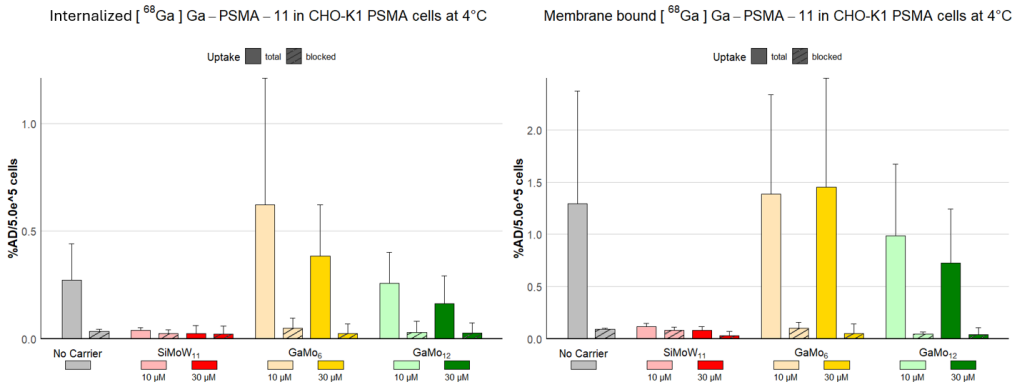

Figure 66 Membrane bound and internalized percentage of applied dosage (%AD) of [^{68}Ga]Ga-PSMA-11 in CHO-K1 PSMA cells at 4 °C

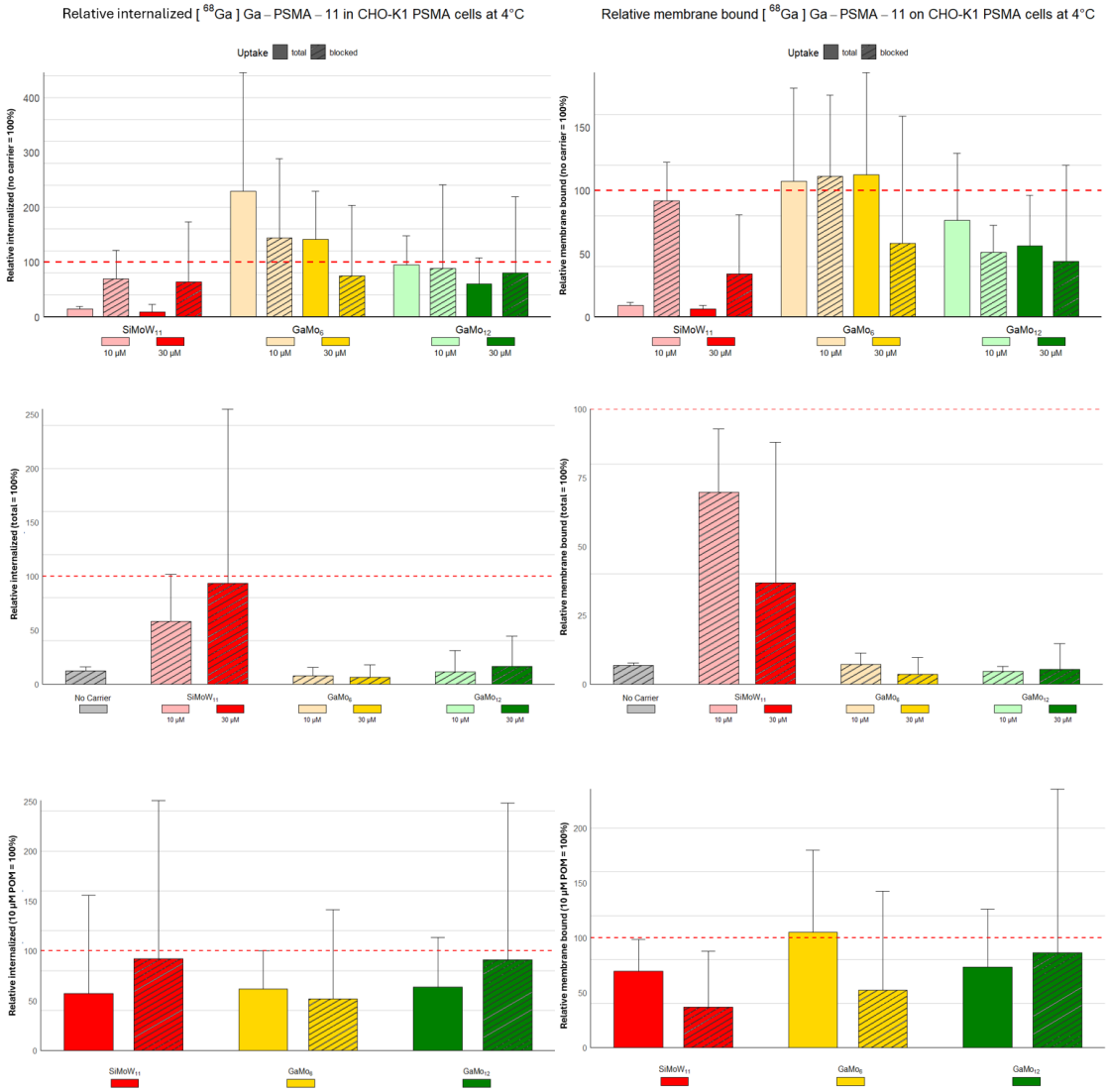

Figure 67 Relative membrane-bound and internalized fractions of [^{68}Ga]Ga–PSMA-11 in CHO–K1 PSMA cells at 4 °C

Top row: Uptake and blocked fractions normalized shown relative to their respective "No carrier" values (= 100 %)

Middle row: Blocked fractions normalized to the respective total uptake (= 100 %)

Bottom row: Uptake at 30 µM normalized to uptake at 10 µM (= 100 %)

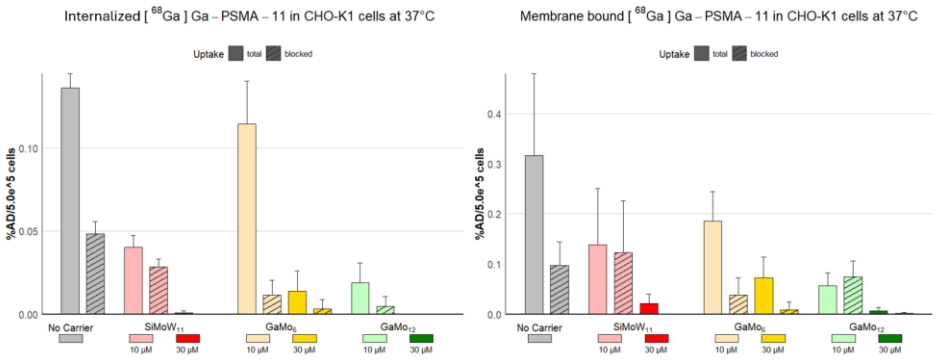

Figure 68 Membrane bound and internalized percentage of applied dosage (%AD) of [^{68}Ga]Ga-PSMA-11 in CHO-K1 cells at 37 °C

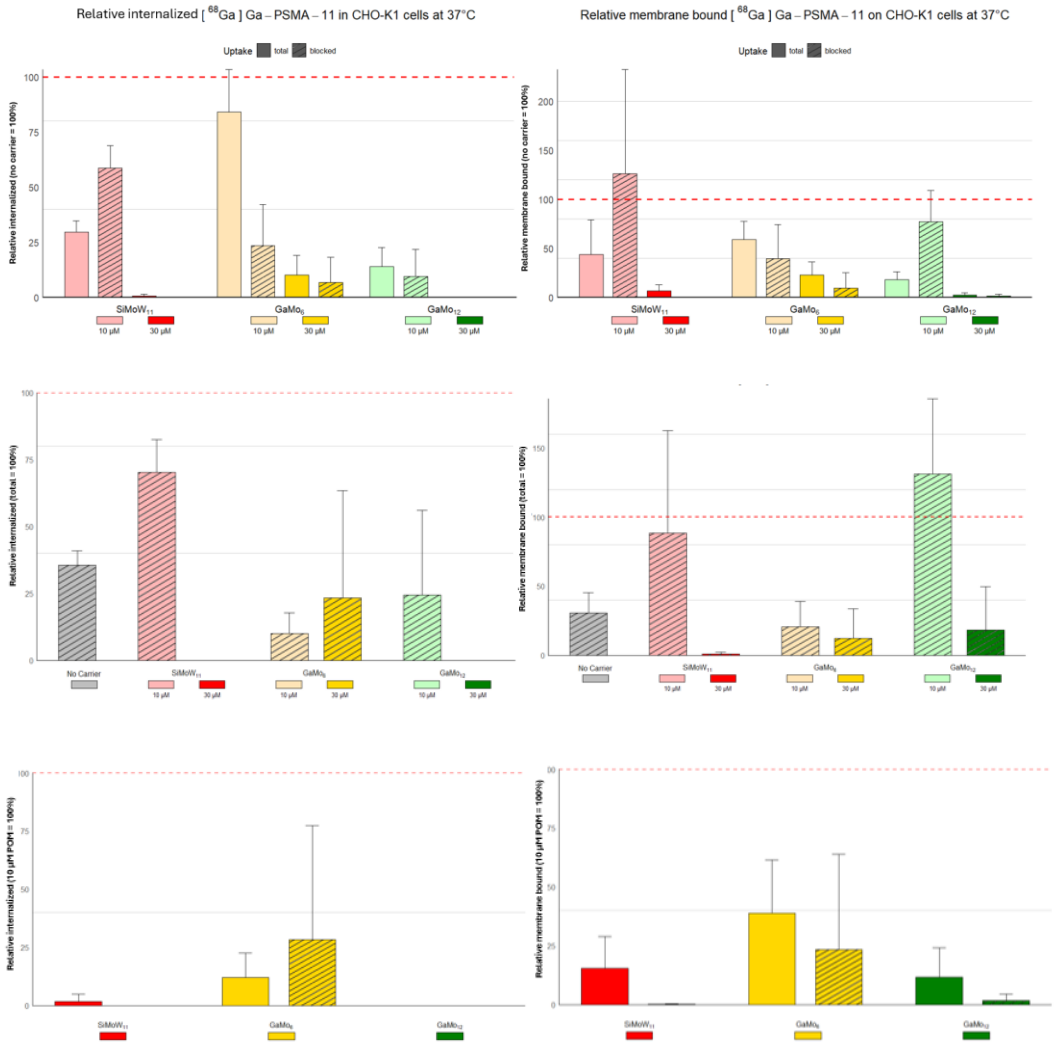

Figure 69 Relative membrane-bound and internalized fractions of [^{68}Ga]Ga–PSMA-11 in CHO–K1 cells at 37 °C

Top row: Uptake and blocked fractions normalized shown relative to their respective "No carrier" vs (= 100 %)
Middle row: Blocked fractions normalized to the respective total uptake (= 100 %)
Bottom row: Uptake at 30 µM normalized to uptake at 10 µM (= 100 %)

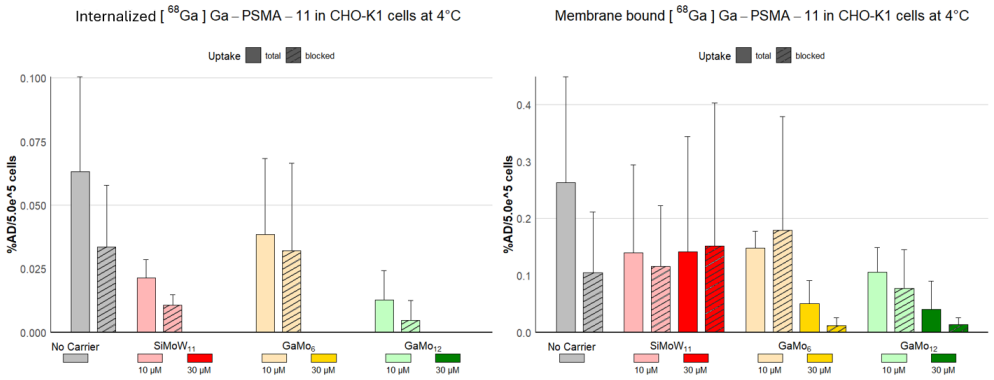

Figure 70 Membrane bound and internalized percentage of applied dosage (%AD) of [^{68}Ga]Ga-PSMA-11 in CHO-K1 cells at 4 °C

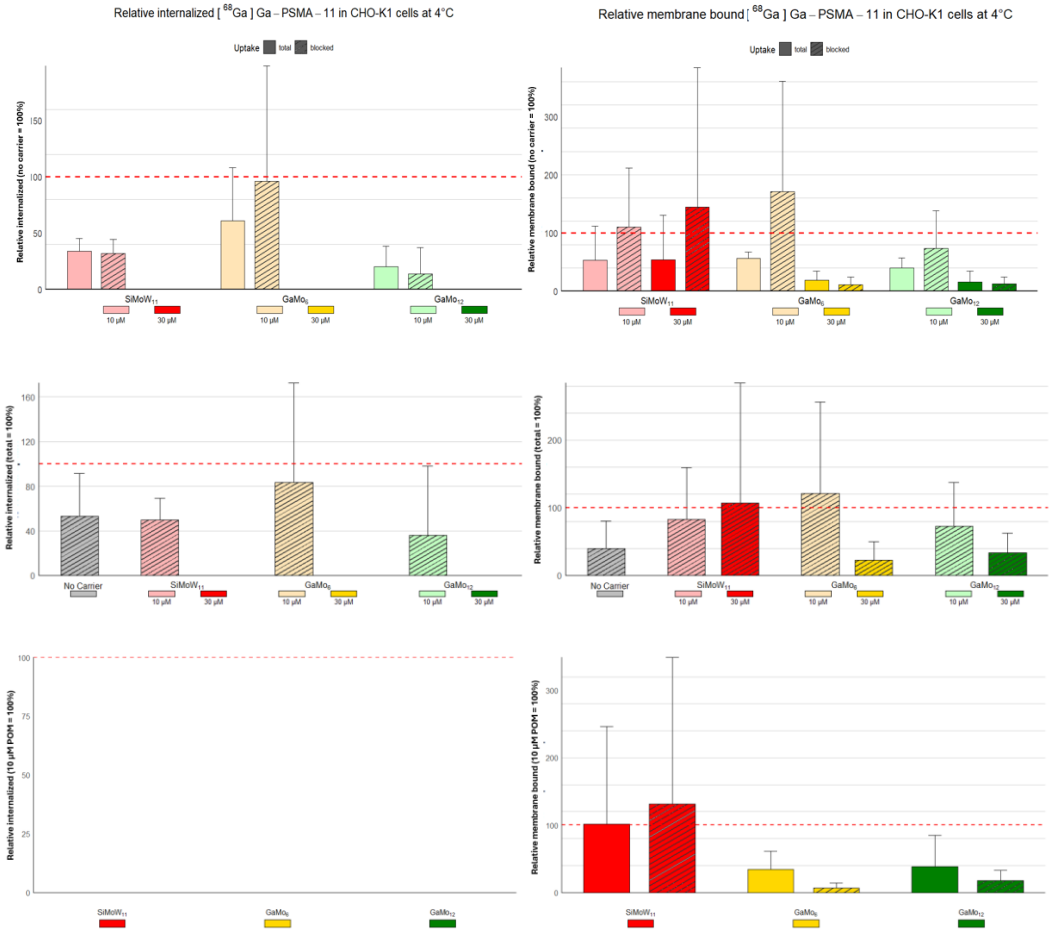

Figure 71 Relative membrane-bound and internalized fractions of [^{68}Ga]Ga–PSMA-11 in CHO–K1 cells at 4 °C

Top row: Uptake and blocked fractions normalized shown relative to their respective "No carrier" values (= 100 %)
Middle row: Blocked fractions normalized to the respective total uptake (= 100 %)
Bottom row: Uptake at 30 µM normalized to uptake at 10 µM (= 100 %)

2.6.6. Discussion

[^{68}Ga]Ga-Pentixafor

The most promising candidate among the tested POMs is $SiMoW_{11}$, who showed astonishing increase in [^{68}Ga]Ga-Pentixafor internalization compared to the no carrier control in both cell lines, especially when CXCR4 is inhibited. While the obtained data does not provide any kinetic data about this internalization process, it is speculated that this effect could be caused by a higher availability of [^{68}Ga]Ga-Pentixafor when CXCR4 is inhibited. Membrane binding seems to be largely unaffected by $SiMoW_{11}$, it was only determined to decrease membrane binding compared to the control in HT29 at 37 °C with a concentration of 30 µM when the receptor was not inhibited. Since the decrease in membrane binding appeared in the cells where internalization was highly increased, it could be hypothesized that these two effects might be connected. A higher rate of receptor internalization facilitated by POM which would lead to a lower availability of tracer could be a possible explanation. Contradictory, in CHO-K1 at 37 °C with target inhibition $SiMoW_{11}$ caused a significant increase of membrane binding compared to the no carrier control. However, since the mechanism of that effect is not known, it is abstained from drawing any definite conclusions. Since the increased levels of internalization compared to the no carrier control are present in both tested cell lines at 37 °C (though the effect is not as strong in CHO-K1) and in HT29 at 4 °C at least at 30 µM $SiMoW_{11}$ without inhibition, it is not conclusive whether that phenomenon involves the targeted receptor CXCR4 or another active internalization pathway. Inhibiting the target receptor displayed inconsistent results among the cell lines. Whereas in HT29 at 37 °C inhibiting the receptor showed only a significant increase in internalization at 10 µM, in CHO-K1 at the same temperature, inhibition showed an increasing effect at both concentrations. This could indicate that the enhancing effect of receptor inhibition could reach a saturation point. In both cell lines at 4 °C a difference between blocked and total internalization was not detected. An increase in $SiMoW_{11}$ concentration from 10 to 30 µM showed a significant increase in internalization without inhibition, which could indicate concentration dependence.

$GaMo_{12}$ seems to be another promising candidate, although not as strongly as $SiMoW_{11}$, since it also showed increased internalization compared to no carrier in HT29 at 37 °C without inhibition. However, inhibition did not show any significant differences. Membrane binding showed to be largely unaffected by $GaMo_{12}$ compared to the no carrier control except for CHO-K1 at 4 °C with target inhibition, where it led to a significant increase in binding. However, a reduction in membrane binding in HT29 at 37 °C compared to the not inhibited counterpart was determined at both tested concentrations. No concentration dependance was determined either in internalization or membrane binding for $GaMo_{12}$. Since $GaMo_{12}$ and $SiMoW_{11}$ are of the Keggin type and both show an increase in internalization of [^{68}Ga]Ga-Pentixafor to varying degrees, it can be assumed that the structure could be a factor in this observed phenomena.

To further verify this claim, these experiments could be expanded utilizing other Keggin type POMs. Given that both POMs did show at least partial increase in internalization, it indicates that they possess membrane carrier properties for Pentixafor.

The Anderson type POM $GaMo_6$ did not show an increase in internalization in any of the cell lines at any temperature compared to the no carrier control. It did however decrease membrane binding at 30 µM when the receptor was not inhibited. In HT29 at 37 °C, receptor inhibition only led to a decreased internalization and membrane binding compared to the not inhibited counterpart at 10 µM and a decrease in membrane binding at 30 µM. In the same cell line at 4 °C $GaMo_6$ only displayed a decrease in membrane binding at 30 µM comparing inhibited and not inhibited conditions. Membrane binding behavior facilitated by $GaMo_6$ seems to be only concentration dependent in HT29 at 37 °C with no inhibition, where an increase of POM concentration leads to decrease in membrane binding. Since the only determined effects of this POM were determined in terms of membrane binding, it can be assumed that $GaMo_6$ does not have any significant functionality as a membrane carrier for Pentixafor.

[^{68}Ga]Ga-PSMA-11

Contrary to the experiments with [^{68}Ga]Ga-Pentixafor, $SiMoW_{11}$ and $GaMo_{12}$ showed decreased internalization of [^{68}Ga]Ga-PSMA-11 in CHO-K1 PSMA and CHO-K1 at 37 °C at both tested concentrations. In CHO-K1 PSMA, this effect was only visible when the receptor was accessible, in CHO-K1 however internalization was decreased with and without inhibition. Interestingly, membrane binding was only impaired by $SiMoW_{11}$ and $GaMo_{12}$ in CHO-K1 PSMA without target inhibition. Compared between inhibited and not inhibited internalization, only in CHO-K1 PSMA at 37 °C internalization was significantly impaired by $SiMoW_{11}$. This inhibitory effect on internalization of $SiMoW_{11}$ is shown to be concentration dependent only in CHO-K1 PSMA at 37 °C. In other conditions, an increase of concentration did not impact either internalization or membrane binding. $GaMo_{12}$ did not show any significant differences between inhibited and uninhibited membrane binding or internalization and did not show any concentration dependance. Since $SiMoW_{11}$ and $GaMo_{12}$ are both Keggin type POMs and both exhibit similar inhibitory effects on [^{68}Ga]Ga-PSMA-11 internalization, it should also be tested whether other Keggin type POMs exert the same effects, to clarify whether these inhibitory effects are structure-related or dependent on the metals of the POMs.

Interestingly, in $GaMo_6$, inhibitory effects were only in CHO-K1 at 37 °C, where it caused a decrease in internalization at both concentrations with receptor inhibition, and at 30 µM even without receptor inhibition. Membrane binding remained unaffected compared to the no carrier control. Comparing internalization between blocked and total internalization and membrane binding, it is shown that both are impaired with this POM in both cell lines at 37 °C at a concentration of 10 µM. Concentration dependance was determined with $GaMo_6$ in CHO-K1

PSMA for the decrease in membrane binding at 37 °C and in CHO-K1 for the decrease in internalization at the same temperature. It seems that $GaMo_6$ might not be completely inert in terms of peptide interactions, since it did show some inhibitory effects on PSMA-11 internalization in CHO-K1 at 37 °C. It should be verified if this is also the case for other Anderson type POMs to determine a possible structure-effect relationship.

In some experiments with particularly low overall uptake, certain fractions displayed activity levels below the detection limit, complicating statistical analyses. To investigate the POMs behavior under those conditions more thoroughly, it is recommended to upscale these experiments. Using cell culture vessels with larger surface areas to increase cell numbers would increase the overall detected radioactivity per fraction, potentially helping to obtain values above the detection limit.

The decrease in [^{68}Ga]Ga-PSMA-11 could result from an interaction of the POMs either with the tracer itself or with the PSMA receptor before tracer binding. A competitive inhibition mechanism is supported by the observation that both membrane binding and internalization are decreased, with $SiMoW_{11}$ and $GaMo_{12}$ in CHO-K1 PSMA at 37 °C especially. This could suggest that the obstructive effect of the POMs probably happens before [^{68}Ga]Ga-PSMA-11 binds to the receptor. Potential interactions between POMs and [^{68}Ga]Ga-PSMA-11 could be investigated using size-exclusion chromatography. However, it is also possible that the POMs act as PSMA inhibitors and do not primarily interact with the tracer at all. This could be evaluated by performing affinity assays between the POMs and PSMA.

Comparison between [^{68}Ga]Ga-PSMA-11 and [^{68}Ga]Ga-Pentixafor results

The most interesting effect observed in these assays is the fact that the same POMs interact with two different peptides in different ways. Whereas the Keggin type POMs caused a significant increase in internalization for [^{68}Ga]Ga-Pentixafor, a decrease was observed with [^{68}Ga]Ga-PSMA-11. The Anderson type POM showed barely any effect with [^{68}Ga]Ga-Pentixafor, and a partial decrease of internalization with [^{68}Ga]Ga-PSMA-11. These observations point out that the underlying process is more complex than a simple permeabilization of the cell membrane by the POMs. Both tracers contain one positively charged peptide ([^{68}Ga]Ga-Pentixafor contains arginine, [^{68}Ga]Ga-PSMA-11 contains lysine), as it was established previously that they act as membrane carriers for positively charged peptides.[1] However, they do not contain the same linker, Pentixafor contains 4-AMBA, whereas [^{68}Ga]Ga-PSMA-11 contains AHX. Both contain a carbonyl group, however 4-AMBA possesses an aromatic ring, which could potentially influence interaction via π-stacking. AHX in contrast is aliphatic, which offers more flexibility at the hinge between the peptide and the chelator of PSMA-11. POMs are known to interact with strongly with conjugated systems.[98]

However, the data obtained unfortunately do not point towards a certain mechanism how that influences the internalization of these tracers.

Those results could be potentially exploited for medical applications, since the ligands of the PET tracers are currently under investigation for therapeutic applications by switching out gallium-68 with other radionuclides.[99] Modifications made to POM or connecting them to the tracer could make the effect more specific, posing the possibility of a targeted therapy approach. Also, if the inhibition arises from an interaction between receptor and POM, the inhibition of PSMA-11 could be medically useful.[100]

While those results are indeed interesting and highly relevant, certain parameters of that phenomenon are still unclear and demand further investigation. While an effect was observed, the collected data does not sufficiently indicate an underlying mechanism. While kinetic data would have been obtainable if the LigandTracer® experiments worked, it was not possible to solve the issue surrounding the high background signal during this master's thesis. If there is a solution to be found, repeating the LigandTracer® experiments could provide useful kinetic data of how cells and tracer interact in the presence of POM. An alternative approach to further explore the underlying mechanisms would be to test whether the POMs themselves bind to the cell membrane or even get internalized, using the same experimental setup, but with radioactive POMs instead of PET tracers. Prior to the start of this thesis, $GaMo_6$ was successfully synthesized with gallium-68 ($[^{68}Ga]GaMo_6$) instead of gallium-69 and internalization experiments were performed. Different concentrations (1 to 100 nmol) and incubation times (10 to 60 min) were tested. However, uptake was only negligible (<0.5%AD/1×10^6 cells), consistent with the lack of effect of $GaMo_6$ on the uptake of tested peptide-based tracers, [^{68}Ga]Ga-PSMA-11 and [^{68}Ga]Ga-Pentixafor. Attempts were also made to synthesize $GaMo_{12}$ with gallium-68 ($[^{68}Ga]GaMo_{12}$), but these were not successful, hence no uptake experiments were performed using this POM. Alternatively, electron microscopy could be employed to visualize interaction of POMs with cells by localizing metals such as gallium, tungsten or vanadium, as already used with gold-nanoparticles.[101]

3. General discussion and conclusions

The main aim of the MTT experiments was to determine the IC_{50} values of $GaMo_6$ and $GaMo_{12}$ to ensure that the concentrations used in subsequent experiments would not induce cytotoxic effects that might confound interpretation. Since the subsequent experiments were conducted at concentrations not exceeding 30 µM, it is safe to assume that cytotoxicity did not interfere with the results. Additionally, no proliferative effects were observed in estrogen receptor-positive T47D cells, which had previously been reported for other molybdenum-containing structures and MCF7 cells.[2] Due to the low solubility of $GaMo_{12}$ in water, full S-curves could not be established in most experiments as the bottom plateau was not reached. Although IC_{50} values could still be determined, these may be slightly inaccurate due to a possibly incomplete curve fitting. Since $SiMoW_{11}$ had already been used in prior cell experiments,[1] toxicity testing for this POM was not repeated.

For fluorescence experiments, an in-house synthesis of FITC-octaarginine was attempted. However, the synthesis was not successful under the utilized conditions. Given that this was not the main objective of this thesis and an optimization of the reaction conditions as well as the purification would be time-consuming, further optimizations were not made. Instead, commercially available FITC-octaarginine was used in the subsequent experiments.

Fluorescence microscopy experiments were performed using commercially available FITC-protamine and FITC-octaarginine. Although $SiMoW_{11}$ was previously reported to exhibit membrane carrier properties for both peptides,[1] this was not confirmed in the fluorescence microscopy experiments performed according to the published protocol, even after consulting the authors. The discrepancy in results for FITC-protamine may be explained by the fact that the original study used artificial membranes for evaluation of membrane carrier properties of $SiMoW_{11}$ for protamine, whereas this thesis used cells and a different type of experiment. One possible explanation is the presence of an AHX-linker in the commercial FITC-octaarginine used here, whereas this was not specified in the published study. For FITC-protamine, there was no specification of a linker by the manufacturer. Additional experimental factors may also have contributed: a very high background signal was a reoccurring problem during those experiments, possibly due to peptide adhesion to the plastic surface, which could also impact uptake. In the published paper, improved imaging was achieved using live cells and a confocal microscope, although effects were visible also in fixed cells. Unfortunately, confocal microscopy was not available for this thesis. A different method, such as FACS, might be better suitable for quantifying cellular uptake than the rather subjective image-based assessments and comparisons.

LigandTracer® technology was employed to investigate POM effects in real time. However, [^{68}Ga]Ga-Pentixafor showed elevated non-specific binding to the plastic of the used cell culture dish, producing a background signal nearly as strong as the cell-associated signal. Various pre-treatment strategies, including surface coating and use of surfactants like Tween-20, were previously tested without success (unpublished). Given these limitations, but also since conventional well-plate assays are less susceptible to plastic binding, this method was not further used.

Using conventional well-plate internalization experiments, $SiMoW_{11}$ and $GaMo_{12}$ showed effects on internalization, either due to their interaction with peptide-based tracers [^{68}Ga]Ga-PSMA-11 and [^{68}Ga]Ga-Pentixafor, or with their biological targets - enzyme PSMA and G-protein-coupled receptor CXCR4. Of particular interest is the differential behavior of these POMs depending on the tracer used.

The mode of action for the increased [^{68}Ga]Ga-Pentixafor uptake is not entirely clear, it is uncertain whether the POMs influence passive or active processes and whether they act on the receptor or radiotracer itself. Furthermore, a potential synergistic effect on [^{68}Ga]Ga-Pentixafor uptake was observed when combining the CXCR4 inhibitor AMD3100 (pharmacological, inhibitory concentrations) with $SiMoW_{11}$. Since[^{68}Ga]Ga-Pentixafor has a therapeutic analogue, [^{177}Lu]Lu-Pentixather (and other radiotherapeutic variants),[102] these findings may be relevant for enhancing delivered radioactivity dose to the treated cancer cells. While the observed effects seem partly untargeted, conjugation of POMs to specific targeting ligands may overcome this limitation.

While both $SiMoW_{11}$ and $GaMo_{12}$ reduced the internalization of [^{68}Ga]PSMA-11, they increased the internalization of [^{68}Ga]Ga-Pentixafor. This suggests that the effects are not due to non-specific mechanisms such as membrane perforation but likely involve tracer- or receptor-specific interactions. In the case of [^{68}Ga]Ga-PSMA-11, the data suggest that $SiMoW_{11}$, $GaMo_{12}$ and to a lower extent also $GaMo_6$ may act as PSMA inhibitors, which would also have useful medical applications, if the interaction is proven to be between POM and receptor. However, the data does not exclude a possible interaction between [^{68}Ga]Ga-PSMA-11 and POM, which could also be a plausible explanation for the reduced internalization.

4. Summary

- MTT assays allowed determination of highest possible, non-cytotoxic concentrations for $GaMo_6$ and $GaMo_{12}$ for subsequent experiments, enabling unbiased interpretation of the results
- No proliferative effects on T47D by $GaMo_6$ and $GaMo_{12}$ were determined *via* MTT
- In house synthesis of FITC-octaarginine was not successful with the attempted conditions
- Attempts to reproduce published results on membrane carrier properties of $SiMoW_{11}$ using fluorescence experiments were unsuccessful and therefore, these properties could not be evaluated using these types of experiments for $GaMo_6$ and $GaMo_{12}$
- LigandTracer® experiments were not conclusive due to high background signal
- $SiMoW_{11}$ and $GaMo_{12}$ influenced the internalization of [^{68}Ga]Ga-PSMA-11 and [^{68}Ga]Ga-Pentixafor in opposing ways, suggesting receptor- or tracer-specific interactions rather than a non-specific membrane effects
- $GaMo_6$ showed no interaction with [^{68}Ga]Ga-Pentixafor but partial decrease in [^{68}Ga]Ga-PSMA-11, giving the impression that POMs of the Anderson type might not be completely inert towards peptides

5. References

[1] A. Barba-Bon *et al.*, 'All-Inorganic Polyoxometalates Act as Superchaotropic Membrane Carriers', *Adv. Mater.*, vol. 36, no. 1, Jan. 2024, doi: 10.1002/adma.202309219.

[2] M. Domínguez-García *et al.*, 'New tungstenocenes containing 3-hydroxy-4-pyrone ligands: antiproliferative activity on HT-29 and MCF-7 cell lines and binding to human serum albumin studied by fluorescence spectroscopy and molecular modeling methods', *JBIC J. Biol. Inorg. Chem.*, vol. 18, no. 2, pp. 195–209, Feb. 2013, doi: 10.1007/s00775-012-0964-2.

[3] B. Artetxe *et al.*, in *Polyoxometalates*, New York: Jenny Stanford Publishing, 2022, pp. 2–8 and 310. doi: 10.1201/9781003277446.

[4] F. Carvalho *et al.*, 'Polyoxometalates Impact as Anticancer Agents', *Int. J. Mol. Sci.*, vol. 24, no. 5, Mar. 2023, doi: 10.3390/ijms24055043.

[5] B. Sarr *et al.*, 'Two new inorganic–organic hybrid materials based on β- and γ-octamolybdate clusters: Synthesis, structure determination and solid-state photochromic properties', *Polyhedron*, vol. 194, p. 114919, Jan. 2021, doi: 10.1016/j.poly.2020.114919.

[6] N. I. Gumerova *et al.*, 'Antibacterial activity of polyoxometalates against Moraxella catarrhalis', *Front. Chem.*, vol. 6, no. AUG, Aug. 2018, doi: 10.3389/fchem.2018.00336.

[7] A. Bijelic *et al.*, 'The antibacterial activity of polyoxometalates: Structures, antibiotic effects and future perspectives', *Chem. Commun.*, vol. 54, no. 10, pp. 1153–1169, 2018, doi: 10.1039/c7cc07549a.

[8] S. Y. Lee *et al.*, 'Polyoxometalates - Potent and selective ecto-nucleotidase inhibitors', *Biochem. Pharmacol.*, vol. 93, no. 2, pp. 171–181, Jan. 2015, doi: 10.1016/j.bcp.2014.11.002.

[9] K. Stroobants *et al.*, 'Polyoxometalate Reactivity toward Biomolecules and their Model Systems', in *Trends in Polyoxometalates Research*, Nova Science Publishers Inc., 2015.

[10] A. Bijelic *et al.*, 'Im Kampf gegen Krebs: Polyoxometallate als nächste Generation metallhaltiger Medikamente', *Angew. Chem.*, vol. 131, no. 10, pp. 3008–3029, Mar. 2019, doi: 10.1002/ange.201803868.

[11] S. Shigeta *et al.*, 'Anti-RNA virus activity of polyoxometalates', *Biomed. Pharmacother.*, vol. 60, no. 5, pp. 211–219, June 2006, doi: 10.1016/j.biopha.2006.03.009.

[12] K. Ben Zaken *et al.*, 'Polyoxometalates bind multiple targets involved in Alzheimer's disease', *JBIC J. Biol. Inorg. Chem.*, vol. 30, no. 3, pp. 299–309, Mar. 2025, doi: 10.1007/s00775-025-02111-2.

[13] J. J. Borrás-Almenar *et al.*, *Polyoxometalate Chemistry: From Topology via Self-Assembly to Applications*. Springer, 2001.

[14] N. I. Gumerova *et al.*, 'Polyoxometalates in solution: speciation under spotlight', *Chem. Soc. Rev.*, vol. 49, no. 21, pp. 7568–7601, 2020, doi: 10.1039/D0CS00392A.

[15] D.-L. Long *et al.*, 'Polyoxometalate clusters, nanostructures and materials: From self assembly to designer materials and devices', *Chem Soc Rev*, vol. 36, no. 1, pp. 105–121, 2007, doi: 10.1039/B502666K.

[16] N. I. Gumerova, 'Powerpoint presentation "POM"'.

[17] C. Sanchez *et al.*, 'Electron delocalization in mixed-valence molybdenum polyanions', *J. Am. Chem. Soc.*, vol. 104, no. 11, pp. 3194–3202, June 1982, doi: https://doi.org/10.1021/ja00375a044.

[18] S. Himeno *et al.*, 'A route to a Keggin-Type α-[(XIIIO4)Mo12O35(OH)]4− anion through an Anderson-type [XIII(OH)6Mo6O18]3− anion: X = Ga', *Dalton Trans*, no. 31, pp. 6114–6119, 2009, doi: 10.1039/B902794G.

[19] L. P. Tsiganok *et al.*, 'UV, IR, 71Ga and 17O NMR Spectroscopic studies of the 12-Molybdogallate Heteropolyanion', *Polyhedron*, vol. 8, no. 23, pp. 2739–2742, Jan. 1989, doi: 10.1016/S0277-5387(00)80529-X.

[20] B. Alberts *et al.*, 'Molecular Biology of the Cell', 711 Third Avenue, New York, NY 10017, US: Garland Science, 2015, pp. 597–603 and 700.
[21] G. van Meer *et al.*, 'Membrane lipids: where they are and how they behave', *Nat. Rev. Mol. Cell Biol.*, vol. 9, no. 2, pp. 112–124, Feb. 2008, doi: 10.1038/nrm2330.
[22] S. M. Smith *et al.*, 'Weak Molecular Interactions in Clathrin-Mediated Endocytosis', *Front. Mol. Biosci.*, vol. 4, Nov. 2017, doi: 10.3389/fmolb.2017.00072.
[23] N. J. Yang *et al.*, 'Getting Across the Cell Membrane: An Overview for Small Molecules, Peptides, and Proteins', 2015, pp. 29–53. doi: 10.1007/978-1-4939-2272-7_3.
[24] S. Sagan *et al.*, 'Homeoproteins and Homeoprotein-derived Peptides: Going in and Out', *Curr. Pharm. Des.*, vol. 19, no. 16, pp. 2851–2862, Mar. 2013, doi: 10.2174/1381612811319160002.
[25] C. Bechara *et al.*, 'Cell-penetrating peptides: 20 years later, where do we stand?', *FEBS Lett.*, vol. 587, no. 12, pp. 1693–1702, June 2013, doi: 10.1016/j.febslet.2013.04.031.
[26] S. Futaki *et al.*, 'Arginine-rich Peptides: Methods of Translocation Through Biological Membranes', *Curr. Pharm. Des.*, vol. 19, no. 16, pp. 2863–2868, Mar. 2013, doi: 10.2174/1381612811319160003.
[27] N. Schmidt *et al.*, 'Arginine-rich cell-penetrating peptides', *FEBS Lett.*, vol. 584, no. 9, pp. 1806–1813, May 2010, doi: 10.1016/j.febslet.2009.11.046.
[28] L. Z. Benet *et al.*, 'BDDCS, the Rule of 5 and drugability', *Adv. Drug Deliv. Rev.*, vol. 101, pp. 89–98, June 2016, doi: 10.1016/j.addr.2016.05.007.
[29] K. M. Corbett *et al.*, 'Cyclosporin Structure and Permeability: From A to Z and Beyond', *J. Med. Chem.*, vol. 64, no. 18, pp. 13131–13151, Sept. 2021, doi: 10.1021/acs.jmedchem.1c00580.
[30] T. R. White *et al.*, 'On-resin N-methylation of cyclic peptides for discovery of orally bioavailable scaffolds', *Nat. Chem. Biol.*, vol. 7, no. 11, pp. 810–817, Nov. 2011, doi: 10.1038/nchembio.664.
[31] Y.-U. Kwon *et al.*, 'Quantitative Comparison of the Relative Cell Permeability of Cyclic and Linear Peptides', *Chem. Biol.*, vol. 14, no. 6, pp. 671–677, June 2007, doi: 10.1016/j.chembiol.2007.05.006.
[32] J. S. Appelbaum *et al.*, 'Arginine Topology Controls Escape of Minimally Cationic Proteins from Early Endosomes to the Cytoplasm', *Chem. Biol.*, vol. 19, no. 7, pp. 819–830, July 2012, doi: 10.1016/j.chembiol.2012.05.022.
[33] B. Thaa *et al.*, 'Viruses as vesicular carriers of the viral genome: A functional module perspective', *Biochim. Biophys. Acta BBA - Mol. Cell Res.*, vol. 1803, no. 4, pp. 507–519, Apr. 2010, doi: 10.1016/j.bbamcr.2010.01.011.
[34] H. Stricker, 'Phospholipid Liposomes as Drug Carriers: Preparation and Properties', in *Phospholipids*, I. Hanin and G. Pepeu, Eds, Boston, MA: Springer US, 1990, pp. 115–122. doi: 10.1007/978-1-4757-1364-0_9.
[35] C. Lapa *et al.*, '[^{68}Ga]Pentixafor-PET/CT for imaging of chemokine receptor CXCR4 expression in multiple myeloma - Comparison to [^{18}F]FDG and laboratory values.', *Theranostics*, vol. 7, no. 1, pp. 205–212, 2017, doi: 10.7150/thno.16576.
[36] S. Kraus *et al.*, '^{68} Ga-Pentixafor PET/CT for Detection of Chemokine Receptor CXCR4 Expression in Myeloproliferative Neoplasms', *J. Nucl. Med.*, vol. 63, no. 1, pp. 96–99, Jan. 2022, doi: 10.2967/jnumed.121.262206.
[37] L. Lindenberg *et al.*, 'Advances in PET Imaging of the CXCR4 Receptor: [68Ga]Ga-PentixaFor', *Semin. Nucl. Med.*, vol. 54, no. 1, pp. 163–170, Jan. 2024, doi: 10.1053/j.semnuclmed.2023.09.002.
[38] C. Bouter *et al.*, '^{68} Ga-Pentixafor PET/CT Imaging of Chemokine Receptor CXCR4 in Chronic Infection of the Bone: First Insights', *J. Nucl. Med.*, vol. 59, no. 2, pp. 320–326, Feb. 2018, doi: 10.2967/jnumed.117.193854.
[39] B. Debnath *et al.*, 'Small Molecule Inhibitors of CXCR4', *Theranostics*, vol. 3, no. 1, pp. 47–75, 2013, doi: 10.7150/thno.5376.
[40] A. Marchese, 'Endocytic trafficking of chemokine receptors', *Curr. Opin. Cell Biol.*, vol. 27, pp. 72–77, Apr. 2014, doi: 10.1016/j.ceb.2013.11.011.

[41] A. Weich *et al.*, ‘Wnt/β-Catenin Signaling Regulates CXCR4 Expression and [68Ga] Pentixafor Internalization in Neuroendocrine Tumor Cells’, *Diagnostics*, vol. 11, no. 2, p. 367, Feb. 2021, doi: 10.3390/diagnostics11020367.
[42] G. Rodríguez-Berriguete *et al.*, ‘MAP Kinases and Prostate Cancer.’, *J. Signal Transduct.*, vol. 2012, p. 169170, 2012, doi: 10.1155/2012/169170.
[43] B. Vanhaesebroeck *et al.*, ‘The PI3K-PDK1 connection: more than just a road to PKB’, *Biochem. J.*, vol. 346 Pt 3, no. Pt 3, pp. 561–576, Mar. 2000.
[44] Y.-N. Wu *et al.*, ‘The roles of phospholipase C-β related signals in the proliferation, metastasis and angiogenesis of malignant tumors, and the corresponding protective measures’, *Front. Oncol.*, vol. 13, July 2023, doi: 10.3389/fonc.2023.1231875.
[45] D. E. Clapham, ‘Calcium Signaling’, *Cell*, vol. 131, no. 6, pp. 1047–1058, Dec. 2007, doi: 10.1016/j.cell.2007.11.028.
[46] X. Cao *et al.*, ‘A phosphorylation switch controls the spatiotemporal activation of Rho GTPases in directional cell migration’, *Nat. Commun.*, vol. 6, no. 1, p. 7721, July 2015, doi: 10.1038/ncomms8721.
[47] M. B. Dwinell *et al.*, ‘SDF-1/CXCL12 regulates cAMP production and ion transport in intestinal epithelial cells via CXCR4’, *Am. J. Physiol.-Gastrointest. Liver Physiol.*, vol. 286, no. 5, pp. G844–G850, May 2004, doi: 10.1152/ajpgi.00112.2003.
[48] X. Hu *et al.*, ‘The JAK/STAT signaling pathway: from bench to clinic’, *Signal Transduct. Target. Ther.*, vol. 6, no. 1, p. 402, Nov. 2021, doi: 10.1038/s41392-021-00791-1.
[49] N. Alouche *et al.*, ‘Cxcr4 desensitization is an essential regulatory mechanism controlling the extra-follicular B cell response’. Feb. 01, 2019. doi: 10.1101/537761.
[50] O. B. Goodman *et al.*, ‘β-Arrestin acts as a clathrin adaptor in endocytosis of the β2-adrenergic receptor’, *Nature*, vol. 383, no. 6599, pp. 447–450, Oct. 1996, doi: 10.1038/383447a0.
[51] A. Fletcher-Jones *et al.*, ‘Protein Interactors and Trafficking Pathways That Regulate the Cannabinoid Type 1 Receptor (CB1R)’, *Front. Mol. Neurosci.*, vol. 13, p. 108, Nov. 2020, doi: 10.3389/fnmol.2020.00108.
[52] R. Islam *et al.*, ‘The Role of PSMA PET Imaging in Prostate Cancer: Current Applications and Future Directions’, *Curr. Urol. Rep.*, vol. 26, no. 1, p. 46, Dec. 2025, doi: 10.1007/s11934-025-01268-2.
[53] C. Lauri *et al.*, ‘PSMA Expression in Solid Tumors beyond the Prostate Gland: Ready for Theranostic Applications?’, *J. Clin. Med.*, vol. 11, no. 21, p. 6590, Nov. 2022, doi: 10.3390/jcm11216590.
[54] B. Sheehan *et al.*, ‘Prostate-specific Membrane Antigen Biology in Lethal Prostate Cancer and its Therapeutic Implications’, *Eur. Urol. Focus*, vol. 8, May 2021, doi: 10.1016/j.euf.2021.06.006.
[55] R. E. Conway *et al.*, ‘Prostate-specific membrane antigen regulates angiogenesis by modulating integrin signal transduction.’, *Mol. Cell. Biol.*, vol. 26, no. 14, pp. 5310–24, July 2006, doi: 10.1128/MCB.00084-06.
[56] R. E. Conway *et al.*, ‘Prostate-specific membrane antigen (PSMA)-mediated laminin proteolysis generates a pro-angiogenic peptide’, *Angiogenesis*, vol. 19, no. 4, pp. 487–500, Oct. 2016, doi: 10.1007/s10456-016-9521-x.
[57] G. Winter *et al.*, ‘Modelling the internalisation process of prostate cancer cells for PSMA-specific ligands’, *Nucl. Med. Biol.*, vol. 72–73, pp. 20–25, May 2019, doi: 10.1016/j.nucmedbio.2019.05.003.
[58] Y. Gao *et al.*, ‘Prostate-Specific Membrane Antigen (PSMA) Promotes Angiogenesis of Glioblastoma Through Interacting With ITGB4 and Regulating NF-κB Signaling Pathway’, *Front. Cell Dev. Biol.*, vol. 9, Mar. 2021, doi: 10.3389/fcell.2021.598377.
[59] O. Sartor *et al.*, ‘Lutetium-177–PSMA-617 for Metastatic Castration-Resistant Prostate Cancer’, *N. Engl. J. Med.*, vol. 385, no. 12, pp. 1091–1103, Sept. 2021, doi: 10.1056/NEJMoa2107322.
[60] M. Sathekge *et al.*, ‘^{225}Ac-PSMA-617 in chemotherapy-naive patients with advanced prostate cancer: a pilot study’, *Eur. J. Nucl. Med. Mol. Imaging*, vol. 46, no. 1, pp. 129–138, Jan. 2019, doi: 10.1007/s00259-018-4167-0.

[61] O. C. Rogers *et al.*, ‘Targeted delivery of cytotoxic proteins to prostate cancer via conjugation to small molecule urea-based PSMA inhibitors’, *Sci. Rep.*, vol. 11, no. 1, p. 14925, July 2021, doi: 10.1038/s41598-021-94534-5.
[62] ‘Cell culture basics handbook’.
[63] Dr. M. O’Kane, ‘How Does A Laminar Flow Hood Work?’ Accessed: May 10, 2025. [Online]. Available: https://www.ossila.com/pages/how-does-a-laminar-flow-hood-work#:~:text=A%20laminar%20flow%20hood%20works,smoothly%20over%20the%20work%20surface
[64] L. Llobet *et al.*, ‘Side Effects of Culture Media Antibiotics on Cell Differentiation’, *Tissue Eng. Part C Methods*, vol. 21, no. 11, pp. 1143–1147, Nov. 2015, doi: 10.1089/ten.tec.2015.0062.
[65] ‘Cell Line Profile CHO-K1’, UK Health Security Agency. Accessed: Feb. 21, 2025. [Online]. Available: https://www.culturecollections.org.uk/products/cell-cultures/ecacc-cell-line-profiles/cho-k1/#:~:text=CHO%20cell%20lines%20and%20their,Modoc%20virus%20and%20Buttonwillow%20virus.
[66] ‘CHO-K1’, ATCC. Accessed: Feb. 21, 2025. [Online]. Available: https://www.atcc.org/products/ccl-61
[67] ‘HT-29’, ATCC. Accessed: June 21, 2025. [Online]. Available: https://www.atcc.org/products/htb-38
[68] D. Martínez-Maqueda *et al.*, ‘HT29 Cell Line’, in *The Impact of Food Bioactives on Health*, Cham: Springer International Publishing, 2015, pp. 113–124. doi: 10.1007/978-3-319-16104-4_11.
[69] ‘T-47D’, ATCC. Accessed: Feb. 21, 2025. [Online]. Available: https://www.atcc.org/products/htb-133
[70] ‘T47D Cell Line’, Creative Biogene. Accessed: Feb. 21, 2025. [Online]. Available: https://www.creative-biogene.com/support/t47d-cell-line.html#:~:text=The%20T47D%20cell%20line%20has%20been%20used,estrogen%20receptors%20and%20are%20responsive%20to%20estrogen.
[71] C. Giammei *et al.*, ‘Towards Dual-Tracer SPECT for Prostate Cancer Imaging Using [99mTc]Tc-PSMA-I&S and [111In]In-RM2’, *Pharmaceuticals*, vol. 18, no. 7, p. 1002, July 2025, doi: 10.3390/ph18071002.
[72] Merck, *Corning® CoolCell™ LX Zelleinfrierbehälter*. Accessed: May 10, 2025. [Online]. Available: https://www.sigmaaldrich.com/AT/de/product/sigma/cls432004?utm_source=google&utm_medium=cpc&utm_campaign=21795116152&utm_content=171621665667&gad_source=1&gbraid=0AAAAAD8kLQSdqwB70vnlGM7lP6gxZ2ZUq&gclid=Cj0KCQjwzrzABhD8ARIsANlSWNOXfTbQkkt3vp6hJU6onlIU3VU7iAjEFp4MtRMRThgACSytcQE3lCAaAhg7EALw_wcB
[73] ‘MycoAlert® Mycoplasma Detection Kit’.
[74] M. Ghasemi *et al.*, ‘The MTT Assay: Utility, Limitations, Pitfalls, and Interpretation in Bulk and Single-Cell Analysis’, *Int. J. Mol. Sci.*, vol. 22, no. 23, p. 12827, Nov. 2021, doi: 10.3390/ijms222312827.
[75] T. Riss, ‘Is Your MTT Assay Really the Best Choice?’ Accessed: May 10, 2025. [Online]. Available: https://at.promega.com/en/resources/pubhub/is-your-mtt-assay-really-the-best-choice/
[76] ‘FITC-labeling’, PeptideWeb.com. Accessed: May 10, 2025. [Online]. Available: https://www.peptideweb.com/fitc-labeling
[77] ‘FITC (Fluorescein isothiocyanate)’, AAT Bioquest. Accessed: May 10, 2025. [Online]. Available: https://www.aatbio.com/resources/application-notes/fitc-fluorescein-isothiocyanate
[78] M. Jullian *et al.*, ‘N-terminus FITC labeling of peptides on solid support: the truth behind the spacer’, *Tetrahedron Lett.*, vol. 50, no. 3, pp. 260–263, Jan. 2009, doi: 10.1016/j.tetlet.2008.10.141.
[79] Cortes Sergio, ‘Basic Principles of Chromatography’, LibreTexts Chemistry. Accessed: June 13, 2025. [Online]. Available:

https://chem.libretexts.org/Ancillary_Materials/Laboratory_Experiments/Wet_Lab_Experiments/Organic_Chemistry_Labs/Lab_I/06%3A_Exp_5-_A_and_B_TLC/6.01%3A_Basic_Principles_of_Chromatography
[80] Howard G. Barth, 'Chromatography Fundamentals, Part VIII: The Meaning and Significance of Chromatographic Resolution', LCGC International. Accessed: June 13, 2025. [Online]. Available: https://www.chromatographyonline.com/view/chromatography-fundamentals-part-viii-meaning-and-significance-chromatographic-resolution
[81] Resch William, 'Mass Spectrometry'. Accessed: June 13, 2025. [Online]. Available: https://www2.chemistry.msu.edu/faculty/reusch/virttxtjml/spectrpy/massspec/masspec1.htm
[82] Aryal Sagar, 'Mass Spectrometry Explained: Principle, Steps & Uses', Mass Spectrometry Explained: Principle, Steps & Uses. Accessed: Sept. 15, 2025. [Online]. Available: https://microbenotes.com/mass-spectrometry-ms-principle-working-instrumentation-steps-applications/
[83] K. Schaefer, 'How do I label N-teminus of a peptide with FITC?' Nov. 2015. Accessed: Oct. 02, 2025. [Online]. Available: https://www.researchgate.net/post/How_do_I_label_N-teminus_of_a_peptide_with_FITC
[84] G. Paës, 'The best protocol for FITC labeling of proteins'. Nov. 2013. Accessed: Oct. 02, 2025. [Online]. Available: https://www.researchgate.net/post/The_best_protocol_for_FITC_labeling_of_proteins
[85] 'Fluorescence', Scientific Volume Imaging. Accessed: Feb. 05, 2026. [Online]. Available: https://svi.nl/Fluorescence
[86] Ardimas, 'Report in the Optical Microscopy for Nanotechnology course Microscopy 2020'. Aug. 2020.
[87] 'IF imaging: Widefield versus confocal microscopy', proteintech. Accessed: Feb. 05, 2026. [Online]. Available: https://www.ptglab.com/news/blog/if-imaging-widefield-versus-confocal-microscopy/?srsltid=AfmBOorX-H1OHWBP6HwLD-hCf0jdwteVTgpyrp9XJyhVyTvZ540RjlWq
[88] H. C. Ishikawa-Ankerhold *et al.*, 'Advanced Fluorescence Microscopy Techniques—FRAP, FLIP, FLAP, FRET and FLIM', *Molecules*, vol. 17, no. 4, pp. 4047–4132, Apr. 2012, doi: 10.3390/molecules17044047.
[89] I. Mäger *et al.*, 'Assessing the uptake kinetics and internalization mechanisms of cell-penetrating peptides using a quenched fluorescence assay', *Biochim. Biophys. Acta BBA - Biomembr.*, vol. 1798, no. 3, pp. 338–343, Mar. 2010, doi: 10.1016/j.bbamem.2009.11.001.
[90] L. K. Chaganti *et al.*, 'An efficient method for FITC labelling of proteins using tandem affinity purification', *Biosci. Rep.*, vol. 38, no. 6, Dec. 2018, doi: 10.1042/BSR20181764.
[91] A. Markowska *et al.*, 'The Importance of 6-Aminohexanoic Acid as a Hydrophobic, Flexible Structural Element.', *Int. J. Mol. Sci.*, vol. 22, no. 22, Nov. 2021, doi: 10.3390/ijms222212122.
[92] 'Content Ligand Tracer', LigandTracer. Accessed: May 10, 2025. [Online]. Available: https://www.ligandtracer.com/product/ligandtracer/#tab-description
[93] 'Picture Ligand Tracer', LigandTracer. Accessed: May 10, 2025. [Online]. Available: https://www.umu.se/en/research/infrastructure/biochemical-imaging-centre-umea-bicu/ligand-tracer/#:~:text=The%20LigandTracer%20technology%20is%20based,A)
[94] M. Zeilinger *et al.*, 'New approaches for the reliable in vitro assessment of binding affinity based on high-resolution real-time data acquisition of radioligand-receptor binding kinetics', *EJNMMI Res.*, vol. 7, no. 1, p. 22, Dec. 2017, doi: 10.1186/s13550-016-0249-9.
[95] B. J. Burkett *et al.*, 'A Review of Theranostics: Perspectives on Emerging Approaches and Clinical Advancements', *Radiol. Imaging Cancer*, vol. 5, no. 4, July 2023, doi: 10.1148/rycan.220157.
[96] N. Jouini *et al.*, 'Evaluation of a Radiolabeled Macrocyclic Peptide as Potential PET Imaging Probe for PD−L1', *ChemMedChem*, vol. 17, no. 12, June 2022, doi: 10.1002/cmdc.202200091.

[97] S. U. Dalm *et al.*, 'Comparison of the Therapeutic Response to Treatment with a ^{177}Lu-Labeled Somatostatin Receptor Agonist and Antagonist in Preclinical Models', *J. Nucl. Med.*, vol. 57, no. 2, pp. 260–265, Feb. 2016, doi: 10.2967/jnumed.115.167007.
[98] M. Lu *et al.*, 'Hybrid Molecular Dumbbells: Bridging Polyoxometalate Clusters with an Organic π-Conjugated Rod', *Angew. Chem. Int. Ed.*, vol. 41, no. 9, pp. 1566–1568, May 2002, doi: 10.1002/1521-3773(20020503)41:9%3C1566::AID-ANIE1566%3E3.0.CO;2-Q.
[99] V. Benfante *et al.*, 'An Update on DOTA-Peptides PET Imaging and Potential Advancements of Radioligand Therapy in Intracranial Meningiomas', *Life*, vol. 15, no. 4, p. 617, Apr. 2025, doi: 10.3390/life15040617.
[100] J. D. Young *et al.*, 'Dipeptide inhibitors of the prostate specific membrane antigen (PSMA): A comparison of urea and thiourea derivatives', *Bioorg. Med. Chem. Lett.*, vol. 42, p. 128044, June 2021, doi: 10.1016/j.bmcl.2021.128044.
[101] D. Belić *et al.*, 'Imaging of Nanoscale Gold in "Intact" Biological Cells by Environmental Electron Microscopy', *J. Phys. Chem. C*, vol. 125, no. 50, pp. 27865–27875, Dec. 2021, doi: 10.1021/acs.jpcc.1c09104.
[102] M. Schottelius *et al.*, '[^{177}Lu]pentixather: Comprehensive Preclinical Characterization of a First CXCR4-directed Endoradiotherapeutic Agent', *Theranostics*, vol. 7, no. 9, pp. 2350–2362, 2017, doi: 10.7150/thno.19119.

6. Appendix

6.1. Detailed results cell toxicity experiments

The values marked green were used to determine the average and standard deviation.

CHO-K1

Table 15 Appendix - IC_{50} results $GaMo_6$ in CHO-K1

Date	IC_{50} - 3 parameter	R^2	IC_{50} - 4 parameter	R^2
7/10/2024	0.2148	0.8484	0.1986	0.9923
7/7/2024	0.1841	0.9214	0.1805	0.9913
6/26/2024	0.1704	0.9085	0.198	0.934
6/23/2024	0.1922	0.9118	0.1946	0.9754
6/16/2024	0.1319	0.9467	0.1495	0.1632
6/19/2024	0.1378	0.9405	0.1637	0.9474
6/11/2024	0.3128	0.9834	0.2767	0.9896
7/14/2024	0.1749	0.8375	0.1695	0.9906
6/4/2024	0.1863	0.9046	0.1673	0.9706
6/9/2024	-	-	-	-
5/26/2024	0.0199	0.6511	1.77E-05	0.6553
		Average	0.189	
		SD	0.0371	

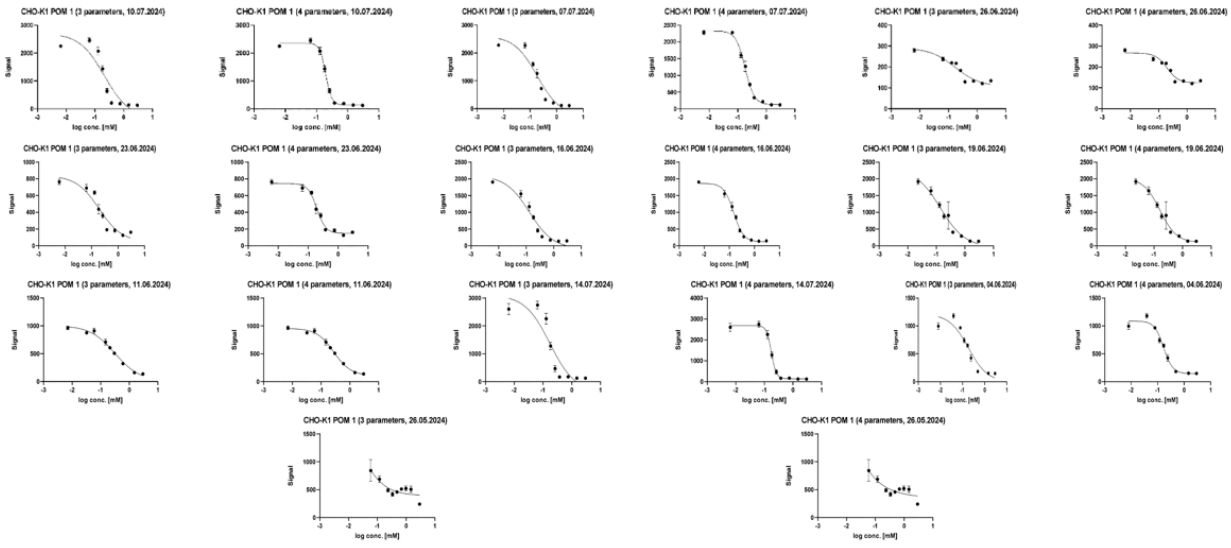

Figure 72 Appendix - IC_{50} results $GaMo_6$ in CHO-K1

Table 16 Appendix - IC_{50} results $GaMo_{12}$ in CHO-K1

Date	IC_{50} - 3 parameter	R^2	IC_{50} - 4 parameter	R^2
7/10/2024	3340	0.9449	0.195	0.9783
7/7/2024	445.7	0.9236	0.145	0.9435
6/26/2024	94335	???	0.2664	0.2574
6/23/2024	1.922	0.9493	57.73	0.9494
6/16/2024	312.3	0.7618	0.1115	0.8376
6/19/2024	0.1301	0.9551	0.2563	0.9565
6/11/2024	362.5	0.859	0.5456	0.8678
7/14/2024	659.8	0.7923	0.9109	0.8331
6/4/2024	1.668	0.6661	0.1273	0.8068
6/9/2024	0.4691	0.966	0.1158	0.9781
5/26/2024	0.1372	0.9628	0.09374	0.9646
		Average	0.131	
		SD	0.0355	

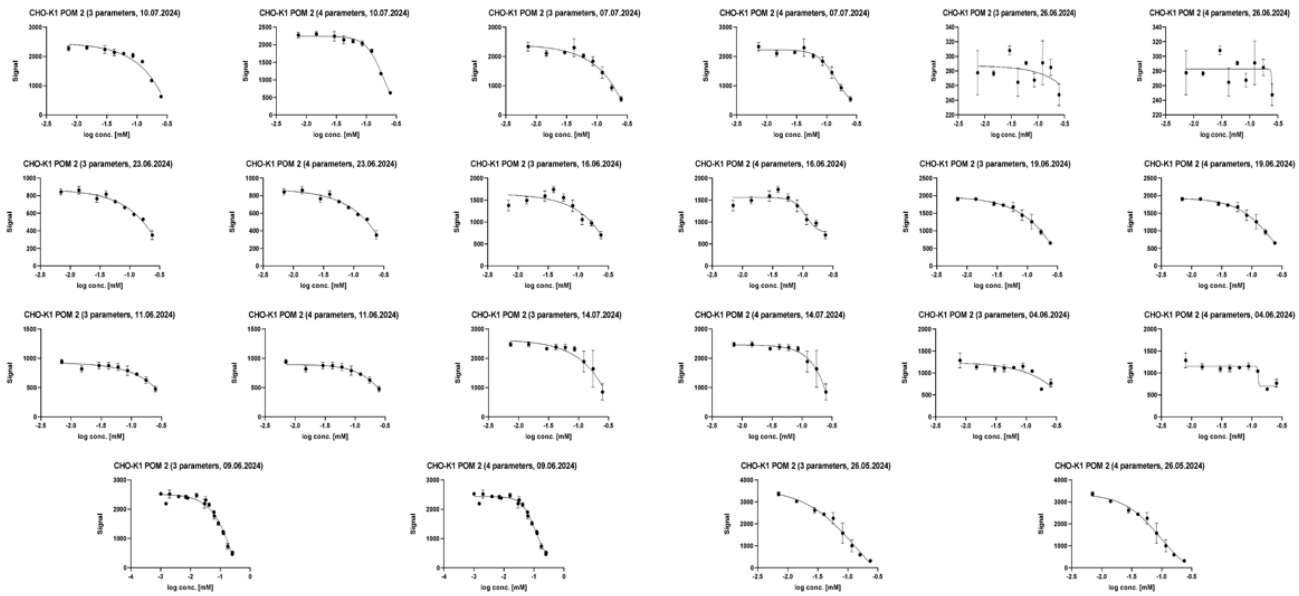

Figure 73 Appendix - IC_{50} results $GaMo_{12}$ in CHO-K1

HT29

Table 17 Appendix – IC_{50} results $GaMo_6$ in HT29

Date	IC50 – 3 parameter	R2	IC50 – 4 parameter	R2
6/26/2024	0.05984	0.9672	0.07278	0.9688

6/23/2024	0.01612	0.9809	0.03134	0.9858
7/10/2024	0.06459	0.9522	0.08483	0.9632
6/19/2024	0.05669	0.9765	0.06075	0.9767
7/7/2024	0.05544	0.9455	0.07526	0.9616
7/3/2024	0.05055	0.9392	0.04386	0.9393
6/30/2024	0.05485	0.9592	0.07357	0.9632
6/16/2024	0.01578	0.9312	0.03976	0.9499
6/9/2024	0.06561	0.9813	0.08137	0.9872
6/11/2024	2977	0.8659	13982	0.8676
5/20/2024	1.827	0.9158	2300279	0.9278
7/14/2024	0.03244	0.9495	0.05467	0.9575
5/26/2024	1.827	0.9158	2300279	0.9278
		Average	0.0618	
		SD	0.0177	

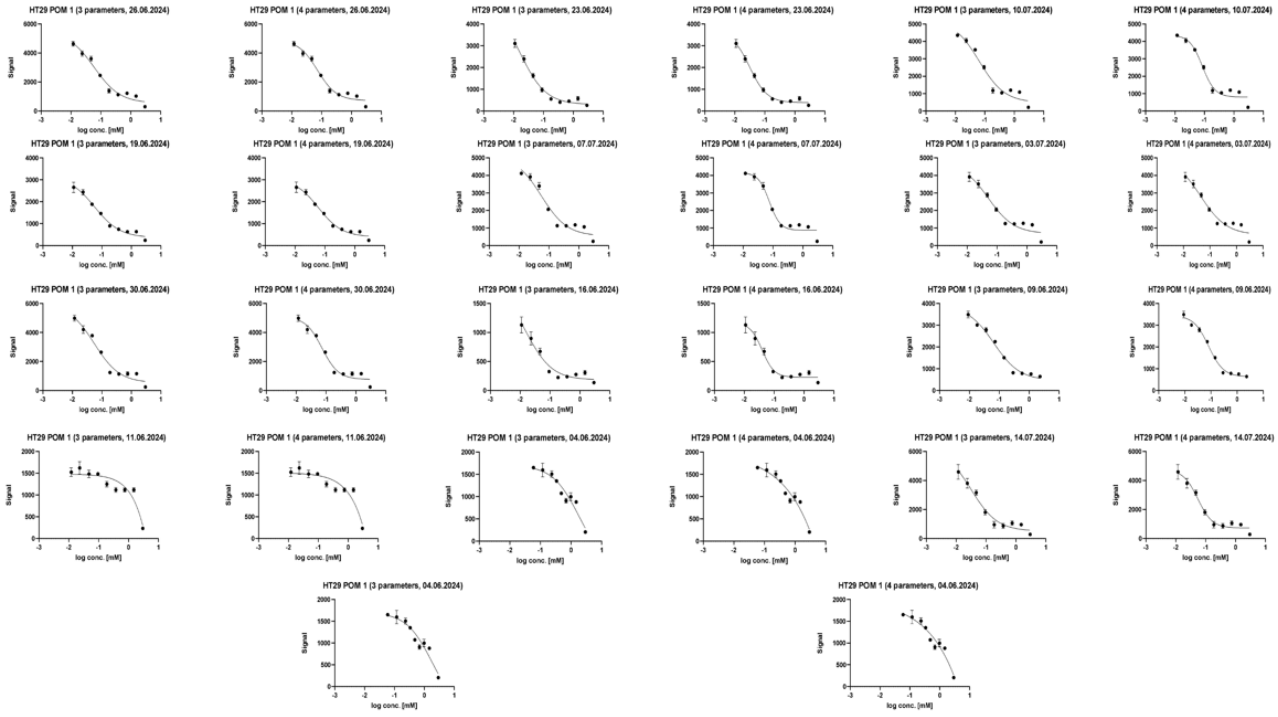

Figure 74 Appendix – IC_{50} results $GaMo_6$ in HT29

Table 18 Appendix - IC_{50} results $GaMo_{12}$ in CHO-K1

Date	IC_{50} - 3 parameter	R^2	IC_{50} - 4 parameter	R^2
6/26/2024	0.1329	0.9464	0.1261	0.9465
6/23/2024	0.08262	0.9579	0.07613	0.9581
7/10/2024	0.1078	0.9363	0.1265	0.9365
6/19/2024	0.0415	0.9607	0.04264	0.9627
7/7/2024	0.1009	0.9277	651411	0.9352
7/3/2024	0.0264	0.7696	0.03321	0.7726
6/30/2024	0.05431	0.8278	0.05262	0.8305
6/16/2024	0.01414	0.6703	0.02927	0.7178
6/9/2024	0.1243	0.9611	0.4221	0.9621
6/11/2024	0.04699	0.6226	2143197580	0.6503
5/20/2024	0.1372	0.9628	0.09374	0.9646
7/14/2024	0.06422	0.9739	0.0801	0.9748
5/26/2024	0.1372	0.9628	0.09374	0.9646
		Average	0.104	
		SD	0.0211	

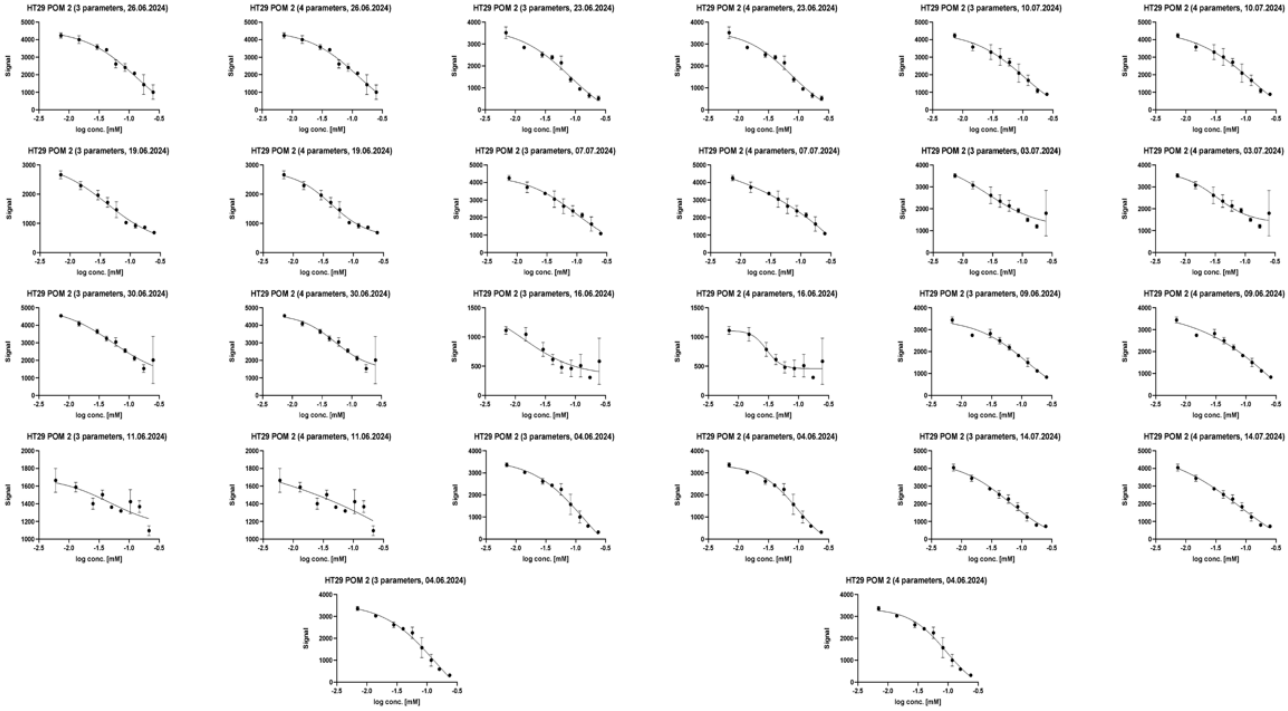

Figure 75 Appendix - IC_{50} results $GaMo_{12}$ in CHO-K1

Table 19 Appendix - IC_{50} results $GaMo_6$ in T47D

Date	IC_{50} - 3 parameter	R^2	IC_{50} - 4 parameter	R^2
7/7/2024	1.374	0.8855	0.7134	0.9039
7/10/2024	1.102	0.9204	0.9481	0.9207
7/14/2024	1.178	0.9417	1.1	0.9418
7/3/2024	0.9441	0.9196	0.5907	0.9326
6/30/2024	1.655	0.9022	1.13	0.9041
6/19/2024	0.2971	0.9454	0.2265	0.9686
6/16/2024	0.5229	0.9058	0.3706	0.9123
6/9/2024	0.2657	0.8567	0.2097	0.8784
6/11/2024	294.1	0.7831	1357	0.7835
6/4/2024	0.52	0.766	0.3322	0.8648
5/26/2024	0.0627	0.9193	0.05327	0.9193
		Average	0.28475	
		SD	0.07884011246	

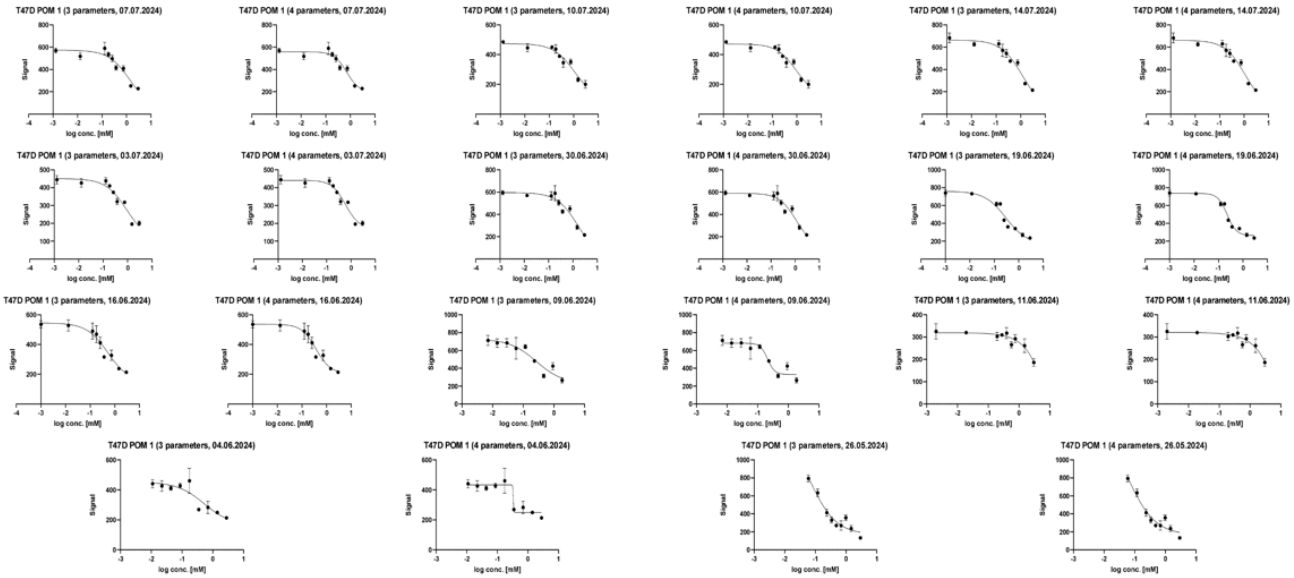

Figure 76 Appendix - IC_{50} results $GaMo_6$ in T47D

Table 20 Appendix - IC_{50} results $GaMo_{12}$ in T47D

Date	IC_{50} - 3 parameter	R^2	IC_{50} - 4 parameter	R^2
7/7/2024	0.0222	0.8818	0.02532	0.8826
7/10/2024	0.02338	0.8662	2029064623255	0.8968
7/14/2024	0.05471	0.8808	0.04927	0.8809
7/3/2024	0.03096	0.8427	0.02432	0.8563
6/30/2024	0.4461	0.01464	159580868	0
6/19/2024	0.01863	0.962	0.01955	0.9623
6/16/2024	0.03886	0.97	0.05473	0.9713
6/9/2024	0.01878	0.851	0.1294	0.868
6/11/2024	0.06526	0.7586	15648	0.7791
6/4/2024	0.02875	0.8907	0.216	0.8989
5/26/2024	0.008036	0.9138	5.20E-09	0.9246
Average	0.02593714286			
SD	0.007362809052			

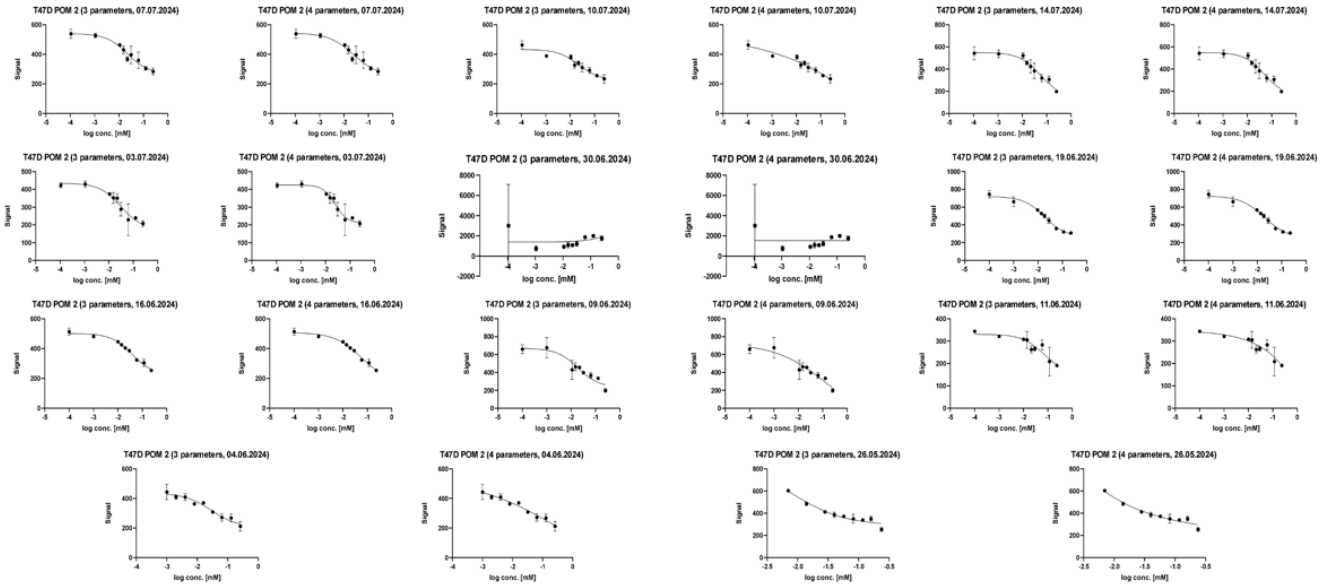

Figure 77 Appendix - IC_{50} results $GaMo_{12}$ in T47D

6.2. Results cell uptake experiments

L	cell line (positive = target high expressing, negative = target low expressing)
T	temperature
P	POM
C	concentration of POM
M	uptake
AverageE	%AD/5.00E^5 cells
SDE	standard deviation of %AD/5.00E^5 cells across experiments
VarianceE	variance of %AD/5.00E^5 cells across experiments

[^{68}Ga]Ga-PSMA-11

Table 21 Appendix – [^{68}Ga]Ga-PSMA-11 internalized

L	T	P	C	M	AverageE	SDE	VarianceE
negative	37 °C	GaMo12	10	blocked	0.004578	0.005972	3.57E-05
negative	37 °C	GaMo12	10	total	0.0188	0.012042	0.000145
negative	37 °C	GaMo12	30	blocked	0	0	0
negative	37 °C	GaMo12	30	total	0	0	0
negative	37 °C	GaMo6	10	blocked	0.011367	0.008952	8.01E-05
negative	37 °C	GaMo6	10	total	0.114456	0.026033	0.000678
negative	37 °C	GaMo6	30	blocked	0.003222	0.005581	3.11E-05

negative	37 °C	GaMo6	30	total	0.013867	0.01201	0.000144
negative	37 °C	No Carrier	0	blocked	0.048389	0.007259	5.27E-05
negative	37 °C	No Carrier	0	total	0.136078	0.008618	7.43E-05
negative	37 °C	SiMoW11	10	blocked	0.028322	0.004932	2.43E-05
negative	37 °C	SiMoW11	10	total	0.040333	0.006966	4.85E-05
negative	37 °C	SiMoW11	30	blocked	0	0	0
negative	37 °C	SiMoW11	30	total	0.000711	0.001232	1.52E-06
negative	4°C	GaMo12	10	blocked	0.004578	0.007929	6.29E-05
negative	4°C	GaMo12	10	total	0.012767	0.011471	0.000132
negative	4°C	GaMo12	30	blocked	0	0	0
negative	4°C	GaMo12	30	total	0	0	0
negative	4°C	GaMo6	10	blocked	0.0321	0.03429	0.001176
negative	4°C	GaMo6	10	total	0.038478	0.029873	0.000892
negative	4°C	GaMo6	30	blocked	0	0	0
negative	4°C	GaMo6	30	total	0	0	0
negative	4°C	No Carrier	0	blocked	0.033456	0.024434	0.000597
negative	4°C	No Carrier	0	total	0.063244	0.037178	0.001382
negative	4°C	SiMoW11	10	blocked	0.010633	0.004202	1.77E-05
negative	4°C	SiMoW11	10	total	0.021422	0.007181	5.16E-05
negative	4°C	SiMoW11	30	blocked	0	0	0
negative	4°C	SiMoW11	30	total	0	0	0
positive	37 °C	GaMo12	10	blocked	0.0126	0.016393	0.000269
positive	37 °C	GaMo12	10	total	0.894767	0.535873	0.287159
positive	37 °C	GaMo12	30	blocked	0.003167	0.005485	3.01E-05
positive	37 °C	GaMo12	30	total	0.298144	0.297	0.088209
positive	37 °C	GaMo6	10	blocked	0.028667	0.03867	0.001495
positive	37 °C	GaMo6	10	total	2.3628	0.560802	0.314498
positive	37 °C	GaMo6	30	blocked	0.002656	0.0046	2.12E-05
positive	37 °C	GaMo6	30	total	1.934756	1.540003	2.371608
positive	37 °C	No Carrier	0	blocked	0.059611	0.029159	0.00085

positive	37 °C	No Carrier	0	total	2.260622	0.486964	0.237134
positive	37 °C	SiMoW11	10	blocked	0.020756	0.021122	0.000446
positive	37 °C	SiMoW11	10	total	0.135367	0.019435	0.000378
positive	37 °C	SiMoW11	30	blocked	0.016089	0.013945	0.000194
positive	37 °C	SiMoW11	30	total	0.031478	0.030252	0.000915
positive	4°C	GaMo12	10	blocked	0.029333	0.050807	0.002581
positive	4°C	GaMo12	10	total	0.258089	0.143358	0.020551
positive	4°C	GaMo12	30	blocked	0.026644	0.04615	0.00213
positive	4°C	GaMo12	30	total	0.163622	0.128844	0.016601
positive	4°C	GaMo6	10	blocked	0.0479	0.04792	0.002296
positive	4°C	GaMo6	10	total	0.623311	0.587259	0.344873
positive	4°C	GaMo6	30	blocked	0.024722	0.04282	0.001834
positive	4°C	GaMo6	30	total	0.384656	0.237883	0.056588
positive	4°C	No Carrier	0	blocked	0.033244	0.009287	8.63E-05
positive	4°C	No Carrier	0	total	0.271989	0.168053	0.028242
positive	4°C	SiMoW11	10	blocked	0.023033	0.017351	0.000301
positive	4°C	SiMoW11	10	total	0.039744	0.011715	0.000137
positive	4°C	SiMoW11	30	blocked	0.021122	0.036585	0.001338
positive	4°C	SiMoW11	30	total	0.022622	0.039183	0.001535

Table 22 Appendix – [^{68}Ga]Ga- PSMA-11 membrane bound

L	**T**	**P**	**C**	**M**	**AverageE**	**SDE**	**VarianceE**
negative	37 °C	GaMo12	10	blocked	0.074767	0.03105	0.000964
negative	37 °C	GaMo12	10	total	0.056944	0.025092	0.00063
negative	37 °C	GaMo12	30	blocked	0.0012	0.002078	4.32E-06
negative	37 °C	GaMo12	30	total	0.006589	0.007195	5.18E-05
negative	37 °C	GaMo6	10	blocked	0.038056	0.034123	0.001164
negative	37 °C	GaMo6	10	total	0.185589	0.059024	0.003484
negative	37 °C	GaMo6	30	blocked	0.008889	0.015396	0.000237
negative	37 °C	GaMo6	30	total	0.071978	0.041976	0.001762
negative	37 °C	No Carrier	0	blocked	0.097178	0.046635	0.002175

negative	37 °C	No Carrier	0	total	0.316211	0.163298	0.026666
negative	37 °C	SiMoW11	10	blocked	0.122667	0.102982	0.010605
negative	37 °C	SiMoW11	10	total	0.138689	0.111594	0.012453
negative	37 °C	SiMoW11	30	blocked	0.000178	0.000308	9.48E-08
negative	37 °C	SiMoW11	30	total	0.021244	0.018859	0.000356
negative	4°C	GaMo12	10	blocked	0.076856	0.06842	0.004681
negative	4°C	GaMo12	10	total	0.105667	0.043615	0.001902
negative	4°C	GaMo12	30	blocked	0.013411	0.011837	0.00014
negative	4°C	GaMo12	30	total	0.040378	0.049334	0.002434
negative	4°C	GaMo6	10	blocked	0.179411	0.199495	0.039798
negative	4°C	GaMo6	10	total	0.148067	0.029195	0.000852
negative	4°C	GaMo6	30	blocked	0.0114	0.013794	0.00019
negative	4°C	GaMo6	30	total	0.050344	0.040754	0.001661
negative	4°C	No Carrier	0	blocked	0.104922	0.106357	0.011312
negative	4°C	No Carrier	0	total	0.262744	0.186077	0.034625
negative	4°C	SiMoW11	10	blocked	0.115478	0.10696	0.011441
negative	4°C	SiMoW11	10	total	0.139411	0.155148	0.024071
negative	4°C	SiMoW11	30	blocked	0.151278	0.251499	0.063252
negative	4°C	SiMoW11	30	total	0.141567	0.202179	0.040876
positive	37 °C	GaMo12	10	blocked	0.048889	0.028558	0.000816
positive	37 °C	GaMo12	10	total	1.403244	0.743302	0.552498
positive	37 °C	GaMo12	30	blocked	0.007822	0.013548	0.000184
positive	37 °C	GaMo12	30	total	0.4459	0.426269	0.181705
positive	37 °C	GaMo6	10	blocked	0.066011	0.051487	0.002651
positive	37 °C	GaMo6	10	total	3.671722	1.098986	1.207769
positive	37 °C	GaMo6	30	blocked	0.013478	0.023344	0.000545
positive	37 °C	GaMo6	30	total	1.842578	1.266245	1.603377
positive	37 °C	No Carrier	0	blocked	0.134589	0.094697	0.008968
positive	37 °C	No Carrier	0	total	3.590167	0.790551	0.62497
positive	37 °C	SiMoW11	10	blocked	0.111356	0.112859	0.012737
positive	37 °C	SiMoW11	10	total	0.280067	0.110754	0.012266

positive	37 °C	SiMoW11	30	blocked	0.0153	0.013817	0.000191
positive	37 °C	SiMoW11	30	total	0.074033	0.081956	0.006717
positive	4°C	GaMo12	10	blocked	0.045056	0.018841	0.000355
positive	4°C	GaMo12	10	total	0.988322	0.684632	0.468721
positive	4°C	GaMo12	30	blocked	0.038833	0.067261	0.004524
positive	4°C	GaMo12	30	total	0.723956	0.521158	0.271605
positive	4°C	GaMo6	10	blocked	0.098333	0.056702	0.003215
positive	4°C	GaMo6	10	total	1.387844	0.9526	0.907447
positive	4°C	GaMo6	30	blocked	0.051322	0.088893	0.007902
positive	4°C	GaMo6	30	total	1.454456	1.041036	1.083756
positive	4°C	No Carrier	0	blocked	0.088333	0.010516	0.000111
positive	4°C	No Carrier	0	total	1.291411	1.082982	1.17285
positive	4°C	SiMoW11	10	blocked	0.081278	0.026825	0.00072
positive	4°C	SiMoW11	10	total	0.1166	0.030008	0.0009
positive	4°C	SiMoW11	30	blocked	0.029911	0.041537	0.001725
positive	4°C	SiMoW11	30	total	0.081222	0.033841	0.001145

[^{68}Ga]Ga-Pentixafor

Table 23 Appendix – [^{68}Ga]Ga-Pentixafor internalized

L	T	P	C	M	AverageE	SDE	VarianceE
negative	37 °C	GaMo12	10	blocked	0.115678	0.011967	0.000143
negative	37 °C	GaMo12	10	total	0.065833	0.048521	0.002354
negative	37 °C	GaMo12	30	blocked	0.318122	0.140177	0.01965
negative	37 °C	GaMo12	30	total	0.027	0.045044	0.002029
negative	37 °C	GaMo6	10	blocked	0.035489	0.029136	0.000849
negative	37 °C	GaMo6	10	total	0.056222	0.056217	0.00316
negative	37 °C	GaMo6	30	blocked	0.011278	0.019534	0.000382
negative	37 °C	GaMo6	30	total	0.038722	0.039614	0.001569
negative	37 °C	No Carrier	0	blocked	0.040211	0.038715	0.001499
negative	37 °C	No Carrier	0	total	0.065011	0.039468	0.001558
negative	37 °C	SiMoW11	10	blocked	2.754078	0.797115	0.635393
negative	37 °C	SiMoW11	10	total	0.669933	0.401389	0.161113

negative	37 °C	SiMoW11	30	blocked	3.545811	0.881963	0.777859
negative	37 °C	SiMoW11	30	total	1.141356	0.41459	0.171885
negative	4°C	GaMo12	10	blocked	0.367711	0.304832	0.092923
negative	4°C	GaMo12	10	total	0.135433	0.080803	0.006529
negative	4°C	GaMo12	30	blocked	0.496489	0.473662	0.224355
negative	4°C	GaMo12	30	total	0.107978	0.151476	0.022945
negative	4°C	GaMo6	10	blocked	0.073433	0.057469	0.003303
negative	4°C	GaMo6	10	total	0.0041	0.007101	5.04E-05
negative	4°C	GaMo6	30	blocked	0.132911	0.230209	0.052996
negative	4°C	GaMo6	30	total	0.010378	0.017975	0.000323
negative	4°C	No Carrier	0	blocked	0.034756	0.060198	0.003624
negative	4°C	No Carrier	0	total	0.0398	0.068936	0.004752
negative	4°C	SiMoW11	10	blocked	0.763833	1.006339	1.012718
negative	4°C	SiMoW11	10	total	0.3429	0.39275	0.154252
negative	4°C	SiMoW11	30	blocked	1.315189	0.978011	0.956505
negative	4°C	SiMoW11	30	total	1.0256	0.590494	0.348683
positive	37 °C	GaMo12	10	blocked	0.811789	0.564753	0.318946
positive	37 °C	GaMo12	10	total	0.812389	0.116859	0.013656
positive	37 °C	GaMo12	30	blocked	1.770533	0.799088	0.638542
positive	37 °C	GaMo12	30	total	0.880089	0.065134	0.004242
positive	37 °C	GaMo6	10	blocked	0.100756	0.12578	0.015821
positive	37 °C	GaMo6	10	total	0.627333	0.048436	0.002346
positive	37 °C	GaMo6	30	blocked	0.157322	0.081019	0.006564
positive	37 °C	GaMo6	30	total	0.493811	0.17754	0.03152
positive	37 °C	No Carrier	0	blocked	0.056189	0.024778	0.000614
positive	37 °C	No Carrier	0	total	0.525478	0.10107	0.010215
positive	37 °C	SiMoW11	10	blocked	1.854022	0.339045	0.114952
positive	37 °C	SiMoW11	10	total	1.0153	0.215667	0.046512
positive	37 °C	SiMoW11	30	blocked	1.919689	0.473086	0.223811
positive	37 °C	SiMoW11	30	total	1.662578	0.205649	0.042292
positive	4°C	GaMo12	10	blocked	2.1779	1.931749	3.731654
positive	4°C	GaMo12	10	total	0.557056	0.414461	0.171778

positive	4°C	GaMo12	30	blocked	1.295589	1.078213	1.162543
positive	4°C	GaMo12	30	total	2.488111	2.126248	4.520929
positive	4°C	GaMo6	10	blocked	0.027744	0.023413	0.000548
positive	4°C	GaMo6	10	total	0.125833	0.055947	0.00313
positive	4°C	GaMo6	30	blocked	0.312933	0.328734	0.108066
positive	4°C	GaMo6	30	total	0.055356	0.046374	0.002151
positive	4°C	No Carrier	0	blocked	0.046422	0.010486	0.00011
positive	4°C	No Carrier	0	total	0.126378	0.030464	0.000928
positive	4°C	SiMoW11	10	blocked	1.798178	0.756634	0.572496
positive	4°C	SiMoW11	10	total	1.193311	0.517164	0.267459
positive	4°C	SiMoW11	30	blocked	2.428656	1.023482	1.047515
positive	4°C	SiMoW11	30	total	2.376922	0.314985	0.099215

Table 24 Appendix – [^{68}Ga]Ga-Pentixafor membrane bound

L	**T**	**P**	**C**	**M**	**AverageE**	**SDE**	**VarianceE**
negative	37 °C	GaMo12	10	blocked	0.151022	0.0744	0.005535
negative	37 °C	GaMo12	10	total	0.198278	0.050702	0.002571
negative	37 °C	GaMo12	30	blocked	0.201522	0.144609	0.020912
negative	37 °C	GaMo12	30	total	0.325133	0.196132	0.038468
negative	37 °C	GaMo6	10	blocked	0.1232	0.0176	0.00031
negative	37 °C	GaMo6	10	total	0.175144	0.03686	0.001359
negative	37 °C	GaMo6	30	blocked	0.156189	0.144684	0.020934
negative	37 °C	GaMo6	30	total	0.127278	0.125998	0.015875
negative	37 °C	No Carrier	0	blocked	0.1806	0.145187	0.021079
negative	37 °C	No Carrier	0	total	0.365856	0.284562	0.080975
negative	37 °C	SiMoW11	10	blocked	0.989756	0.15195	0.023089
negative	37 °C	SiMoW11	10	total	0.715633	0.134611	0.01812
negative	37 °C	SiMoW11	30	blocked	0.881756	0.352481	0.124243
negative	37 °C	SiMoW11	30	total	0.804411	0.233086	0.054329
negative	4°C	GaMo12	10	blocked	0.268478	0.172095	0.029617
negative	4°C	GaMo12	10	total	0.270722	0.090553	0.0082
negative	4°C	GaMo12	30	blocked	0.399878	0.131095	0.017186

negative	4°C	GaMo12	30	total	0.217067	0.066311	0.004397
negative	4°C	GaMo6	10	blocked	0.131267	0.091304	0.008336
negative	4°C	GaMo6	10	total	0.099044	0.0161	0.000259
negative	4°C	GaMo6	30	blocked	0.036356	0.055606	0.003092
negative	4°C	GaMo6	30	total	0.0563	0.056701	0.003215
negative	4°C	No Carrier	0	blocked	0.094478	0.031156	0.000971
negative	4°C	No Carrier	0	total	0.127	0.040845	0.001668
negative	4°C	SiMoW11	10	blocked	1.115278	0.611716	0.374197
negative	4°C	SiMoW11	10	total	1.453733	0.690298	0.476511
negative	4°C	SiMoW11	30	blocked	0.572922	0.10932	0.011951
negative	4°C	SiMoW11	30	total	1.698844	0.772928	0.597418
positive	37 °C	GaMo12	10	blocked	0.171367	0.040246	0.00162
positive	37 °C	GaMo12	10	total	1.731433	0.485212	0.235431
positive	37 °C	GaMo12	30	blocked	0.309267	0.113889	0.012971
positive	37 °C	GaMo12	30	total	1.551344	0.208139	0.043322
positive	37 °C	GaMo6	10	blocked	0.160378	0.10817	0.011701
positive	37 °C	GaMo6	10	total	1.781856	0.219931	0.04837
positive	37 °C	GaMo6	30	blocked	0.241833	0.09967	0.009934
positive	37 °C	GaMo6	30	total	0.758856	0.056702	0.003215
positive	37 °C	No Carrier	0	blocked	0.224767	0.193734	0.037533
positive	37 °C	No Carrier	0	total	1.734578	0.088465	0.007826
positive	37 °C	SiMoW11	10	blocked	0.643689	0.416262	0.173274
positive	37 °C	SiMoW11	10	total	1.456544	0.212079	0.044977
positive	37 °C	SiMoW11	30	blocked	0.377089	0.084973	0.00722
positive	37 °C	SiMoW11	30	total	1.071156	0.267795	0.071714
positive	4°C	GaMo12	10	blocked	1.620011	1.388867	1.928952
positive	4°C	GaMo12	10	total	2.251178	1.242129	1.542885
positive	4°C	GaMo12	30	blocked	1.010489	0.726234	0.527417
positive	4°C	GaMo12	30	total	2.964967	1.061727	1.127264
positive	4°C	GaMo6	10	blocked	0.196944	0.074008	0.005477
positive	4°C	GaMo6	10	total	2.352233	1.211887	1.468671
positive	4°C	GaMo6	30	blocked	0.315011	0.237761	0.05653

positive	4°C	GaMo6	30	total	2.122978	0.746539	0.557321
positive	4°C	No Carrier	0	blocked	0.227156	0.126821	0.016084
positive	4°C	No Carrier	0	total	2.412078	0.394023	0.155254
positive	4°C	SiMoW11	10	blocked	1.612222	0.863883	0.746295
positive	4°C	SiMoW11	10	total	3.270756	1.375644	1.892397
positive	4°C	SiMoW11	30	blocked	1.431956	0.882728	0.779209
positive	4°C	SiMoW11	30	total	3.332711	1.738185	3.021287

6.3. Calculation and statistical evaluation of cell uptake experiments

Below is the code utilised in the program R to statistically evaluate the cell uptake results

```
rm(list=ls());gc();library(readxl);library(dplyr);library(car);library(purrr);library(nortest);library(ggplot2);library(ggpattern);library(writexl);library(scales);library(grid);library(gridExtra);RawData<-read_excel(file.choose());RawData<-RawData%>%mutate(E=as.factor(E),R=as.factor(R),U=as.numeric(U),C=as.factor(C),T=as.factor(T),L=as.factor(L),M=as.factor(M),P=as.factor(P));class(RawData);str(RawData);OutlierR<-RawData%>%group_by(L,T,P,C,M,E)%>%mutate(Z=(U-mean(U,na.rm=T))/sd(U,na.rm=T),Is_Outlier=abs(Z)>2)%>%filter(is.na(Is_Outlier)|!Is_Outlier)%>%mutate(n=n());NormalShapiroR<-OutlierR%>%summarise(ShapiroP=ifelse(var(U,na.rm=T)>0,shapiro.test(U)$p.value,NA),Normal=ifelse(!is.na(ShapiroP)>0.05,T,F));DescriptiveStatR<-OutlierR%>%summarise(AverageR=mean(U,na.rm=T),SDR=sd(U,na.rm=T),VarianceR=var(U,na.rm=T));OutlierE<-DescriptiveStatR%>%group_by(L,T,P,C,M)%>%mutate(Z=(AverageR-mean(AverageR,na.rm=T))/sd(AverageR,na.rm=T),Is_Outlier=abs(Z)>2)%>%filter(is.na(Is_Outlier)|!Is_Outlier)%>%mutate(n=n());DescriptiveStatE<-OutlierE%>%summarise(AverageE=mean(AverageR,na.rm=T),SDE=sd(AverageR,na.rm=T),VarianceE=var(AverageR,na.rm=T));NormalShapiroE<-OutlierE%>%summarise(ShapiroP=ifelse(var(AverageR,na.rm=T)>0,shapiro.test(AverageR)$p.value,NA),Normal=ifelse(!is.na(ShapiroP)>0.05,T,F));VarHomLeveneE<-OutlierR%>%group_by(L,T,P,C,M)%>%group_split()%>%map_dfr(function(data){if(n_distinct(data$E)>1){test<-leveneTest(U~as.factor(E),data=data);tibble(L=unique(data$L),T=unique(data$T),P=unique(data$P),C=unique(data$C),M=unique(data$M),Group_DF=test$Df[1]
```

```
,Residual_DF=test$Df[2],F_value=test$`F
value`[1],P_value=test$`Pr(>F)`[1],Homogen=ifelse(test$`Pr(>F)`[1]>0.05,"YES","NO"))}else{
tibble(L=unique(data$L),T=unique(data$T),P=unique(data$P),C=unique(data$C),M=unique(
data$M),Group_DF=NA_integer_,Residual_DF=NA_integer_,F_value=NA_real_,P_value=N
A_real_,Homogen=NA_character_)}});RelativeUptake<-
OutlierE%>%filter(C%in%c(0,10,30))%>%group_by(L,T,M,E)%>%mutate(No_Carrier_Mean=
mean(AverageR[P=="No
Carrier"&C==0],na.rm=T),Relative_Uptake=(AverageR/No_Carrier_Mean)*100)%>%filter(P!=
"No
Carrier")%>%group_by(L,T,M,P,C)%>%summarise(Mean_Relative_Uptake=mean(Relative_
Uptake,na.rm=T),SD_Relative_Uptake=sd(Relative_Uptake,na.rm=T),.groups="drop");tTestT
otBlock<-
OutlierE%>%group_by(L,T,P,C)%>%summarise(p_value=t.test(AverageR~M,data=cur_data(
))$p.value,significance=case_when(p_value<0.001~"***",p_value<0.01~"**",p_value<0.05~"*
",T~"ns"),.groups="drop");tTestConc<-
OutlierE%>%filter(C!=0)%>%group_by(L,T,M,P)%>%summarise(p_value=t.test(AverageR~C
,data=cur_data())$p.value,significance=case_when(p_value<0.001~"***",p_value<0.01~"**",p
_value<0.05~"*",T~"ns"),.groups="drop");tTestNoCarrier<-
OutlierE%>%filter(C%in%c(0,10,30))%>%group_by(L,T,M)%>%group_split()%>%map_dfr(fu
nction(data){no_carrier<-data%>%filter(P=="No Carrier",C==0);others<-
data%>%filter(P!="No
Carrier");if(nrow(no_carrier)>0&nrow(others)>0){map_dfr(unique(others$P),function(substanc
e){map_dfr(unique(others$C),function(conc){test_data<-
bind_rows(no_carrier,others%>%filter(P==substance,C==conc));if(n_distinct(test_data$P)==
2){test<-
t.test(AverageR~P,data=test_data);tibble(L=unique(data$L),T=unique(data$T),M=unique(dat
a$M),Substance=substance,Concentration=conc,P_value=test$p.value,Significance=case_w
hen(test$p.value<0.001~"***",test$p.value<0.01~"**",test$p.value<0.05~"*",T~"ns"))}else{tibb
le(L=unique(data$L),T=unique(data$T),M=unique(data$M),Substance=substance,Concentra
tion=conc,P_value=NA_real_,Significance=NA_character_)}})}else{tibble(L=unique(data$L),T
=unique(data$T),M=unique(data$M),Substance=NA_character_,Concentration=NA_real_,P_
value=NA_real_,Significance=NA_character_)}})
```